Towards Patient-Specific Modeling of Hearts in Children with Congenital Heart Defects

A morphing technique for patient-inspired biventricular models of young hearts in a diverse population

Biomedical Engineering Msc Thesis

P.H. (Puck) Pentenga

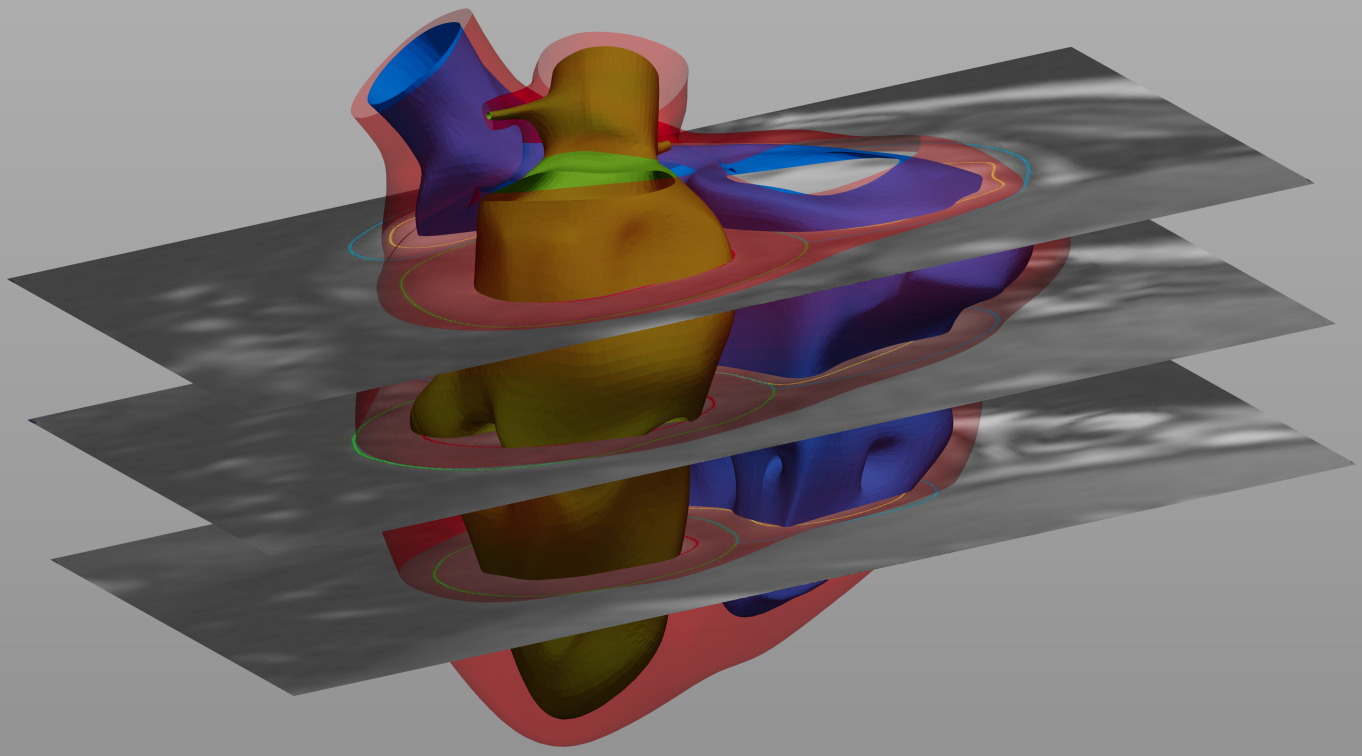

Delft University of Technology

Erasmus MC
Universitair Medisch Centrum Rotterdam

TU Delft

Towards Patient-Specific Modeling of Hearts in Children with Congenital Heart Defects

A morphing technique for patient-inspired biventricular models of young hearts in a diverse population

by

P.H. (Puck) Pentenga

Student number:	5149509
Main supervisor:	Dr. ir. Mathias Peirlinck
Institution:	Delft University of Technology
Place:	Faculty of Mechanical, Maritime and Materials Engineering, Delft
Master program:	Biomedical Engineering
Specialization:	Medical Devices and Bioelectronics
Date:	January 19, 2023

Thesis committee members:	Dr.ir. A.C. Akyildiz
	Dr.ir. M.P. Peirlinck
	Prof.dr. W.A. Helbing
	M.D. W.J. van Genuchten

Erasmus MC
University Medical Center Rotterdam

TU Delft

Summary

Introduction: A congenital heart defect (CHD) is an anomaly in the structure of the heart that is present at birth. In the last 15 years, a CHD is present in 9 per 1,000 live births, making it the most prevalent birth defect (van der Linde et al., 2011). CHD's prevalence coupled with its inherent complexity culminates into situations that are both complicated and unique. This makes the treatment of patients with CHDs highly patient-specific. Patient-specific physics-based computational models can aid in selecting the optimal course of treatment for the patient and serve as a predictive tool for different surgical plans (Capelli et al., 2018). The creation of patient-specific geometric heart models of children with CHDs will be the first crucial step towards a patient-specific approach in ameliorating this challenge. Approaches have to be found to face challenges including: a lack of high quality imaging data of the target population; slice misalignment due to breathing in a breath-hold procedure; and a lack of protocols in image segmentation.

Materials and Methods: To accomplish the objective, seven biventricular geometric models and meshes are created for healthy hearts, tetralogy of Fallot hearts and Fontan hearts. Slice misalignment is corrected using contours of the papillary muscle and the epicardium as a reference. Lastly, ground truth geometries are constructed by stacking disks that originate directly from the MRI segmentation.

Results: To validate the geometric models, global and local approaches are used. The global validation includes ventricular mass and volume analyses with a relative error (RE) ranging from 0.00036 to 0.79. The Dice similarity coefficient (DSC) for the local validation is between 0.711 ± 0.138 and 0.968 ± 0.018. The slice misalignment correction is validated using qualitative and quantitative measures. A quantitative measure is the 4-chamber long-axis local validation which has a DSC of 0.877 for the epicardium and 0.916 for the papillary muscle correction method. Global validation in the ground truth exercise has a mean RE of 0.010 ± 0.0066. Results of the local validation show a minimum DSC of 0.960 ± 0.008.

Discussion: Large differences in RE can be explained by the small number of MRI slices available, segmentation variability, the complex geometry of the right ventricle, and the methods of volume and mass computations. The DSC computed in the local validation of the models shows good to excellent agreement for all models. According to the long-axis local validation, the papillary muscle is the best reference method proposed for the slice misalignment correction. The ground truth exercise reveals close correlation to the Medis Suite measurements, possibly leading to underestimation of the computed volumes.

Conclusion: Patient-specific biventricular geometric models are created and validated in this thesis. The models are representative of a range of patients including healthy hearts and hearts with complex CHDs. A patient-specific model of the heart would be beneficial for clinicians to understand complex pathological cases, as the ones described in this work. Herein, a patient-specific biventricular geometric model is presented. By including a healthy population as well as patients affected by complex congenital heart defects, this work can be used as a starting point for the development of more patient-specific computational models of the heart.

Contents

Nomenclature

Abbreviations

Abbreviation	Definition
AA	Aortic Arch
CHD	Congenital Heart Defect
CT	Computed Tomography
DSC	Dice Similarity Coefficient
ED	End-Diastolic
EDV	End-Diastolic Volume
ES	End-Systolic
ESV	End-Systolic Volume
HLHS	Hypoplastic Left Heart Syndrome
LCA	Left Coronary Artery
LHHM	Living Heart Human Model
LV	Left Ventricle
MRI	Magnetic Resonance Imaging
MV	Mitral Valve
PCA	Principal Component Analysis
PT	Pulmonary Trunk
RCA	Right Coronary Artery
RE	Relative Error
RV	Right Ventricle
SSM	Statistical Shape Model
TOF	Tetralogy of Fallot
TV	Tricuspid Valve

Patient list

Patient	Age	Sex	Case
1	8	Female	Healthy
2	9	Female	Healthy
3	7	Male	Tetralogy of Fallot
4	8	Male	Tetralogy of Fallot
5	5	Male	Fontan
6	8	Male	Fontan
7	19	Male	Fontan

List of Figures

List of Tables

1

Introduction

The heart is the primary organ in the circulatory system. It pumps blood through the body to provide oxygen and nutrients to the organs. A typically functioning heart has two sides and is divided into four chambers. The right side of the heart provides the lungs with deoxygenated blood and the left side of the heart provides the organs with oxygenated blood. In a healthy heart, all chambers contract rhythmically and blood flows efficiently through the heart and into the arteries. However, anomalies in the heart structure are common.

Congenital heart defects (CHD) are abnormalities in the heart structure present at birth with a prevalence of 9 per 1,000 live births. This pathological condition is assessed to be highly heterogeneous, with a range from no symptoms to life-threatening heart conditions (van der Linde et al., 2011). Severe congenital heart defects require surgical intervention. Historically, the treatment was focused on palliative procedures. However, improvements in imaging and surgical procedures allow for more corrective surgeries at a younger age. This has resulted in a higher long-term survival rate and a higher quality of life (Martin & Jonas, 2018). Congenital heart defects can roughly be divided into two categories: simple and complex CHDs. Simple CHDs can be treated using interventional cardiac catheterization (Martin & Jonas, 2018). Complex CHDs present differently in every patient. Open-heart surgeries are often required, sometimes in different stages, with a patient-specific approach due to the uniqueness of the defects. Clinicians use noninvasive imaging techniques to visualize the defect and plan the surgical approach. Decisions have to be made on the timing of the surgery and different surgical plans are based on the patients' particular cardiac anatomy.

The creation of patient-specific geometric heart models of children with congenital heart defects can be the first step towards a patient-specific physics-based computational model to use in the treatment of CHDs.

1.1. Physics-Based Computational Modeling

Computational cardiac models provide a powerful tool for integrating theoretical principles with experimental data. By implementing multi-physics, cardiac function can be studied in terms of anatomy, electro-mechanics, fluid behavior, and cellular function (Levine et al., 2022). Complex computational models require the integration of multi-disciplinary efforts (Ordas et al., 2007). The models can be made patient-specific, while risk is minimized and patient benefit is maximized (Rufaihah et al., 2021). With the aim of improving the surgical procedure, minimizing the risk and

increasing the clinical outcome, patient-specific computational models can be useful (Formato et al., 2022).

The creation of a physics-based computational model follows a general workflow with a number of subsequent steps. The construction of a patient-specific geometry is the first step. The geometry forms the anatomical structure, which is based on medical imaging. Image segmentation partitions the images into segments according to their function and cardiac modeling applications (Vieira et al., 2015). From the contours, a patient-specific 3D surface is defined. The second step is discretizing the model into a computational mesh (Formato et al., 2022). The geometry is broken down into elements and nodes. Equations of motion can be set up and solved by using the individual elements and nodes (Vieira et al., 2015). The third step is assigning material properties to the myocardial wall and valve leaflets (Yu et al., 2020). Additionally, it is important to include the fiber orientation in the computational model to accurately represent the mechanical contraction in the myocardium. Ventricular mechanics depend on the myocardial arrangement and this arrangement affects both the local mechanics and global ventricular behavior (Bayer et al., 2012). In the left ventricle, these fibers follow a right-handed helical pathway from the endocardium towards the mid-wall and a left-handed helical pathway from the mid-wall towards the epicardium (Wong & Kuhl, 2014). Boundary conditions are defined in the fourth step. Conditions are determined at every inlet and outlet of the model (Vieira et al., 2015). They provide the model information on motion, flow and resistance to make the simulation realistic. The fifth and final step is solving the partial differential equations in a computational simulation and the post-processing of the results to evaluate the variables of interest.

1.2. Patient-Specific Geometry

The creation of patient-specific geometric heart models of children with congenital heart defects will be the first crucial step towards a patient-specific approach to the treatment of patients with a complex CHD and further research into patient-specific computational heart models. Once a validated workflow is set up to create patient-specific geometries, the models can be explored and expanded to evaluate pathologies and surgical planning.

Geometric models of different CHDs can help gain experience and expertise in complex cases and increase the understanding of anatomical details. Every case of complex congenital heart defect is unique. This makes the treatment of patients with CHDs highly patient-specific. The uniqueness, combined with the prevalence, makes it very difficult for doctors to understand all the aspects of the specific CHD, learn from previous cases, and select the best course of treatment. These cases are not seen frequently, making it difficult to build up expertise. This is one of the reasons why children's heart centers are centralized. Specialized hospitals with experienced pediatric cardiologists treat patients from all over The Netherlands (Van der Geest, 2022).

Not only can the model be used as an educational tool for the clinician, but also the patient, parents, and/or caretakers can benefit from a 3D anatomically correct model. Congenital heart defects often involve complex surgical operations. In these situations, communication between the clinician and the patient is important for the patient and family to be well-informed on the condition, and prepared for the treatment of the patient. Studies have indicated that the parents of children with CHDs have a lack of knowledge on the condition of their children (Cheuk et al., 2004). It has been shown that both parents and clinicians of patients with a CHD appreciate and benefit from 3D patient-specific models during consultations (Biglino et al., 2015). To gain an understanding of the experience of the patient and family and their needs on forms of communication, an interview is conducted. The full interview is in Appendix A. The interview indicates that parents of a child born with a CHD have many questions and uncertainties. Cardiac

Table 1.1: CHD subtypes prevalence and distribution

(Gatzoulis et al., 2018; van der Linde et al., 2011)

CHD	Prevalence per 1000 live births	Distribution
Ventricular Septal Defect	2.62	34%
Atrial Septal defect	1.64	13%
Patent Ductus Arteriosus	0.87	10%
Pulmonary Stenosis	0.50	8%
Tetralogy of Fallot	0.34	5%
Hypoplastic Left Heart Syndrome	0.17	<1%

images are difficult to comprehend, and parents are not cardiac experts. On top of that, once parents understand the anatomy of their child, they get many questions from family and friends that are involved. Having a patient-specific geometric model that is intuitive and understandable to people without anatomical expertise would be helpful in communication.

1.2.1. Research problem

A patient-specific geometric heart model requires high-quality cardiac imaging data from the target population. Cardiac imaging in children is challenging due to a number of reasons. The target population of children with CHDs is small, especially for complex CHDs. Table 1.1 shows the most common CHDs subtypes with their worldwide prevalence per 1000 live births. The second column shows the distribution of CHDs. The table shows that children with CHDs make up a small population with a wide variety of defects. The most common complex CHD is tetralogy of Fallot (TOF) with an occurrence of under 0.05% of births (van der Linde et al., 2011). Furthermore, it is important to understand that every case of complex CHD is unique.

Obtaining high-quality imaging from the target population is also challenging. There are different imaging techniques which can be used to obtain data, including echocardiography, computed tomography (CT) and cardiovascular magnetic resonance imaging (MRI). All the techniques have their advantages and disadvantages, which are summarized in Table 1.2. It is essential that the imaging technique is safe for the patient and high spatial resolution and reproducibility are desired for a better quality model.

Young children have a high heart rate and a small anatomy, requiring both high temporal resolution and spatial resolution (Lederlin et al., 2011). Next to that, breath-holding and lying still are generally required in the acquisition of cardiac images. This puts forward an additional challenge: slice misalignment. During an MRI, a child is asked to lie still, take a deep breath, and hold this breath. The child may be unable to do this and move or breathe out too early. Breathing out too early leads to the lungs moving and therefore relocating the heart. This will result in a slice misalignment. The produced contours will be misaligned as well, misrepresenting the true shape of the heart.

The final challenge is the segmentation of the obtained imaging data. High-quality segmentation is a research problem due to lower quality of the imaging data in the target population, the lack of protocols and the difficult geometries. The myocardial wall of the right ventricle (RV) is about one-third of the thickness of the left ventricle (LV), due to a lower vascular resistance (Muresian, 2016; Weinhaus, 2015). This makes segmentation more difficult. Large anatomical variations increase the complexity of segmentation algorithms and manual correction is therefore still required when using automated segmentation (Trusty et al., 2018). To address the research problems stated, possible approaches are suggested next.

Table 1.2: Advantages and disadvantages of different imaging techniques

Imaging Technique	Advantages	Disadvantages
Echocardiography	+ Widely available + Easy to use + High temporal resolution + Radiation and sedation free (Olivieri et al., 2015) (Babu-Narayan et al., 2016)	- Low spatial resolution (Mertens et al., 2008)
Magnetic resonance imaging	+ Radiation free + High spatial resolution + High reproducibility (Gilbert et al., 2014) (Babu-Narayan et al., 2016)	- Contrast agent on occasion - Low temporal resolution - General anesthesia for children - High cost and expertise (Dietz et al., 2015) (Sahu & Slesnick, 2017)
Computed tomography	+ High spatial resolution + High temporal resolution (Babu-Narayan et al., 2016) (Mertens et al., 2008)	- Harmful ionizing radiation (Mertens et al., 2008)
(3D) Angiography	+ High spatial resolution + High temporal resolution (Lederlin et al., 2011)	- Invasive procedure - Harmful ionizing radiation (Lederlin et al., 2011) (Mertens et al., 2008)

1.3. Approaches

1.3.1. Statistical shape modeling

In order to describe the variation in geometric shape and analyze the human anatomy, a Statistical Shape Model (SSM) can be constructed. A statistical shape model provides the modes that are most relevant for describing the cardiac anatomy by estimating the shape variability within a sample. To create an SSM, imaging data from a population are gathered first. From the acquired data, the anatomy is represented in a single average mesh. Principal Component Analysis (PCA), a process of computing the principal components of the data, is used to find the orthogonal directions of deformation (or modes). Each cardiac anatomy can now be reconstructed as a linear combination of the modes that deform the average mesh (Rodero et al., 2021).

Although SSMs are useful tools for expressing a range of variation on top of a mean shape, they cannot be used for patient-specific geometries of children with CHDs. The anatomies in this population are non-standard geometries that lie too far outside the range of variation for the Statistical Shape Models. The hearts with complex congenital heart defects are too unique to be represented by a linear combination of modes. Additionally, SSMs require a large population of representative training samples. This is not possible for children with CHDs.

1.3.2. Morphing

Morphing aims at matching an initial geometry to a desired target by performing shape alterations. As discussed, obtaining high-quality imaging data from children is challenging. There is, however, sufficient high-quality imaging data available from adult hearts. This data can still be valuable when using morphing techniques. The mesh of an adult heart can be used as a baseline model, which can be subsequently morphed into a young, anatomically correct heart (Sigal et al., 2010). Again, every heart with a CHD is unique. Morphing allows for the creation of patient-specific models by making changes to the shapes of the individual patients. Lastly, the existing baseline model and mesh can be preserved. This prevents the time-consuming and inconsistent process of building a completely new model for every case (Weissmann et al., 2021).

Attempts have been made to use morphing techniques for cardiac modeling. Weissmann et al. propose a morphing algorithm to make anatomical changes to cardiac remodeling (Weissmann et al., 2021). However, this method is based on a porcine model. Multiple cardiac MRI scans are taken before and after the induction of heart failure. This allows for comparison within the same subject (Weissmann et al., 2021). Additionally, the pigs were pre-medicated for imaging. They were ventilated, intubated, and under general anesthesia (Charles et al., 2020). Furthermore, after the last scan, the pigs were terminated and their hearts were removed to take additional measurements (Charles et al., 2020).

Animal testing is a way to avoid risks to human patients. Animal and human physiology is different, however, and results cannot always be directly transferred (Mathur et al., 2016). Besides being expensive and challenging, animal testings requires to sacrifice a large amount of animals which can be considered cruel. In 2005, 12.1 million animals have been used for animal experimentation in Europe. 57% of these animals were used for scientific purposes (Liebsch et al., 2011). To overcome the issues of cost, lower order animals can be used. These animals have fast reproduction times, genetic traceability, and are easier in animal care. Unfortunately, the lower order animal hearts are not complex enough to study intricate CHDs in humans (Rufaihah et al., 2021).

Applying the Weissmann et al. algorithm to cardiac models for children with CHDs is much more challenging. Firstly, the population of patients is very small. The occurrence of all CHDs combined is just under 1% for all births (van der Linde et al., 2011). Secondly, an important aspect of creating an anatomically accurate model is the need for availability and use of high-quality data. MRI images have a slightly lower spatial resolution compared to CT images (Lederlin et al., 2011). However, CT images are not generally obtained from young children, due to radiation exposure. MRI also poses challenges for young children, including not being allowed to move for a longer time period, holding their breath, and the loud noises from the MRI machine (Lederlin et al., 2011; Sahu & Slesnick, 2017). In contrast to the porcine MRI scans, unnecessarily medicating children and performing a series of scans are avoided. This also means a lower resolution and a larger slice thickness. This all results in difficulties in obtaining high-quality images of young children with a CHD.

A separate study, from Conca (2015), was aimed at making monoventricular models of young patients with Hypoplastic Left Heart Syndrome (HLHS). Patient-specific data was gathered and visualized in a 3D format. An RV mesh template, consisting of 28 elements and 66 nodes, was used to fit this patient-specific data (Conca, 2015). However, by doing this, a lot of information gets lost because of oversimplification of the patient-specific data.

Ventricles are overall complex and irregular in shape, but the RV is the most irregular chamber given the crescent shape and the irregularities inside the cavity (Arega et al., 2022; Weissmann et al., 2021). Furthermore, there is high variability between subjects. And, boundaries to sur-

rounding structures, such as the right ventricular outflow tract and tricuspid valve plane, are not well defined (Tautz et al., 2022). Additionally, the right ventricular wall is significantly thinner compared to its left counterpart (Wang et al., 2019). This all makes it difficult to shape using a simplified template mesh.

Medis Suite, a post-processing software for cardiac MRI, uses Simpson's method to determine the end-diastolic volume (EDV) and end-systolic volume (ESV) of the ventricles (Medis, 2020). Simpson's method is a summation-of-disks method where the acquired short-axis images are stacked and the volume is the sum of the separate disks (Cho Kim et al., 2022). By applying this method, the ventricular volume is calculated as the sum of the contour area multiplied by the slice thickness. Medis Suite also creates 3D geometries of the hearts. However, as shown in Figure 1.1, this is a low-quality and rugged shape.

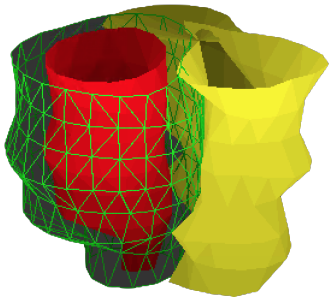

Figure 1.1: 3D geometry Medis Suite
Patient 4

The technique has also shown to provide inaccurate results after comparing the method to different computational techniques. Using Simpson's method with short-axis views leads to an underestimation of the RV volume (Moroseos et al., 2010) and an overestimation of the LV volume(Cho Kim et al., 2022). Incorporating long-axis views into the measurements can improve the accuracy (Cho Kim et al., 2022; Moroseos et al., 2010).

1.4. Objectives

To address the challenges and limitations presented, the objective of this master thesis is three-fold.

First objective

Develop a workflow and create biventricular patient-specific geometric heart models of a young and diverse population, including patients with a complex congenital heart defect using morphing techniques.

Second objective

Propose and compare two methods to correct slice misalignment in MRI scanning.

Third objective

Validate the quality of the data provided by Medis Suite through a ground truth experiment and analyze the post-processing purely based on contours.

2

Materials and Methods

This chapter describes the materials and methods that are used for this project. The methodology is separated into 3 parts, representing the 3 objectives of this thesis. The first part illustrates the sequential steps adopted to build the geometric models. These steps involve the data acquisition, the image processing, the geometry construction, the patient specific model, and the mesh construction.

A detailed manual of the methodology is provided in Appendix C.

Part 1

Objective: Develop a workflow and create biventricular patient-specific geometric heart models of a young and diverse population, including patients with a complex congenital heart defect using morphing techniques.

2.1. Data Acquisition

The first step in developing a computational model is data acquisition. For creating a patient-specific model, imaging data of the target population are essential. Furthermore, high-quality data are preferred in order to create an accurate anatomical reconstruction. With the purpose of gaining accurate data several imaging techniques can be used, including echocardiography, CT and cardiovascular MRI.

Children with CHDs make up a small population with a wide variety of defects. Obtaining good quality imaging data is therefore challenging. When it comes to building a computational model of a child's heart, MRI proved to be the most suitable technique given its advantages listed in Table 1.2. A safe environment is essential for the patient, as well as assessing high spatial resolution and reproducibility for a high quality model. The initial imaging data were obtained from the Erasmus University Medical Center and are from seven patients: two healthy female patients aged 8 and 9 years old, two male patients with tetralogy of Fallot hearts aged 7 and 8 years old, and three male single ventricle patients with a Fontan physiology aged 5, 8 and 19. A list of the patients is shown in a table in the Nomenclature Chapter. The focus is on two types of CHDs. As mentioned, TOF is the most common complex CHD (Nelson et al., 2014). Because of this, there is more imaging data available on this defect. The patients after the Fontan operation are included in this thesis for their unique and complex geometries and to test the boundaries of

the workflow and methodology. By including the data of both healthy and diseased children, one can compare the different patient models and create a workflow which can be applied on a wider range of cases.

The imaging data is presented in Medis Suite, an image analysis software. Typical imaging parameters are: repetition time 3.41-3.75 ms, echo time 1.31-1.62 ms, flip angle 45 deg, and slice thickness 8 mm. Prior to any data processing, all imaging data is anonymized to protect the privacy of the patient.

2.2. Image Processing

After the acquisition of the imaging data, the anatomical model can be developed by image post-processing. During image segmentation, the image is partitioned into multiple segments by drawing contours, according to their function and cardiac modeling applications.

For this thesis project, contours are drawn using a combination of automatic and manual segmentation inside Medis Suite. In both cases, the epicardium and endocardium of the LV and the epicardium of the RV are segmented. The right side of the heart pumps blood to the lungs and the left side to the rest of the body, resulting in a thicker muscle layer in the left ventricle. The endocardium of the RV is not segmented in every case because of this thin muscle layer. This thinner layer in the right ventricle makes it more difficult to segment both the epicardium and the endocardium of the RV. Figure 2.1 shows the segmentation step in Medis Suite. The yellow contour represents the RV, the green contour represents the LV epicardium, and the red contour represents the LV endocardium.

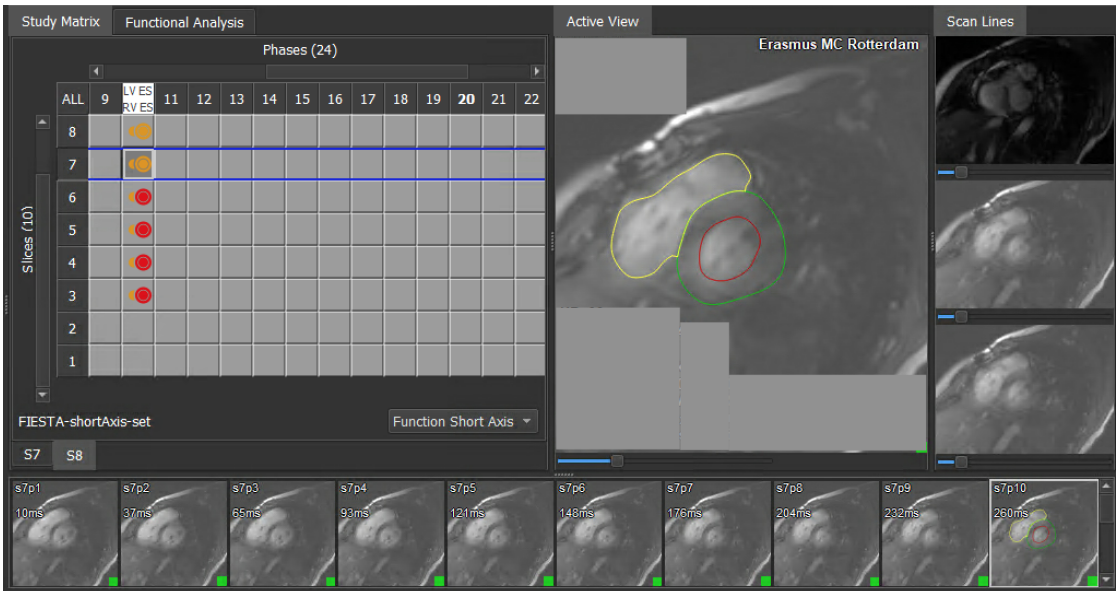

Figure 2.1: Screen capture of Medis Suite.
MRI segmentation: Yellow=RV, Green=LV epicardium and Red=LV endocardium

Segmented data are available for two crucial volumes of the cardiac cycle. The first is the end-diastolic (ED) volume, which is obtained at the end of the ventricular relaxation, when the expansion of the chamber causes a decrease in pressure. The second is the end-systolic (ES) volume, which is obtained at the end of the ventricular contraction. The ES stage of the heart is chosen for this project as the volume of the ventricle is smallest in this stage.

Next, the contours are exported from Medis Suite in .vtp files. Thus, the contours are further processed in ParaView, a visualization platform. Figure 2.2 shows all contours of the endocardium and epicardium of the LV and the epicardium of the RV. Using the tube filter that is available in Paraview, the data is converted into 3D shapes and the different segments of the heart are exported as .stl files.

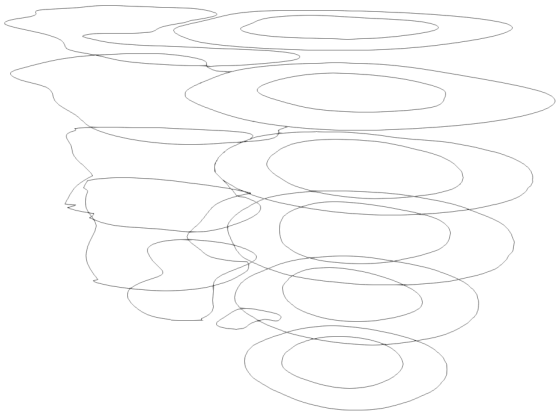

Figure 2.2: LV and RV contours.
Patient 4 as presented in Paraview

2.3. Geometry Construction

The biventricular subdivision surfaces of the Living Human Heart Model (LHHM) serve as the starting point of the geometry construction (Baillargeon et al., 2014). The geometry of this subdivision surface is from The Solid 3D Human Heart from Zygote Media Group Inc (Zygote, 2014). The 3DEXPERIENCE platform from Dassault Systemes is used for the construction of the geometry. This section explains the method of scaling the LHHM to the size and shape of a child's heart. The surfaces in the model are paired. The epicardium of the ventricles is controlled by the left and right ventricular endocardium and must, therefore, be scaled last. The surface of the full LHHM is shown in Figure 2.3.

2.3.1. Scaling

For the models in this project, only the subdivision surfaces of the ventricles of the LHHM are used. The ventricles are sized as a healthy male heart and must, therefore, be scaled down. The subdivisions have a hierarchical structure. The epicardium of the ventricles is controlled by the LV and RV and scales automatically. For the scaling of the right and left ventricular endocardium, a scaling factor is determined based on the size of the reference geometry. The scaling is performed by selecting all nodes of the subdivision. Using the "Affinity" tool, the three-dimensional volume can be adjusted based on the determined scaling factor. After manually scaling the left and right endocardium, the epicardium can be updated to scale automatically. In complex CHDs, such as HLHS, updating the epicardium can result in twisted and relocated nodes. The twisted surface can be corrected manually using the techniques that are explained in the manual morphing section below.

Figure 2.3: LHHM

2.4. Patient-Specific Model

This section describes the steps for morphing the scaled model into the patient-specific model. The goal is to morph the model as closely as possible to the imported reference geometry. This section is subdivided into a number of subsections, covering importing and aligning the reference geometry, adjusting the model parameters, and manual morphing of the model. The "Digitized Shape Preparation" application of CATIA is used for this step of the methodology.

2.4.1. Import and align reference geometry

The "Digitized Shape Preparation" application of CATIA is used to import and align the reference geometry. Patient data can be imported into the model by first creating a new geometric set and importing the .stl file in this set. Next, the reference geometry is manually aligned with the model using the robot tool. Additional .stl files can be aligned directly using the "Axis to Axis" tool. When the reference geometry is completely aligned, the model is ready to be (manually) morphed.

2.4.2. Parameter morphing

Before manual morphing of the model, parameter morphing can be used. This is a quick way to make modifications to the model. Examples of relevant parameters to which adjustments can be made are: "Top LV Diameter"; "Mid LV diameter"; "Apex LV diameter"; and "Long Axis Length". The parameter changes are performed on the endocardium. The epicardium must, therefore, be updated after changing the parameters. The ruler can be used to measure the differences in size between the model and the reference geometry and to find the increase or decrease required to fit the reference geometry for a specific parameter.

2.4.3. Manual morphing

Manual morphing is used to make local surface modifications to the model. Both individual and groups of nodes and lines can be rotated and translated in different ways to morph the surface into the desired shape. There are various different selection functions and surface modification tools available in the "Generative Shape Design" application in CATIA. Again, the model can only be changed in a way that is consistent with the hierarchy. Figures 2.4a and 2.4b show the manual morphing steps of the endocardium of the left ventricle. Figure 2.4a shows the scaled LV

endocardium with the aligned corresponding contours prior to manual morphing. Figure 2.4b shows the same ventricle after manual morphing.

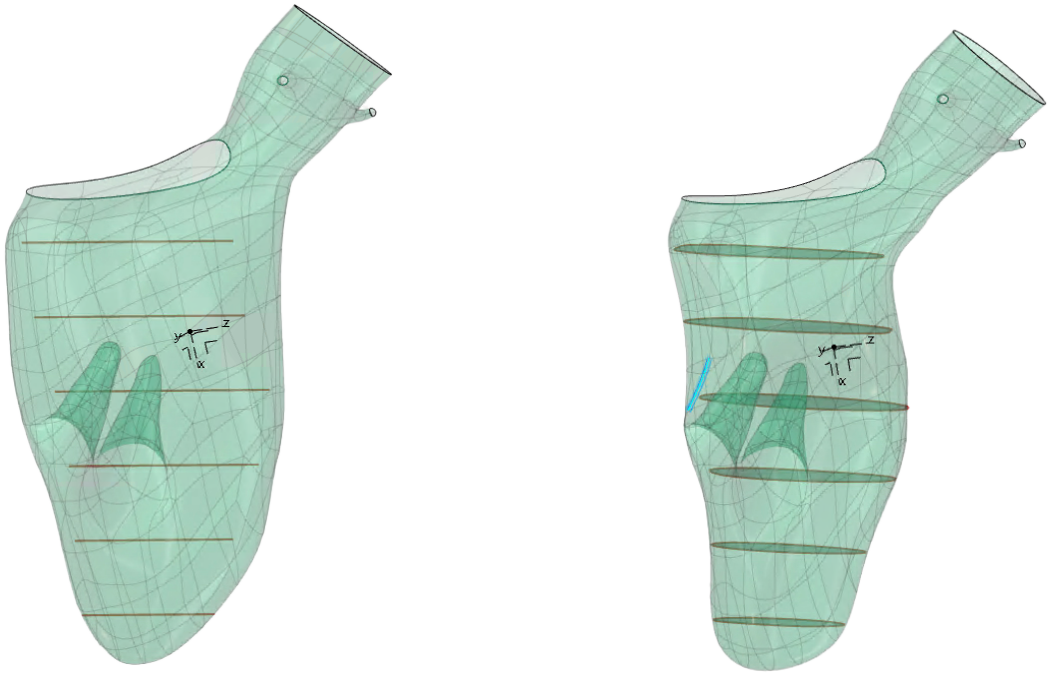

(a) Before **(b)** After

Figure 2.4: LV endocardium.
Comparison before and after morphing for Patient 3.

The endocardium of the left and right ventricle is morphed in a similar fashion. Next, the epicardium is updated to adjust automatically to large changes. After this, the epicardium is manually morphed to fit the contours of the reference geometry as closely as possible. Lastly, intersecting surfaces will lead to errors while creating the mesh. Thus, the model should be checked for interference, which can be done manually or using the interference check in CATIA.

2.5. Mesh

The last step for creating the patient-specific model is the construction of the mesh. A mesh describes the shape of the model using vertices, edges and faces. The faces can be triangles or quadrilaterals.

Inside the "Generative Shape Design" application of CATIA, the "Fill" tool is used to fill the openings in the subdivision surfaces. For the LV, these openings are the mitral valve (MV), the aortic arch (AA), the left coronary artery (LCA) and the right coronary artery (RCA). For the RV, these openings are the tricuspid valve (TV) and the pulmonary trunk (PT). A cavity volume surface is made consisting of the endocardium and its corresponding fill surface. Next, a closed surface of the integrated ventricles is made consisting of the left and right endocardium, the epicardium and fill surfaces between the epicardium and endocardium for all openings. The surface of the integrated ventricles is the basis of the mechanical surface mesh, which has a mesh size of 3 mm with an absolute sag of 0.2 mm. Using the surface mesh as the support, a

tetrahedron mechanical volume mesh is created with a size progression of 1 and a quadratic element type. In this project, a triangular mesh is used and these last steps are performed inside the "Structural Model Creation" application of SIMULIA. The thickness of the mesh is intended to be 3-5 elements thick and the size of the elements can be adjusted to achieve this, which is important when performing a stress and strain analysis on the model. Based on the mesh quality report, the subdivision surfaces can be adjusted to remove bad or poor elements. This is done to avoid failed simulations. The quality of the mesh can be determined based on a number of measures:

- **The aspect ratio:** The ratio of the longest edge length to the shortest edge length (Webster, 2021).
$$Q_{aspect} = \frac{Max(l_1, l_2, ..l_n)}{Min(l_1, l_2, ..l_n)}$$
- **The maximum angle**
- **The minimum angle**
- **The skewness:** The deviation from the ideal shape of the cell (Ansys, 2008).
$$Q_{skewness} = \frac{V_{ideal} - V_{cell}}{V_{ideal}}$$
- **The stretch:** The ratio of the change in size from one cell to the next (Ansys, 2008).
$$Q_{stretch} = k \times \frac{R}{L_{max}}$$

2.6. Validation

The created geometric models can be validated using different methods of analysis. These analyses are divided into global validation and local validation. Global validation is used to analyze the full geometric model in comparison to the Medis Suite measurements and includes ventricular volume and mass. Local validation is used to analyze the correlation between the original data and the models locally, using the individual MRI slices.

2.6.1. Global validation

There are different analysis methods that can be used for global validation. In a ventricular volume analysis, the blood volume of the ventricles of the geometric models can be compared to the Medis Suite measurements. The closed surfaces of the endocardium, which are created in the previous section, are used for this analysis. For a ventricular mass analysis, the closed surface of the integrated ventricles is used. The volume of this closed surface is multiplied by the density of the ventricular wall (1.05 g/ml) to obtain the mass (Buechel et al., 2009; Luijnenburg et al., 2010).

The relative error (RE) can be calculated by dividing the absolute error over the expected value (Medis Suite measurements) as shown in the formula:

$$RE(X, Y) = \frac{|V_x - V_y|}{V_y}$$

Lastly, a deviation analysis can be performed inside CATIA to determine the local thickness between the epicardium and the endocardium, otherwise known as the wall thickness. The analysis carries out local calculations, but the results can be evaluated globally.

2.6.2. Local validation

A method of local validation of the model geometry is by use of the Dice similarity coefficient (DSC). This method examines the statistical overlap between two sets of the same geometry (Zou et al., 2004). The coefficient is often used to evaluate the performance of manual segmentation with automatic segmentation. However, this validation method will be applied to evaluate the reliability of the morphed geometries. The segmented MRI data is compared to the created models. This is done by looking at transverse cross-sections at the same height as the MRI slices. The formula for the DSC is :

$$DSC(X,Y) = \frac{2 * |X \bigcap Y|}{|X| + |Y|}$$

In the formula, X and Y are two sets. It divides the intersection of the two sets by the number of elements in each set (Zou et al., 2004). The coefficient measures the similarity between two sets, X and Y. The values of the coefficient range between 0 and 1. No spatial overlap is equal to a DSC value of 0.0 and complete overlap has a DSC value equal to 1.0 (Zou et al., 2004). Labels are assigned to the ground truth, the segmented MRI data, representing the left and right ventricular volume and the ventricular myocardium. The same is done for the prediction, the model geometry. Examples of labels for the ground truth and prediction are shown in Figures 2.5a and 2.5b. The values for the DSC are then found using Python.

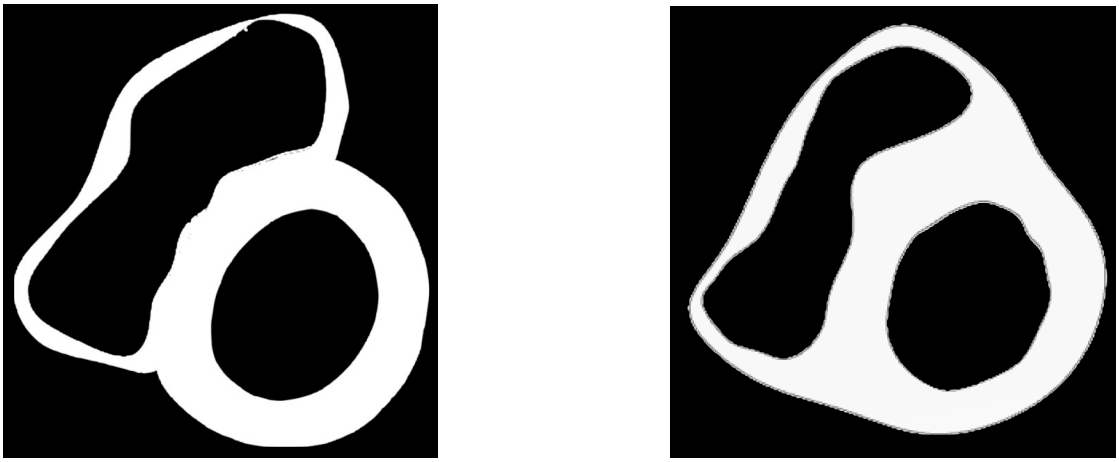

(a) Ground Truth **(b)** Prediction

Figure 2.5: Dice similarity coefficient labels.
Comparison of the ground truth and prediction short-axis cross-section labels from Patient 4.

Part 2

Objective: Propose and compare two methods to correct slice misalignment in MRI scanning.

2.7. Slice Misalignment Correction

During MRI imaging, the patient is asked to stay still and hold their breath. When there is movement, there will be an inaccurate registration of MRI images. This slice misalignment, or slice shift, is shown in Figure 2.6a. The figure shows the contours of the LV of Patient 2. The bottom slices seem misaligned with the top slices.

Slice misalignment is corrected using two different methods. The focus of the correction is on the left ventricle, which has more anatomical reference points compared to the right ventricle. A detailed step-by-step description is provided in the final section of Appendix C.

The first correction method is the alignment of the contours using the papillary muscle. The center of gravity is found for all contours of the papillary muscle in the LV. Next, a line is drawn through two points which are not associated with the slice misalignment. The rest of the center-of-gravity points, with their corresponding contours, are then translated onto the line. This method is shown in Figure 2.6b, where the center points of the papillary muscle are correctly aligned.

The second correction method is the alignment of the contours of the epicardium. For this correction, the center of gravity is found for all contours of the epicardium of the LV. Again, a line is drawn through two center points not associated with the misalignment. The rest of the contours are translated onto the line using their center-of-gravity point. This method is shown in Figure 2.6c, where the slices and the center points of the epicardium contours are correctly aligned.

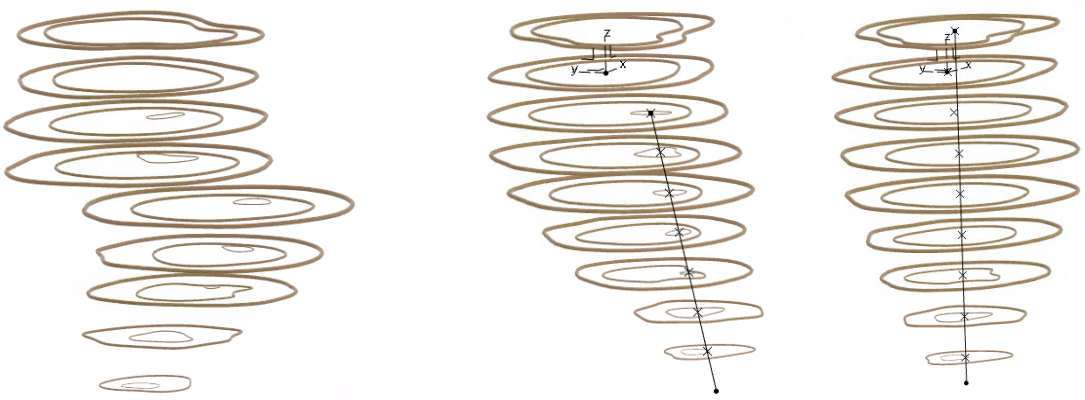

(a) Original contours **(b)** Align through papillary muscle **(c)** Align through epicardium

Figure 2.6: Slice misalignment method comparison.
Correction methods in LV of Patient 2. Comparison of the original data with two correction methods using the center-of-gravity points

2.7.1. Validation

Global validation Similar to Part 1, global validation can be performed using a ventricular volume analysis and a ventricular mass analysis. This part, on slice misalignment, uses a single ventricle model. That means that the closed surfaces for blood volume and the integrated ventricle are also of the single ventricle.

Local validation Two different methods of local validation are explained in this section. The first method is calculation of the DSC, as described in the local validation of Part 1. However, in this case, not the short-axis view is evaluated, but the long-axis view. Slices of the long-axis 2-chamber view and long-axis 4-chamber view are obtained and segmented. The contours of this segmentation serve as the ground-truth and are compared to the cross-sections of the three slice misalignment models. Figure 2.7 shows an overlay of the corrected model using alignment with the epicardium and the long-axis 4-chamber contours of Patient 2. Labels are created from these views and the DSC can be calculated. The same thing is done using the long-axis 2-chamber contours of Patient 2.

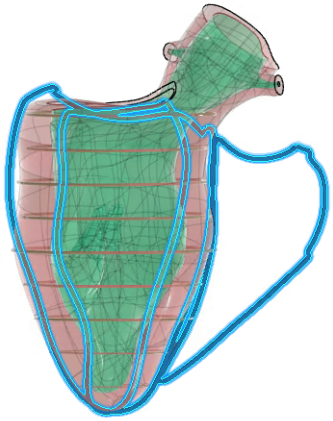

Figure 2.7: LV model with overlay of the long-axis contours
Corrected slice misalignment model with alignment through the epicardium and the long-axis 4-chamber contours of Patient 2

The second method of local validation of the misalignment correction is by comparison to a ground truth. In this case, the ground truth is a different patient, Patient 3. This validation compares the magnitude of the in-plane slice misalignment, or the inter-acquisition variation (Swingen et al., 2003). This method plane is demonstrated in Figure 2.8. A mean vector through the center points of all slices can be computed. Next, the distance to this mean vector for the individual center-of-gravity points can be determined. Using this method, the results for Patient 2 and Patient 3 can be compared and evaluated.

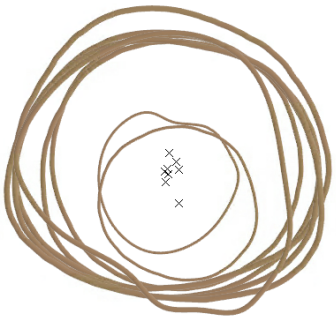

Figure 2.8: In-plane slice misalignment calculation of the LV.
Showing the contours of the epicardium with their corresponding center-of-gravity points.

Part 3

Objective: Validate the quality of the data provided by Medis Suite through a ground truth experiment and analyze the post-processing purely based on contours.

2.8. Ground Truth Experiment

In this last part, the cavity volume results provided by Medis Suite, a commercially available analysis software, are compared to a ground truth geometry. Medis suite computes the volumes of the left and right ventricular cavity using the Simpson's method (Medis, 2020). This is a method of disk summation. The ventricle is considered a sum of disks, where the cross-sectional area is multiplied by the slice thickness (Cho Kim et al., 2022).

The ground truth geometry is created by making a stacked geometry of disks directly from the contours. This is done to simulate the Simpson's method. A disk is made by forming a spline curve around a contour. The "Multi-Sections Surface" tool, inside the "Generative Shape Design" application in CATIA, is used to make a surface between the contours. The "Fill" tool is used to make a surface inside the contour. Next, two fill surfaces are joined with the multi-sections surface to create a volume. This is repeated until all disks are created and closed surfaces are formed. The volume of the ground truth geometry is calculated as the sum of the individual disks (Luijnenburg et al., 2010). Figure 2.9 shows the geometry of Patient 4 created inside Medis Suite. Figure 2.10a shows the ground truth geometry of the stacked disks of the LV of Patient 4, created in CATIA. Figure 2.10b shows this geometry of the RV of Patient 4.

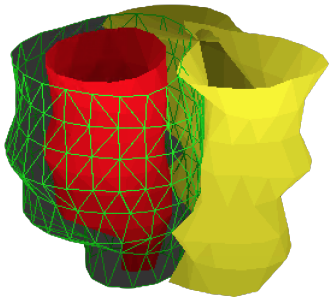

Figure 2.9: 3D geometry Medis Suite Patient 4

2.8.1. Global validation

Similar to Part 1 and 2, global validation can be performed using a ventricular volume analysis. The ground truth geometries are of the left and right ventricular cavities. The relative error can be calculated between the Medis Suite ESV and the ground truth geometry.

In addition to ventricular volume analysis, an inter-observer variability can be used for global validation. The inter-observer variability is a quantification method of feasibility used in literature and can be measured using the method of Bland–Altman (Bland & Altman, 2010). In this method, the coefficient of variability is expressed as a percentage of the standard deviation of the difference divided by the mean of the two measurements (Luijnenburg et al., 2010).

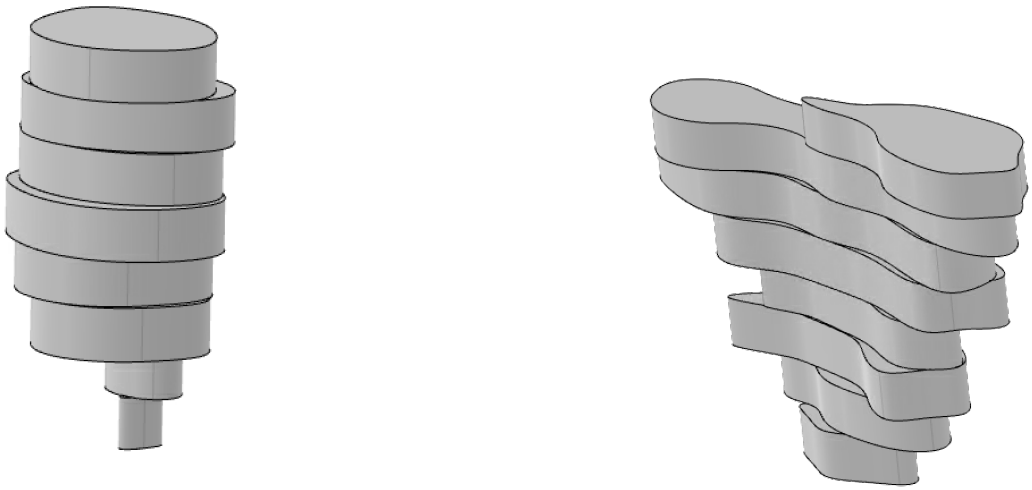

(a) Left ventricle **(b)** Right ventricle

Figure 2.10: Ground truth geometry.
Stacked disk geometries of left and right ventricle from Patient 4.

2.8.2. Local validation

Again, the Dice similarity coefficient can be computed for local validation. This time, the coefficient compares the segmented MRI data to the ground truth geometry, or the individual disks.

3

Results

This chapter illustrates the results obtained in this project. The first part shows the outcomes derived from the patient-specific biventricular geometries developed for the healthy children and for the patients with a CHD. Here, the results of the global validation in the form of the ventricular volume analysis and the ventricular mass analysis are shown together with the deviation analysis. The Dice similarity coefficient is presented for the local validation. Lastly, the mesh results are provided.

For part 2, the results of the two different correction methods are compared against the original data based on both volume and mass in the global validation section. A qualitative and quantitative approach is herein adopted. Next, local validation results of the correction method are validated against a ground truth geometry.

To conclude this chapter, the third part illustrates the global validation results, with the ventricular volume analysis and the inter-observer variability. The final section shows the local validation. Here, the DSC is calculated for the comparison between the ground truth geometry and the segmented MRI data.

Complete results with figures of all patients are provided in Appendix B. Full results can also be found here: https://gitlab.tudelft.nl. It includes all images, 3D models and model files.

Part 1

3.1. Geometry Results

A patient-specific biventricular geometric model is created using manual morphing for 7 different hearts. The results of the geometric models are shown in Figure 3.1. For all patients, the epicardium is represented in red, the LV endocardium in green and the RV endocardium in blue.

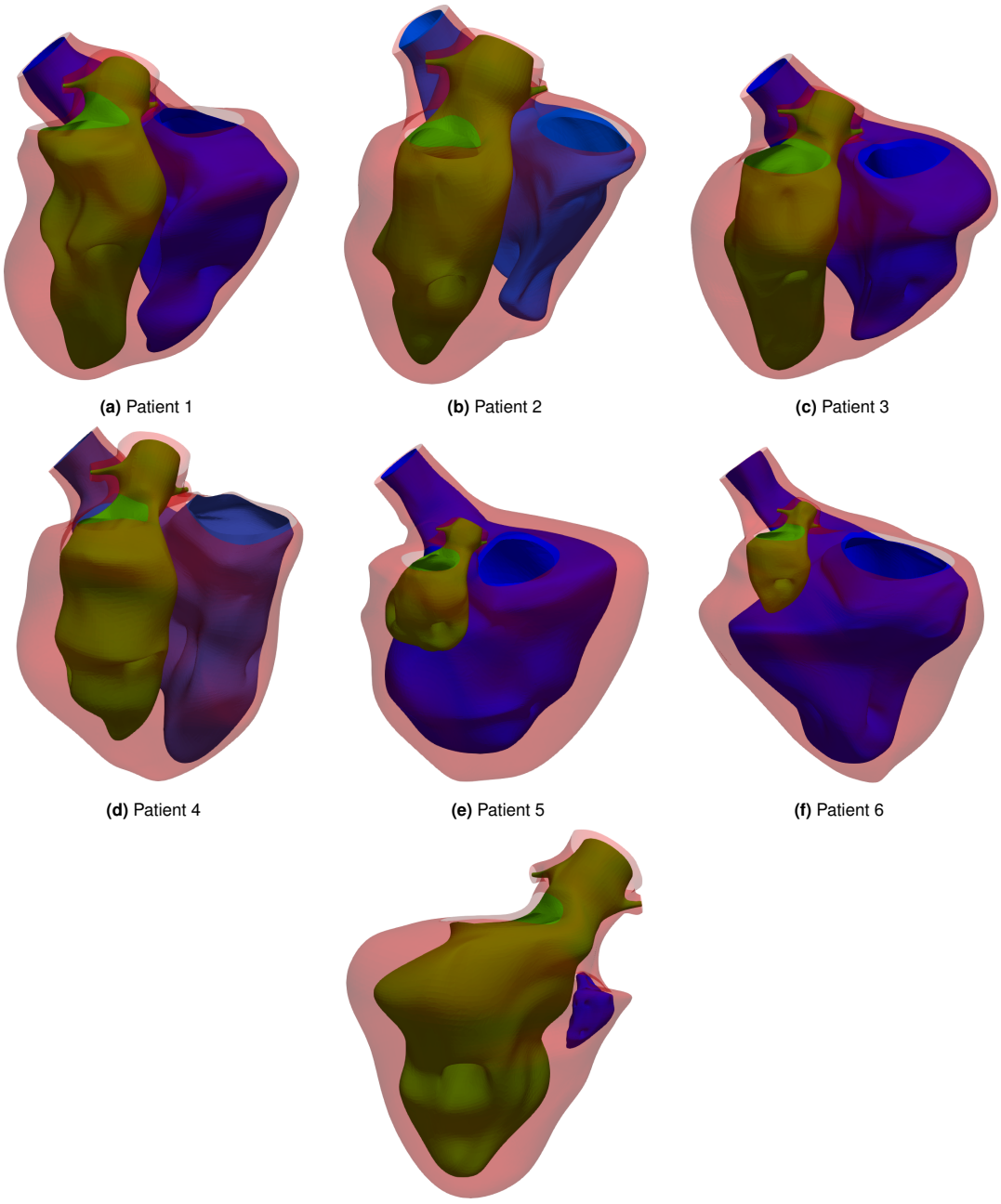

(a) Patient 1 **(b)** Patient 2 **(c)** Patient 3

(d) Patient 4 **(e)** Patient 5 **(f)** Patient 6

(g) Patient 7

Figure 3.1: Biventricular manual morphing results.
Red=epicardium, Green=LV endocardium, Blue=RV endocardium

3.1.1. Mesh

Figure 3.2a shows the complete mesh and Figure 3.2b a cross-section view of this mesh of Patient 2, a healthy 9-year-old female. Similarly, the complete mesh and a cross-section of this mesh of Patient 3, a 7-year-old male with TOF, is presented in Figure 3.3a and Figure 3.3b, respectively.

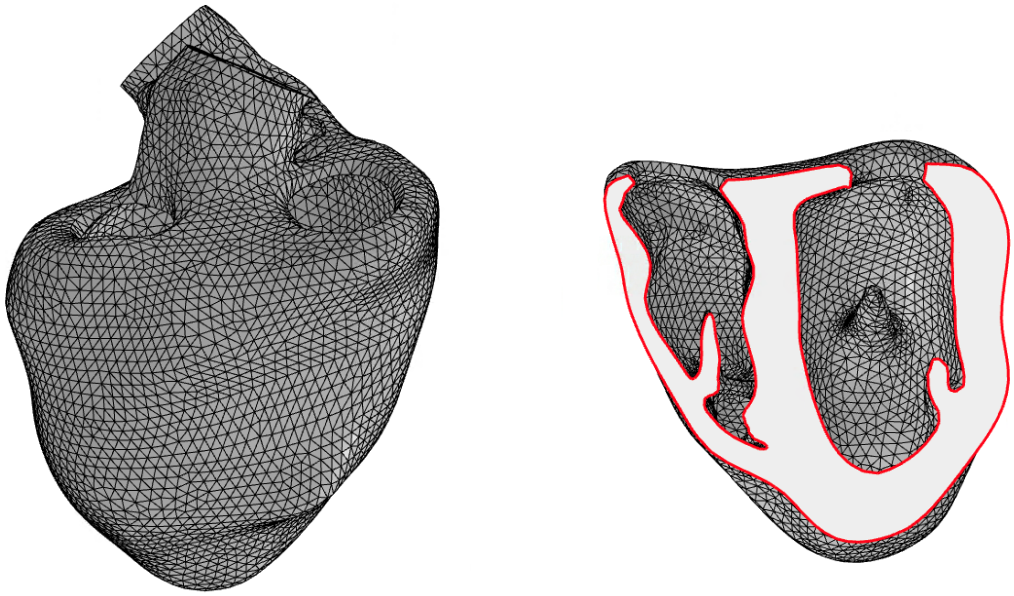

(a) Complete mesh **(b)** Cross-section mesh

Figure 3.2: Patient 2 mesh
Biventricular geometry mesh with cross-section of mesh

Mesh quality The results of the mesh quality reports are presented in this section. The quality of the mesh is determined based on quantitative values described in the previous chapter. These values are: the aspect ratio, the maximum angle, the minimum angle, the skewness, and the stretch. The average values of these measures are presented in Table 3.1. For each indicator, a range of values can be determined to qualify the mesh as good, poor or bad. The mesh generates a warning with poor elements and an error with bad elements. An element is considered poor with an aspect ratio above 5, a maximum angle above 160 deg, a minimum angle below 10 deg, a skewness below 0.25 and a stretch below 0.3. (Ansys, 2008; Smith, 2009; Webster, 2021).

None of the meshes contain bad elements. The average number of poor elements for all meshes is 25 elements. The highest ratio of poor elements is for Patient 7, a 19-year-old male with a Fontan physiology. This mesh has 40 bad elements, corresponding to 0.093 % of all elements. The mesh of Patient 4, an 8-year-old male with TOF, has the lowest number of bad elements. This mesh has 10 bad elements, which corresponds to 0.017 % of all elements.

3.1.2. Deviation analysis

In the ventricular model, deviation analysis can be used to determine local thickness by extracting sections of the epicardium and endocardium. Table 3.2 shows the results of the deviation analysis

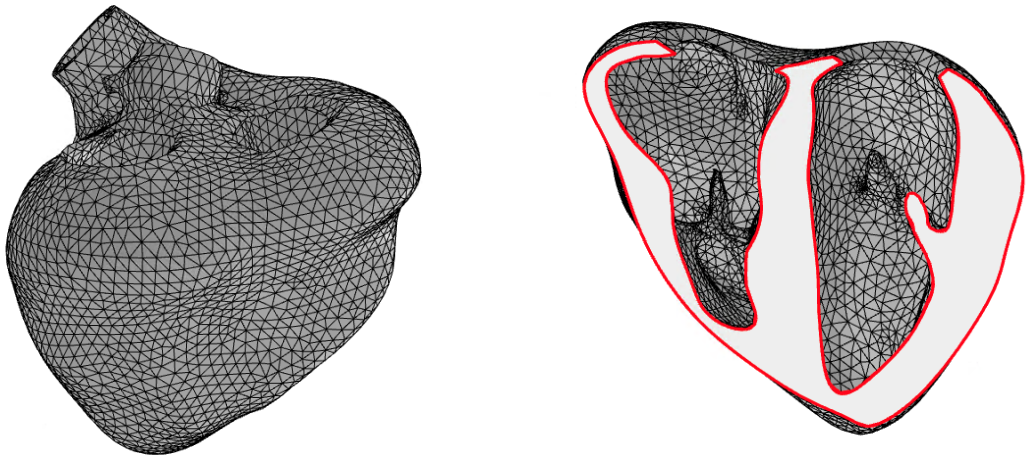

(a) Complete mesh **(b)** Cross-section mesh

Figure 3.3: Patient 3 mesh
Biventricular geometry mesh with cross-section of mesh

Table 3.1: Mesh quality results

	No. elements	Aspect ratio	Max angle	Min angle	Skewness	Stretch
Patient 1	61,178	1.561	96.079 deg	49.387 deg	0.732	0.732
Patient 2	46,890	1.604	96.549 deg	48.602 deg	0.713	0.721
Patient 3	44,886	1.583	96.225 deg	48.917 deg	0.724	0.727
Patient 4	57,997	1.571	95.950 deg	49.140 deg	0.730	0.731
Patient 5	32,836	1.590	96.605 deg	48.711 deg	0.718	0.723
Patient 6	44,807	1.538	95.731 deg	49.722 deg	0.745	0.739
Patient 7	42,813	1.561	96.140 deg	49.362 deg	0.735	0.732

for all models. The mean deviation between the epicardium and endocardium is determined together with the maximum deviation and standard deviation. Figures 3.5 and 3.6 show visuals of the deviation analysis of Patient 3, a 7-year-old male with TOF, and Patient 5, a 5-year-old male with a Fontan physiology, respectively. The figures show the biventricular geometric model with the epicardium covered by a color map representing the deviation transitions. The pink histogram displays the amount of points in each bin.

For a complete overview of all patients, see Appendix B.

3.1.3. Global validation

Ventricular volume analysis The following results show the ventricular volume analysis. For the ventricular models, this is calculated by creating a closed volume of the endocardium. The blood volume of the ventricles of all patients is compared to the measurements provided by Medis Suite and is shown in the following tables: Table 3.3 shows the results for the left ventricle volume analysis and Table 3.4 shows the results for the right ventricle volume analysis. For both tables, the Medis results are shown next to the ventricular model results. The last column shows

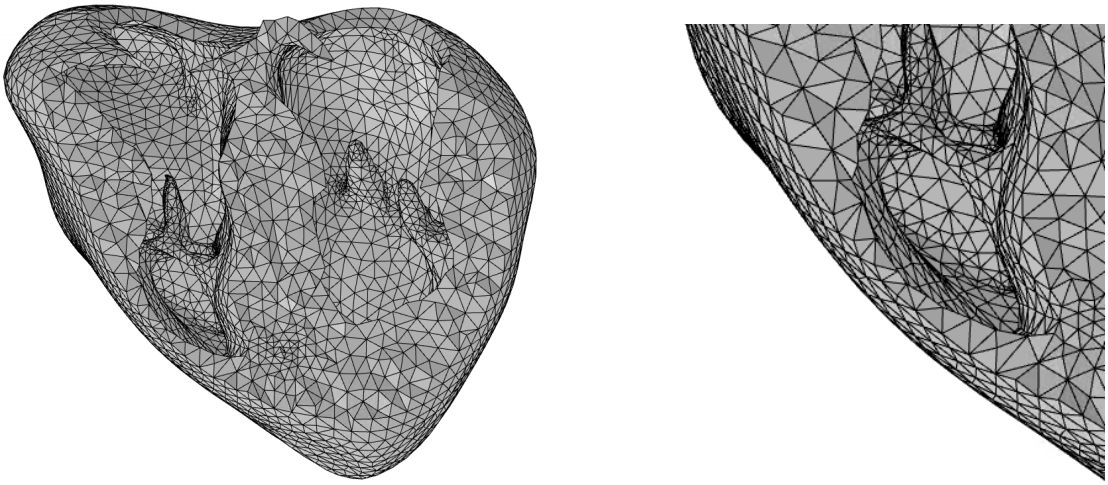

(a) Cross-section exact cut **(b)** Enlarged view cross-section exact cut

Figure 3.4: Patient 3 exact-cut mesh
Biventricular geometry mesh with exact-cut cross-section of mesh and enlarged view

Table 3.2: Results deviation analysis

	Mean Deviation	Maximum Deviation	Standard Deviation
Patient 1	4.81 mm	18.5 mm	3.21 mm
Patient 2	4.48 mm	14.3 mm	2.88 mm
Patient 3	4.07 mm	13.7 mm	3.02 mm
Patient 4	4.50 mm	14.5 mm	2.74 mm
Patient 5	4.06 mm	11.8 mm	2.53 mm
Patient 6	5.07 mm	14.7 mm	5.07 mm
Patient 7	4.87 mm	13.2 mm	3.08 mm

the relative error between the two measurements.

Ventricular mass analysis Table 3.5 shows the result of the ventricular mass analysis. For the geometric models, this is calculated by creating a closed volume between the endocardium of the two ventricles and the epicardium. The mass is obtained by multiplying the myocardial density of the ventricular wall (1.05 g/ml (Buechel et al., 2009)) and the volume of the ventricular wall. The table compares the results from Medis Suite to the created geometric models for every patient in the population. Again, the last column shows the relative error between the two measurements.

3.1.4. Local validation

This section provides the results of the local validation using the Dice similarity coefficient for the models of Patient 2, a healthy patient, Patient 4, a TOF patient, and Patient 7, a Fontan patient. Table 3.6 provides a summary of the results, which are fully illustrated in Appendix B. The outcomes of the statistical analysis are reported for all the slices by including the mean DSC and the standard deviation. This is done for the three labels of the heart models, which are presented by the three columns in the table.

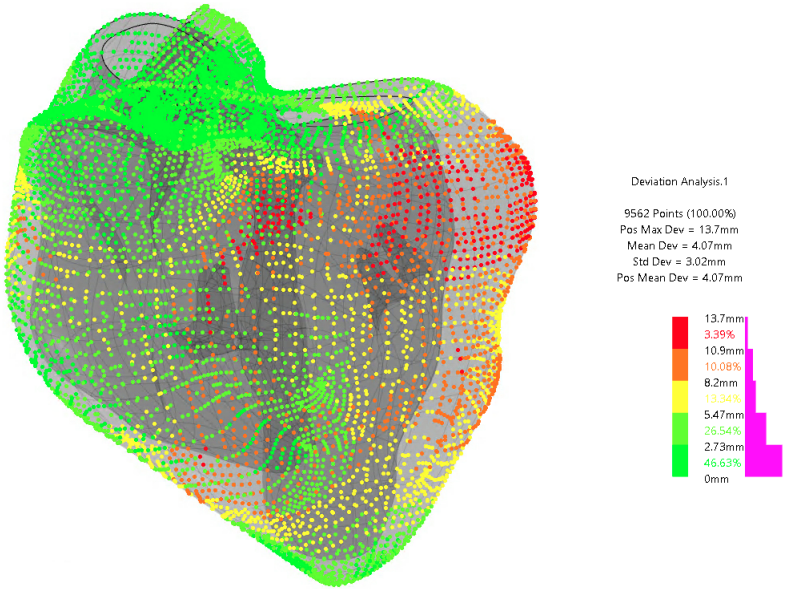

Figure 3.5: Results deviation analysis of Patient 3
LV covered by a color map showing the thickness of the ventricular wall.

Table 3.3: Results LV volume analysis

	Medis LV ESV	Model LV ESV	RE
Patient 1	37.90 ml	43.83 ml	0.16
Patient 2	30.19 ml	35.83 ml	0.19
Patient 3	26.44 ml	28.81 ml	0.090
Patient 4	33.87 ml	39.27 ml	0.16
Patient 5	26.85 ml	5.60 ml	0.79
Patient 6	*no data*	2.85 ml	*n/a*
Patient 7	76.80 ml	90.33 ml	0.18

Table 3.4: Results RV volume analysis

	Medis RV ESV	Model RV ESV	RE
Patient 1	46.91 ml	61.26 ml	0.31
Patient 2	34.43 ml	26.85 ml	0.22
Patient 3	48.21 ml	39.86 ml	0.17
Patient 4	54.83 ml	54.80 ml	0.00036
Patient 5	40.29 ml	60.33 ml	0.50
Patient 6	63.67 ml	83.88 ml	0.32
Patient 7	1.54 ml	1.753 ml	0.14

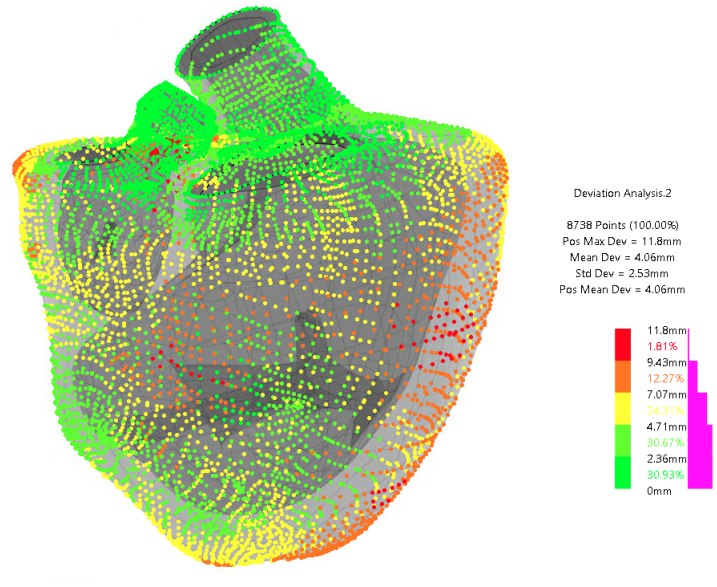

Figure 3.6: Results deviation analysis of Patient 5
LV covered by a color map showing the thickness of the ventricular wall.

Table 3.5: Results ventricular mass analysis

	Medis LV mass	**Medis RV mass**	**Medis total mass**	**Model ventricular mass**	**RE**
Patient 1	70.74 g	28.87 g	99.61 g	131.15 g	0.32
Patient 2	45.08 g	22.23 g	67.31 g	87.78 g	0.30
Patient 3	47.13 g	27.40 g	74.53 g	94.51 g	0.27
Patient 4	56.89 g	26.85 g	83.74 g	122.43 g	0.46
Patient 5	46.81 g	14.58 g	61.39 g	69.13 g	0.13
Patient 6	*no data*	78.69 g	78.69 g	110.04 g	0.40
Patient 7	74.26 g	8.25 g	82.51 g	102.53 g	0.24

Table 3.6: Dice similarity coefficient results summary. Mean $\pm$ SD

	LV Blood volume	**RV Blood Volume**	**Myocardium**
Patient 2	0.937 ± 0.040	0.861 ± 0.066	0.750 ± 0.073
Patient 4	0.968 ± 0.018	0.818 ± 0.113	0.711 ± 0.138
Patient 7	0.939 ± 0.032	0.935	0.830 ± 0.037

Part 2

3.2. Misalignment Correction

This section gives the results of the slice misalignment correction that was performed for Patient 2, a healthy 9-year-old female. The results are presented in both a qualitative and quantitative manner.

3.2.1. Global validation

The qualitative results are obtained by morphing the geometry of the three situations. Figure 3.7a shows the morphed geometry of the left ventricle with the original data without a correction and Figure 3.7b illustrates the morphed geometry after an alignment correction using the papillary muscle. Figure 3.7c shows the morphed geometry after an alignment correction using the epicardium of the left ventricle.

Blood volume and ventricular mass of the left ventricle in Patient 2 are herein used to qualitatively compare the original and the adjusted geometries, as reported in Table 3.7. In addition, Table 3.7 includes these same measurements provided by Medis Suite.

Table 3.7: Results global validation of misalignment correction Patient 2

	Blood volume	**Ventricular mass**
Medis measurements	30.19 ml	45.08 g
Before correction	41.14 ml	59.49 g
Papillary correction	39.71 ml	54.35 g
Epicardium correction	37.61 ml	56.79 g

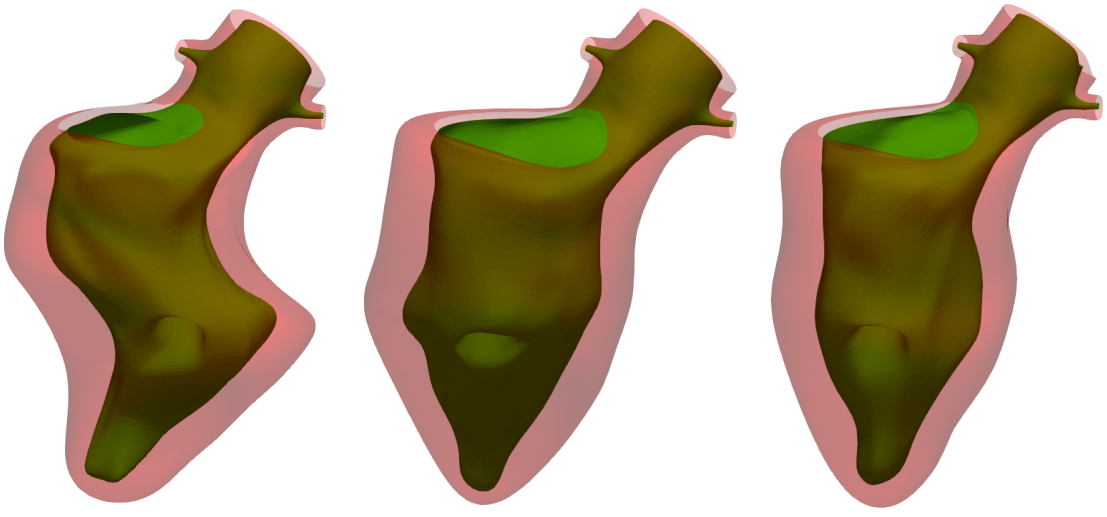

(a) Before correction **(b)** Correction using papillary muscle **(c)** Correction using epicardium

Figure 3.7: Slice misalignment correction comparison.
Morphed geometries of the LV of Patient 2.

3.2.2. Local validation

The results of the first method of local validation, the calculation of the Dice similarity coefficient using the 4-chamber and 2-chamber long-axis slices, are in Table 3.8. The first two columns are the results using the 4-chamber long-axis slices as the ground truth. The results show the calculated DSC for the LV cavity and the myocardium of the two correction methods and the model before correction. The DSC is 0.747 before correction in the 4-chamber view of LV cavity. Notably, the correction based on the papillary muscle improved the Dice score to 0.916, and the correction based on the epicardium improved the score to 0.877. The DSC of the LV cavity using the 2-chamber long-axis view are in the last column. Before correction, the DSC is 0.895 and after correction the scores are 0.948 and 0.895 for the papillary muscle and epicardium correction models, respectively.

Table 3.8: Dice similarity coefficient results of misalignment correction using long-axis views.

	4-chamber LV cavity	**Myocardium**	**2-chamber LV**
Before correction	0.747	0.531	0.895
Papillary correction	0.916	0.656	0.948
Epicardium correction	0.877	0.567	0.895

The results of the inter-acquisition variation, the second method of local validation, are shown in Table 3.9. In this validation, the ground truth is Patient 3, a 7-year-old male with TOF. The table shows the average distance between the center-of-gravity points of the contours to the mean vector of all contours of the left ventricular epicardium. For Patient 2 this distance is 5.94 ± 5.21 mm and for Patient 3 it is 2.89 ± 1.42 mm.

Table 3.9: Results local validation of misalignment correction Patient 2

	Average to the mean	**Standard deviation**
Patient 2	5.94 mm	5.21 mm
Patient 3	2.89 mm	1.42 mm

Part 3

3.3. Ground Truth Exercise

The results of the ground truth exercise are presented in this section. A geometry of stacked disks, representing the ground truth, is validated against the data presented in Medis Suite.

3.3.1. Global validation

This section illustrates the outcomes of the global validation of the left and right ventricular blood volume. For completeness, the exercise on the LV is done for three patients: a healthy patient, a patient with TOF and a patient with a Fontan physiology. These results are shown in Table 3.10. For the RV, both healthy patients are included. These results are shown in Table 3.11. In both tables, the second column provides the blood volume given by Medis Suite for each patient. The third column provides the total volume of the stacked geometry after summation of the individual disks. The last column gives the relative error between the ground truth and the stacked geometry.

Table 3.10: Results global validation of ground truth exercise LV ESV

	Medis Suite data	Ground truth geometry	RE
Patient 2	30.19 ml	30.14 ml	0.0017
Patient 4	33.87 ml	34.09 ml	0.0064
Patient 7	76.80 ml	76.17 ml	0.0082

Table 3.11: Results global validation of ground truth exercise RV ESV

	Medis Suite data	Ground truth geometry	RE
Patient 1	46.91 ml	46.15 ml	0.0163
Patient 2	34.43 ml	35.03 ml	0.0173
Patient 3	48.21 ml	49.03 ml	0.0170
Patient 4	54.83 ml	54.61 ml	0.0041

Variability The results of the inter-observer variability are listed here:

- For the LV ESV, this variability is 0.64%.
- For the RV ESV, this variability is 0.58%.

3.3.2. Local validation

To locally validate the model and to assess the similarity between the segmented MRI data and the ground truth geometry of the stacked disks, the DSC is computed for the LV and RV data of Patient 2 and 4. These values can be used regardless of a slice misalignment in Patient 2, since the disks are independent of one another. Table 3.12 gives the DSC mean $\pm$ standard deviation for both the left and right ventricular cavity. The lowest DSC calculated is 0.960 ± 0.008 for the RV cavity of Patient 2.

Table 3.12: Results Dice similarity coefficient for the ground truth geometry. Mean $\pm$ SD

	LV cavity	RV cavity
Patient 2	0.983 ± 0.006	0.960 ± 0.008
Patient 4	0.983 ± 0.013	0.975 ± 0.005

4

Discussion

A systematic overview of Chapter 3 is herein presented. Also, an analysis of the limitations of the work is provided and some recommendations for future projects are discussed.

4.1. Results

The results of the different parts are explained and the data are interpreted. Also, the importance of the results are evaluated together with how they relate to the original aims. Additionally, unexpected results are examined.

Part 1

4.1.1. Geometric model

The first purpose of this work consists of developing and executing a workflow for the creation of patient-specific geometric biventricular models of healthy children and patients with a CHD. The results show a set of seven geometric models, one for each patient. Patient 1 and 2 are healthy patients; Patients 3 and 4 are patient with TOF; Patients 5, 6 and 7 are patients with a Fontan physiology. The left ventricle is represented by green, the right ventricle by blue, and the epicardium by red. The models show a smooth surface and clearly distinguishable left and right ventricles. Patients 1-4 show biventricular models. Patients 5-7 show single ventricle hearts, however the small, non-functioning ventricle is still visible in a limited number of slices of the MRI data. For Patient 7, there is one MRI slice in which the RV endocardium is visible. This results in a very small, but still existing, ventricle.

For each patient, a mesh with a triangular surface is successfully created. In more details, quadratic elements are used and a refinement process is performed based on the mesh quality report inside SIMULIA. None of the meshes presented in the results show any bad elements and the percentage of poor elements is very low, 0.093% in the worst case mesh for Patient 7. Furthermore, all average values for the measures in the mesh quality results are within the range of what is considered a good mesh. Also, a high number of elements is adopted, with values ranging from 32,836 to 61,178 elements. The finer the mesh, the better the quality of the mesh and the more accurate the results from the mesh. However, a higher number of elements also increases the computational time. For optimal results, a mesh convergence study would be conducted. This type of study is discussed later in this chapter. Other improvements can include

a better distribution of fine and coarse meshing based on the geometric necessity.

To perform a stress analysis across the ventricular wall, 3-5 elements are required across the wall thicknesses of the mesh. The mean deviation ranges from 4 - 5 mm. This means that, on average, there are at least 2 elements across the ventricular wall. The results from the deviation analysis show that much of the thickness from the lower range concentrates around the ventricular outflow tracks, as demonstrated by the abundance of green around this area. This means that the mean deviation around the ventricular wall could be slightly higher. The mesh with the exact cut cross-section (Figure 3.4a) displays the individual elements across the ventricular wall. For most of the models, there are more than 5 elements across the thickness of the wall. However, the enlarged view (Figure 3.4b) shows that on the thinnest part of the geometric model, around the RV, the wall thickness is only one element across. Local mesh modification will have to refine this part of the mesh.

Both the cross-section of the mesh and the transparent epicardium allow for evaluation of the wall thickness. From the results, the difference in wall thickness between the left and right side of the heart is visible. In addition to this, the deviation analysis provides global results of the thickness of the ventricular wall. All models show a concentration of red dots around the left side of the heart. In this analysis, red corresponds to a higher deviation, and therefore a higher wall thickness. This means that all models show a thickening of the ventricular wall around the LV, which is in line with the anatomy of the heart.

Beside for a global qualitative analysis, this deviation analysis can be used as a tool to study right ventricular hypertrophy in patients with TOF. The thickening of the wall can also be measured quantitatively in the cross-sections of the mesh.

Validation

The geometric models are quantitatively validated using both global validation and local validation. The first method of global validation is by a ventricular volume analysis. The blood volumes of both ventricles are measured and compared to the values provided by Medis Suite. For the LV, the relative error is between 0.09 - 0.19 for the biventricular patients (Patient 1-4), showing a relatively good resemblance. The patients after Fontan surgery presented a wide range of relative error, between 0.18 - 0.79. The RE for Patient 5 is very large. This can be explained by the small number of contours available in the MRI data showing this ventricle. A small number of contours corresponds to a relatively larger volume of the ventricle in between the slices and therefore a larger uncertainty.

For the RV, the relative error is between 0.00036-0.31 for the biventricular patients (Patient 1-4). Again, the patients after Fontan surgery show a worse RE range of 0.14 - 0.50. And again, Patient 5 has the highest RE. There are a number of possible explanations for this. Firstly, Fontan anatomy is very complex. This results in a high inter-observer variability which is discussed later in this chapter and demonstrated in Figure 4.1a and Figure 4.1b. The MRI scan can be interpreted differently and, accordingly, the created contours as well. For this patient, the RV is modeled as the functioning ventricle. However, the data could potentially have a better fit if the LV was modeled as the functioning ventricle. As a comparison to literature, Weissmann et al. compares the inner cavity volumes of a meshed porcine model to manual measurements (Weissmann et al., 2021). In their research, the error in all cavities was below 0.06. That is not achieved in this thesis. After all, as mentioned in the introduction, there was more data available for their models. Furthermore, even though the porcine hearts in their study are diseased, they might not be as complex as the hearts used in this thesis. The same study also shows that, for both its models, the RV has a larger error compared with the LV (Weissmann et al., 2021). With regard to this work, this is also the case in three out of four biventricular hearts, which can be explained by the complexity of the right ventricle compared to the left. This also

applies to the single ventricle hearts (Patient 5-7). However, as mentioned, obtaining accurate measurements from the non-functioning ventricle is very difficult for these hearts, which can lead to large errors. Another reason for the volume difference is that a section of the aorta is included in the measurement. The aorta is not segmented and therefore not taken into account in the Medis volume measurements. This can result in a larger volume in the biventricular model compared to the original data.

The second method of global validation is the ventricular mass analysis. This analysis compares the total mass of the ventricular wall of the biventricular geometric model to the Medis Suite measurements for each patient. The results of this analysis show a relative error in the range of 0.13 - 0.46. It is interesting to note that while the model for Patient 5 performed worst in both volume analyses, it has the lowest RE in the mass analysis.

A factor which could explain the poor fit in the geometric models is the method of calculating the ventricular mass. Medis Suite calculates this mass separately for the left and right ventricle. However, the ventricular myocardial wall is a single layer of tissue. The geometric models calculate this mass from one volume, which makes a comparison difficult. A sum of the left and right ventricular mass is taken to obtain a total mass, which is not desired, as it does not result in a smooth epicardial surface and can therefore be an underestimation of the true value. This is shown in the results as the mass of the geometric model is higher for every patient. Another factor potentially contributing to the RE is that the mass is only calculated in Medis Suite if both the epicardium and endocardium are segmented. Initially, contours were missing for the RV in Patient 2, 3 and 4. Extra contours were added to calculate the ventricle mass, but since this was not performed by the same physician as the original, moreover untrained for this purpose, it can lead to error. Ultimately, the aim of this thesis is to create a patient-specific model. To calculate the mass of the ventricular wall, the volume was multiplied by a density. A myocardial density of 1.05 g/ml was used, based on literature (Buechel et al., 2009). This is not a patient-specific value.

The results of the local validation show the Dice similarity coefficients for Patient 2, 4 and 7. The coefficient is calculated for the left and right ventricular blood volume and the myocardial wall. The aim of this validation is to show the surface similarity between the contours from the MRI data and the cross-section of the geometric model at the location of the MRI slices. The mean Dice scores range from 0.711 - 0.968. According to Zou et al., good overlap occurs when the DSC > 0.7 and excellent agreement happens at DSC > 0.75 (Zou et al., 2004). According to this metric, all labels show excellent similarity except the myocardial wall of Patient 4. However, this label still shows good similarity. A different study classifies the Dice scores slightly differently. Hershman et al. state that high spatial agreement is defined as a DSC between 0.7 - 1.0 and moderate agreement between 0.5 - 0.7 (Hershman et al., 2021). According to this standard, all models show high spatial agreement.

On average, the LV has the highest DSC scores and the myocardium the lowest. This can be explained by the complexity of the shapes of the labels. The LV cavity cross-section has a smooth circular shape. The transverse cross-section of the heart, the myocardium label, has more of an eight shape. This myocardial label is more complex, and therefore more difficult to morph. The validation shows that a more complex shape results in a lower similarity coefficient.

Part 2

4.1.2. Misalignment correction

After developing a geometric model, this work focuses on proposing and comparing methods to correct slice misalignment in MRI scans. The results show two proposed methods of correction for the contours of Patient 2.

First, qualitative results present the geometries of three, distinct left ventricle models. An obvious kink halfway through the ventricle is clearly visible in the geometric model before correction. Both correction models, aligned using the papillary muscle and epicardium, display an obvious difference in shape and a much smoother surface. This surface seems to follow a more natural curve of the LV in a healthy patient. Qualitative comparison between the corrected models is difficult, because there are no obvious differences visible. Looking at the geometric model outcomes, it is possible to assume that the correction methods have a positive influence on the wall stress, as the surface is much smoother. However, this has to be tested using a simulation of the model.

Global validation Quantitative results in the global validation present the blood volume and ventricular mass of all geometric models and the Medis Suite measurements. A slight decrease in volume and mass is evident for both corrected models. This can be considered an improvement, as the difference to the Medis Suite measurements is now smaller. Despite being minimal, the difference in outcomes between the two correction methods, both of them improved compared to the original data.

Using the papillary muscle as a reference, the assumption is made that this structure is straight. Also, this muscle does not run all the way to the apex, which means that further assumptions have to be made to align the contours below the papillary muscle. This last issue does not arise when aligning using the epicardium. But also here, the assumption is made that the epicardium is straight. Using an anatomical reference, which can be assumed to be straight or follow a predictable path, outside the heart would be an improvement. An example can be to use the sternum. Nevertheless, this reference is made of calcified tissue which is not visible on the scans and can not be segmented. This condition is relevant when it comes to optimizing soft tissue visualization in MRI setting, as in the context of this work. Thus, sternum is not considered in this specific project but may be beneficial for future improvements.

Local validation The results of the first method of local validation show the Dice similarity coefficient between the three left ventricle models and the 4-chamber and 2-chamber long-axis slices. The dice score of the LV cavity shows an improvement from good to excellent overlap (Zou et al., 2004) with the highest improvement for the correction using the papillary muscle. The Dice scores of the myocardium are lower, but they are still an improvement and give moderate agreement (Hershman et al., 2021). Again, the papillary correction method shows the biggest improvement. The difference in scores between the LV cavity and the myocardium can be explained by the increased complexity of the labels for the myocardium. The DSC results of the 2-chamber long-axis view present excellent agreement for all models (Zou et al., 2004). There is no improvement in the Dice score of the epicardium correction, but the corrected model using the papillary muscle does show a higher score. Due to low quality of the imaging data for the 2-chamber long-axis view, there is no segmentation of the LV cavity, possibly explaining the high scores.

The results of the second method of local validation show whether the use of the epicardium as the reference is an improvement to the model. Patient 3 was used as the ground truth. The

results show that the average distance to the mean and the standard deviation is much lower in the ground truth, but not zero. This shows that using the epicardium as a reference for alignment is beneficial to the model, however not the perfect solution. A positive development to this validation would be to validate against a patient with a healthy heart. A patient with TOF was used in this case as the only other healthy patient included in this thesis also has signs of slice misalignment.

Part 3

4.1.3. Ground truth exercise

The results of the third part of this thesis show the ground truth exercise in which a geometry of stacked disks is created for a subset of the population and the results are compared to the Medis Suite measurements.

Global validation The results of the global validation show the comparison between the Medis Suite measurement and the geometry of the stacked disks. The global validation of the LV shows a relative error below 1% for every patient included in this exercise. For the RV, the highest RE is 1.73%, meaning that there is excellent similarity between the volumes. A slightly higher relative error in the right ventricle can be explained by the more complex geometry of this ventricle. This high level of similarity demonstrates that this method is used by Medis Suite to calculate the volumes of the ventricles, a summation of stacked disks. It was hypothesized that this method provides and overestimation of the LV volume and an underestimation for the RV volume (Cho Kim et al., 2022; Moroseos et al., 2010). However, for all biventricular patients, the measurement of volume is higher in the geometric model compared to the Medis Suite measurements and the ground truth exercise measurements. This implies an underestimation of the LV volume by Medis Suite.

A coefficient of variability is used in the literature to evaluate the inter-observer variability. This coefficient is defined as the difference in measurements between observers (Bland & Altman, 2010). This ground truth exercise can be seen as an inter-observer comparison of the volumes. The inter-observer variability is below 1% for both the left and right ventricular blood volume. A study by Luijnenburg et al. showed an inter-observer variability between 3.9 and 10.2% for a population of children with TOF (Luijnenburg et al., 2010), which was considered a good result. Thus, the outcomes from the ground truth exercise are good when compared with this standard.

Local validation The results of the local validation present the Dice score between the segmented contours and the stacked disks. The results exhibit excellent similarity with a DSC of 0.960 or higher (Zou et al., 2004). High Dice scores are expected in this validation, because the geometry of stacked disks is created directly from the segmented contours.

Again, the LV blood volume has a slightly higher similarity compared to the right side, which can be explained by the more complex geometry of the right ventricle.

4.2. Limitations

The objectives of this thesis project include the creation of a biventricular *patient-specific* heart model. This section discusses the limitations found in the workflow which may have led to a *patient-inspired* model rather than a *patient-specific* model. The following section will provide suggestions on how to move closer to becoming a patient-specific model in the future.

MRI slices The input MRI data itself introduces error to the geometric models. The MRI machine produces a set of slices which are 8 mm apart for the scans used in this project. This may seem small, however, for a child's sized heart with a LV long axis length around 60-65 mm it means that there are close to 6-8 slices available. Information is lost between, above and below these slices. A different limitation this brings about is that it can be difficult to locate the apex of the heart. The apex can be located anywhere between 0 - 8 mm below the lowest contour. The apex is the location of the start of ventricular contraction and, therefore, an important part of the heart. Additionally, as mentioned before, the resolution of the MRI is lower because it is more difficult to ask children to lie completely still for long periods of time.

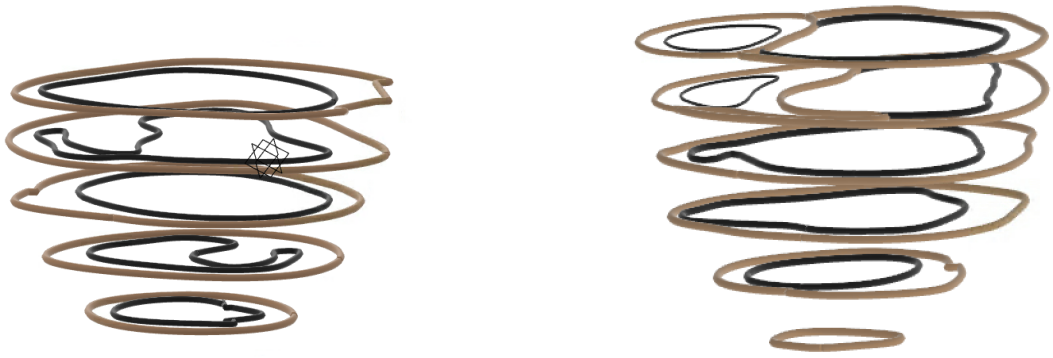

(a) Contours Patient 5

(b) Contours Patient 5

Figure 4.1: Contours Patient 5

Segmentation Another limitation occurs during segmentation and is caused by inter-observer variability to a certain degree. The contours used for this project are created using a combination of automatic and manual segmentation. Manual segmentation can introduce error, especially when it is carried out by different physicians, as shown in the inter-observer variability. However, automatic segmentation introduces error as well. Automatic segmentation relies on large amounts of training data. Hearts with CHDs have complex shapes and this presents challenges for segmentation algorithms due to limited training data for this population. This leads to automatic segmentation still requiring manual corrections, as it remains limited in clinical practice (Li et al., 2016). In this thesis, an effort was made to have the manual segmentation performed by the same physician to limit variability. The importance of this is shown in Figures 4.1a and 4.1b. Both figures show the contours of the epicardium and endocardium of Patient 5, a patient with a Fontan physiology. The contours are of the same patient, and from the same MRI scans, however, there are obvious differences. Both figures show the contours of the epicardium drawn in brown and the epicardium in black. Figure 4.1a on the left shows solely a single ventricle. Figure 4.1b on the right shows a biventricular heart, though one of the ventricles is drawn significantly smaller

than the other. The contour set also consists of 6 slices, rather than five in the other contour set. This shows that MRI scans can be interpreted differently and segmentation is a limitation due to its variability. These contour sets would result in two differently looking geometric models and volume measurements, while being the same heart.

Furthermore, this thesis project has been limited by a lack of consistency and protocols in its input data. Figure 4.2 shows the contours of the left ventricular endocardium of Patient 1. The contours are clearly rugged with many inlets. This is because the inlets show the locations of the papillary muscles. These locations might be important and useful for a different purpose to the physician. However, with regard to this project, smooth contours representing the outside of the endocardium wall layer are more useful for morphing.

Figure 4.2: Segmentation limitation
Contours endocardium LV Patient 1, including papillary muscles

Repeatability The manual morphing and a lack of protocols in segmentation both affect the repeatability of the results. As shown above, imaging data can be interpreted differently when there are no strict protocols in place. This, in combination with manually aligning, scaling and morphing, the model can lead to a low repeatability for the process of creating a geometric biventricular model. Low repeatability means that there is high inter-observer variability, which is unfavorable. Protocols to improve the repeatability of manual segmentation can include the exclusion of the papillary muscles, the inclusion of long-axis views, and consistent and complete labeling. A protocol to improve the repeatability of manual morphing can include following the guideline presented in Appendix C.

Aligning The patient data are imported into the LHHM model as a reference geometry and have to be manually aligned. These contours are placed somewhere in space. Using translations and rotations, the reference geometry can be aligned with the biventricular model. With the contours providing limited anatomic details, accurately aligning the reference geometry with the model is challenging and can introduce error.

Morphing Morphing the model introduces error as well. Morphing is done manually and is therefore not expected to be perfect. Nodes are relocated individually and this can lead to irregularities. Furthermore, there might not be enough nodes to create small alterations in the geometry. Moreover, manual morphing is a time-demanding task.

Unique geometries CHDs are characterized by their unique geometries and can therefore not be easily morphed from the same baseline geometry. Manual morphing can be a very useful tool in a lot of cases, however it can also reach its limits. In this project, the baseline geometry from where the morphing happens is a healthy heart. The healthy heart has two regularly sized ventricles, an aorta and pulmonary tract. In the case of very complex hearts, for example Fontan patients, there are significant differences in geometry. One of the ventricles can be extremely small or non-existent and the great arteries can be rerouted during surgeries. This makes these hearts different in its core geometry. Achieving a patient-specific geometry solely using morphing is challenging. It may require more alterations than morphing can provide.

Validation Validation is important to check the quality of the results, but obtaining validation data remains a limitation. The results of this project can be validated against the data available in Medis Suite. Among other values, Medis Suite provides data on the ventricular mass and volume. However, these values are based on the same segmentation as used for the geometric models and thus use the same input data. It is therefore not possible to validate against the *true* values of mass and volume. This has been attempted by the local validation using the Dice similarity coefficient and the addition of the ground truth exercise. Additionally, the mass of the ventricles is calculated for the left and right ventricles separately. The biventricular model made in this project has one combined ventricular mass. A sum of the two ventricles results in more error and is therefore a limitation for this validation. The slice misalignment correction is validated locally using the left ventricle of a different, non-healthy, patient. To improve this validation, multiple healthy patients could be included in the validation.

4.3. Recommendations For Future Work

A number of points can be implemented for further improvements and continuation of this project. This section lists various recommendations for future work.

Contour expansion The introduction of additional anatomical details in the segmentation process can aid in the improvement of the alignment of the reference geometry step and, therefore, the accuracy of morphing the model. Contour suggestions of anatomical details to include are: the aortic valve, papillary muscles separated from the endocardium, and the sternum. Contours of the sternum can aid in the detection and correction of a slice misalignment. This is because the sternum follows a predictable path. Furthermore, long-axis views are used in only one case for local validation of the slice misalignment correction methods. Applying these views with segmentation can improve both the geometric models (in aligning and morphing) and the slice misalignment correction. Segmentation of long-axis views can possible also improve the volume measurements inside Medis Suite. In addition to the contour expansion, the piecewise smooth subdivision surface method can be included. This method can be used to validate the accuracy of the 3D shape of the ventricles, as well as the ventricular volume (Moroseos et al., 2010).

Mesh convergence study The meshes in this thesis project are evaluated using the mesh quality reports. A recommended step for future work would be to incorporate a mesh convergence study. This is a study to find the best mesh element shape and size. The goal of a mesh convergence study is to create a mesh that generates accurate results whilst using a reasonable number of elements for computational time purposes. To find the best mesh, the number of elements is increased in a simulation to see if the results converge at a certain mesh density. An improvement for the current meshes could be a reduction in the total number of elements, but locally an increase in elements across the ventricular wall.

Simulation The current model is a patient-specific geometry and mesh of the ventricles. For further continuation of this project, this can be eventually made into a simulation. Boundary conditions, constraints and material properties, including fiber orientations, will have to be implemented. A simulation can be used to study the stress and strain in the model during ventricular contraction and relaxation. When both end-systolic and end-diastolic volumes are incorporated, the stroke volume ($SV = EDV - ESV$) can be calculated as well as the ejection fraction ($EF\% = SV/EDV * 100$) of the heart. These measurements can then be used to compare diseased heart models to healthy models.

Single ventricle geometry Lastly, this project shows the morphing process of hearts with congenital heart defects starting from the same healthy geometry. In the case of single ventricle hearts, these anatomies test the limits of the morphing process. A recommendation for future work would therefore be to include a baseline geometry of a single ventricle heart. This will reduce the workload of manual morphing and possibly improve the accuracy of the model. Such a baseline geometry can be created by using the mesh from one of the single ventricle models and transforming it into a subdivision surface.

5

Conclusion

The goal of this thesis project is to use manual morphing to create biventricular patient-specific geometric models of a diverse population of young hearts in order to move closer towards patient-specific modeling of hearts in children with congenital heart defects. In order to assess this goal, it is divided into three objectives.

The first objective is to develop and implement a workflow for the creation of a biventricular patient-specific geometric heart model, using morphing techniques, of a young population, including complex congenital heart defects. The results show seven patient-specific geometric models. Starting from a healthy adult heart model, these models are created using a combination of parameter and manual morphing. The models might be considered *patient-inspired* rather than *patient-specific* due to the comparatively high relative error in the global validation. However, these errors can be explained by a number of factors Medis Suite uses to obtain its results. These factors include, but are not limited to, the small number of contour slices available, the exclusion of the ventricular outflow tracts, the separation of the left and right ventricular mass, and the inter-observer variability. Interestingly, local validation using the Dice similarity coefficient shows good to excellent surface similarity between the segmented MRI data and the created models.

The second objective is to propose and compare two methods of slice misalignment correction, which can occur in an MRI when a patient moves or breathes out too early. The first correction method presented is the alignment of the contours based on the center-of-gravity points of one of the papillary muscles. The second correction method is based on the epicardium. Qualitative analysis, global validation and local validation all show an improvement in comparison to the original data for both correction methods. Based on the Dice similarity coefficients using the long-axis views, the correction method using the papillary muscle shows the largest improvement.

There are also limitations to the methods. Both methods make the assumption that their reference geometry, the papillary muscle and epicardium, is straight. An improvement would be to add contours of the sternum as a reference structure, because it follows a more predictable path.

The third and last objective if this thesis is to perform a ground truth experiment in order to evaluate the quality of the results based on the data and methods by Medis Suite and to test the post-processing results purely based on the contours. Geometries using stacked disks are

made of the left and right ventricular cavities for a number of the included patients. The cavity volume of these geometries is calculated as the sum of the individual volumes, according to the Simpson's method. Validation of these volumes shows an excellent comparison between the stacked models and the Medis Suite measurements. From these results, it can be concluded that Medis Suite uses this method for its calculations. A limitation found, based on this conclusion, is that this method can result in error. Especially in children's hearts, where there are fewer slices available compared to fully grown hearts. This means that there is a relatively larger volume unknown, between the MRI slices. Subsequently, this also means that it might lead to an underestimation of the LV volume when comparing it to the geometric models. Further research will have to be done to support this hypothesis.

In conclusion, patient-specific biventricular geometric models are created in this thesis. These models represent a range of patients, including healthy hearts and hearts with complex congenital heart defects. The geometric models are ready to be used by clinicians to build up expertise from individual complex cases and increase the understanding of individual models. The models can also benefit patients and families directly by using the models as a communication method for patient-specific anatomical understanding. Lastly, these models are a starting point for the development of patient-specific computational models. The geometric model and mesh are a basis on which a material model and boundary conditions can be added in further research. The computational model can be used to study wall stresses and flow dynamics on an individual basis.

References

Ansys, I. (2008). Reporting mesh statistics [Online; accessed 8 December 2022]. https://romeo.univ-reims.fr/documents/fluent/tgrid/ug/chp15.pdf

Arega, T., Legrand, F., Bricq, S., & Meriaudeau, F. (2022). Using mri-specific data augmentation to enhance the segmentation of right ventricle in multi-disease, multi-center and multi-view cardiac mri. *Lecture Notes in Computer Science*, *13131*, 250–258. https://doi.org/10.1007/978-3-030-93722-5_27

Babu-Narayan, S., Giannakoulas, G., Valente, A., Li, W., & Gatzoulis, M. (2016). Imaging of congenital heart disease in adults. *European Heart Journal*, *37*, 1182–1195. https://doi.org/10.1093/eurheartj/ehv519

Baillargeon, B., Rebelo, N., Fox, D., Taylor, R., & Kuhl, E. (2014). The living heart project: A robust and integrative simulator for human heart function. *European Journal of Mechanics*, *48*, 38–47. https://doi.org/10.1016/j.euromechsol.2014.04.001

Bayer, J., Blake, R., Plank, G., & Trayanova, N. (2012). A novel rule-based algorithm for assigning myocardial fiber orientation to computational heart models. *Annals of Biomedical Engineering*, *40*, 2243–2254. https://doi.org/10.1007/s10439-012-0593-5

Biglino, G., Capelli, C., Wray, J., Schievano, S., Leaver, L., Khambadkone, S., Giardini, A., Derrick, G., Jones, A., & Taylor, A. (2015). 3d-manufactured patient-specific models of congenital heart defects for communication in clinical practice: Feasibility and acceptability. *BMJ Open*, *5*, 007165. https://doi.org/10.1136/bmjopen-2014-007165

Bland, J., & Altman, D. (2010). Statistical methods for assessing agreement between two methods of clinical measurement. *International Journal of Nursing Studies*, *47*, 931–936. https://doi.org/10.1016/j.ijnurstu.2009.10.001

Buechel, E., Kaiser, T., Jackson, C., Schmitz, A., & Kellenberger, C. (2009). Normal right- and left ventricular volumes and myocardial mass in children measured by steady state free precession cardiovascular magnetic resonance. *Journal of cardiovascular magnetic resonance : official journal of the Society for Cardiovascular Magnetic Resonance*, *11*, 19. https://doi.org/10.1186/1532-429X-11-19

Capelli, C., Sauvage, E., Giusti, G., Bosi, G., Ntsinjana, H., Carminati, M., Derrick, G., Marek, J., Khambadkone, S., Taylor, A., & Schievano, S. (2018). Patient-specific simulations for planning treatment in congenital heart disease. *Interface Focus*, *8*, 20170021. https://doi.org/http://dx.doi.org/10.1098/rsfs.2017.0021

Charles, C., Lee, P., Li, R., Yeung, T., Ibraham Mazlan, S., Tay, Z., Abdurrachim, D., Teo, X., Wang, W., de Kleijn, D., Cozzone, P., Lam, C., & Richards, A. (2020). A porcine model of heart failure with preserved ejection fraction: Magnetic resonance imaging and metabolic energetics. *ESC Heart Failure*, *7*, 93–103. https://doi.org/10.1002/ehf2.12536

Cheuk, D. K. L., Wong, S. M. Y., Choi, Y. P., Chau, A. K. T., & Cheung, Y. F. (2004). Parents' understanding of their child's congenital heart disease. *Heart*, *90*, 435–439. https://doi.org/10.1136/hrt.2003.014092

Cho Kim, W., Beqiri, A., Lewandowski, A., Puyol-Antón, E., Markham, D., King, A., Leeson, P., & Lamata, P. (2022). Beyond simpson's rule: Accounting for orientation and ellipticity assumptions. *Ultrasound in Medicine and Biology*, *48*, 2476–2485. https://doi.org/10.1016/j.ultrasmedbio.2022.07.013

Conca, G. (2015). Patient-specific monoventricular models of cardiac biomechanics for hypoplastic left heart syndrome [Master's Thesis].

Dietz, S., Tacke, C., Kuipers, I., Wiegman, A., de Winter, R., Burns, J., Gordon, J., Groenink, M., & Kuijpers, T. (2015). Cardiovascular imaging in children and adults following kawasaki disease. *Insights Imaging*, *6*, 697–705. https://doi.org/10.1007/s13244-015-0422-0

Formato, G., Schievano, S., & Biglino, G. (2022). Modelling congenital heart disease. Springer Nature Switzerland AG. https://doi.org/10.1007/978-3-030-88892-3_1

Gatzoulis, M., Webb, G., & Daubeney, P. (2018). *Diagnosis and management of adult congenital heart disease* (Third edition). Elsevier. https://doi.org/10.1016/B978-0-7020-6929-1.01002-9

Gilbert, K., Cowan, B., Suinesiaputra, A., Occleshaw, C., & Young, A. (2014). Rapid d-affine biventricular cardiac function with polar prediction. *Medical Image Computing and Computer Assisted Intervention*, *17*, 546–553. https://doi.org/10.1007/978-3-319-10470-6_68

Hershman, M., Yousefi, B., Serletti, L., Galperin-Aizenberg, M., Roshkovan, L., Luna, J., Thompson, J., Aggarwal, C., Carpenter, E., Kontos, D., & Katz, S. (2021). Impact of interobserver variability in manual segmentation of non-small cell lung cancer (nsclc) applying low-rank radiomic representation on computed tomography. *Cancers*, *13*, 5985. https://doi.org/10.3390/cancers13235985

Lederlin, M., Thambo, J., Latrabe, V., Corneloup, O., Cochet, H., Montaudon, M., & Laurent, F. (2011). Coronary imaging techniques with emphasis on ct and mri. *Pediatric Radiology*, *41*, 1516–1525. https://doi.org/10.1007/s00247-011-2222-0

Levine, S., Battisti, T., Butz, B., D'Souza, K., Costabal, F., & Peirlinck, M. (2022). Modelling congenital heart disease. Springer Nature Switzerland AG. https://doi.org/10.1007/978-3-030-88892-3_25

Li, J., Zhang, R., Shi, L., & Wang, D. (2016). Automatic whole-heart segmentation in congenital heart disease using deeply-supervised 3d fcn. *Lecture Notes in Computer Science*, 111–118. https://doi.org/10.1007/978-3-319-52280-7_11

Liebsch, M., Grune, B., & Seiler, A. e. a. (2011). Alternatives to animal testing: Current status and future perspectives. *Archives of Toxicology*, *85*, 841–858. https://doi.org/10.1007/s00204-011-0718-x

Luijnenburg, S., Robbers-Visser, D., Moelker, A., Vliegen, H., Mulder, B., & Helbing, W. (2010). Intra-observer and interobserver variability of biventricular function, volumes and mass in patients with congenital heart disease measured by cmr imaging. *The international journal of cardiovascular imaging*, *26*, 57–64. https://doi.org/10.1007/s10554-009-9501-y

Martin, G. R., & Jonas, R. A. (2018). Surgery for congenital heart disease: Improvements in outcomes. *American journal of perinatology*, *35*, 557–560. https://doi.org/10.1055/s-0038-1639358

Mathur, A., Ma, Z., Loskill, P., Jeeawoody, S., & Healy, K. (2016). In vitro cardiac tissue models: Current status and future prospects. *Advanced drug delivery reviews*, *96*, 203–213. https://doi.org/10.1016/j.addr.2015.09.011

Medis. (2020). Medis suite mr 3.2 [Product Specification Sheet]. https://medisimaging.com/wp-content/uploads/2021/04/MR-Product-sheet-2020NPI2.pdf

Mertens, L., Ganame, J., & Eyskens, B. (2008). What is new in pediatric cardiac imaging? *European Journal of Pediatrics*, *167*, 1–8. https://doi.org/10.1007/s00431-007-0544-6

Moroseos, T., Mitsumori, L., Kerwin, W., Sahn, D., Helbing, W., Kilner, P., Shurman, A., Litt, H., & Sheehan, F. (2010). Comparison of simpson's method and three-dimensional reconstruction for measurement of right ventricular volume in patients with complete or corrected transposition of the great arteries. *American Journal of Cardiology*, *105*, 1603–1609. https://doi.org/10.1016/j.amjcard.2010.01.025

Muresian, H. (2016). The clinical anatomy of the right ventricle. *Clinical Anatomy*, *29*, 380–398. https://doi.org/10.1002/ca.22484

Nelson, J., Bove, E., & Hirsch-Romano, J. (2014). Tetralogy of fallot. *Pediatric and Congenital Cardiology, Cardiac Surgery and Intensive Care*, 1505–1526. https://doi.org/10.1007/978-1-4471-4619-3_18

Olivieri, L., Krieger, A., Loke, Y.-H., Nath, D., Kim, P., & Sable, C. (2015). Three-dimensional printing of intracardiac defects from three-dimensional echocardiographic images: Feasibility and relative accuracy. *Journal of the American Society of Echocardiography*, *28*, 392–397. https://doi.org/10.1016/j.echo.2014.12.016

Ordas, S., Oubel, E., Leta, R., Carreras, F., & Frangi, A. (2007). A statistical shape model of the heart and its application to model-based segmentation. *Proceedings of SPIE - The International Society for Optical Engineering*, *6511*. https://doi.org/10.1117/12.708879

Rodero, C., Strocchi, M., Marciniak, M., Longobardi, S., Whitaker, J., O'Neill, M., & et al. (2021). Linking statistical shape models and simulated function in the healthy adult human heart. *PLoS computational biology*, *17*. https://doi.org/10.1371/journal.pcbi.1008851

Rufaihah, A., Chen, C., Yap, C., & Mattar, C. (2021). Mending a broken heart: In vitro, in vivo and in silico models of congenital heart disease. *The Company of Biologists*, *14*, 047522. https://doi.org/10.1242/dmm.047522

Sahu, A., & Slesnick, T. (2017). Imaging adults with congenital heart disease part ii. *Journal of Thoracic Imaging*, *32*, 245–257. https://doi.org/10.1097/RTI.0000000000000274

Sigal, I., Yang, H., Roberts, M., & Downs, J. (2010). Morphing methods to parameterize specimen-specific finite element model geometries. *Journal of Biomechanics*, *43*, 254. https://doi.org/10.1016/j.jbiomech.2009.08.036

Smith, M. (2009). *Abaqus/standard user's manual, version 6.9*. Dassault Systèmes Simulia Corp.

Swingen, C., Seethamraju, R., & Jerosch-Herold, M. (2003). An approach to the three-dimensional display of left ventricular function and viability using mri. *The International Journal of Cardiovascular Imaging*, *19*, 325–336. https://doi.org/10.1023/a:1025450211508

Tautz, L., Walczak, L., Manini, C., Hennemuth, A., & Hüllebrand, M. (2022). 3d right ventricle reconstruction from 2d u-net segmentation of sparse short-axis and 4-chamber cardiac cine mri views. *Lecture Notes in Computer Science*, *13131*, 352–359. https://doi.org/10.1007/978-3-030-93722-5_38

Trusty, P., Slesnick, T., Wei, Z., Rossignac, J., Kanter, K., Fogel, M., & Yoganathan, A. (2018). Fontan surgical planning: Previous accomplishments, current challenges and future directions. *Journal of Cardiovascular Translational Research*, *11*, 133–144. https://doi.org/10.1007/s12265-018-9786-0

Van der Geest, M. (2022). Wie mag straks nog een kinderhart opereren? een strijd tussen ziekenhuizen om expertise en aanzien [Online; accessed 23 January 2022]. https://www.volkskrant.nl/nieuws-achtergrond/wie-mag-straks-nog-een-kinderhart-opereren-een-strijd-tussen-ziekenhuizen-om-expertise-en-aanzien~b3a3f48d/

van der Linde, D., Konings, E., Slager, M., Witsenburg, M., Helbing, W., Takkenberg, J., & Roos-Hesselink, J. (2011). Birth prevalence of congenital heart disease worldwide. *Journal of the American College of Cardiology*, *58*, 2241–7. https://doi.org/10.1016/j.jacc.2011.08.025

Vieira, M., Hussain, T., & Figueroa, C. (2015). Patient-specific image-based computational modeling in congenital heart disease: A clinician perspective. *Journal of Cardiology and Therapy*, *2*, 436–448. https://doi.org/10.17554/j.issn.2309-6861.2015.02.96

Wang, J., Rai, R., Carrasco, M., Sam-Odusina, T., Salandy, S., Gielecki, J., Zurada, A., & Loukas, M. (2019). An anatomical review of the right ventricle. *Translational Research in Anatomy*, *17*, 100049. https://doi.org/10.1016/j.tria.2019.100049

Webster, B. (2021). Which abaqus element type should i use - article 4: Element quality check criteria [Online; accessed 8 December 2022]. https://www.fidelisfea.com/post/which-abaqus-element-type-should-i-use-article-4-element-quality-check-criteria

Weinhaus, A. (2015). *Handbook of cardiac anatomy, physiology, and devices* (3rd ed.). Springer Cham. https://doi.org/10.1007/978-3-319-19464-6_5

Weissmann, J., Charles, C., Richards, A., Yap, C., & Marom, G. (2021). Cardiac mesh morphing method for finite element modeling of heart failure with preserved ejection fraction. *Journal of the Mechanical Behavior of Biomedical Materials*, *126*, 104937. https://doi.org/10.1016/j.jmbbm.2021.104937

Wong, J., & Kuhl, E. (2014). Generating fiber orientation maps in human heart models using poisson interpolation. *Computer Methods in Biomechanics and Biomedical Engineering*, *17*, 1217–1226. https://doi.org/10.1080/10255842.2012.739167

Yu, H., del Nido, P., Geva, T., Yang, C., Wu, Z., Rathod, R., Huang, X., Billiar, K., & Tang, D. (2020). Multi-band surgery for repaired tetralogy of fallot patients with reduced right ventricle ejection fraction: A pilot study. *Frontiers in Physiology*, *11*. https://doi.org/10.3389/fphys.2020.00198

Zou, K. H., Warfield, S. K., Bharatha, A., Tempany, C. M., Kaus, M. R., Haker, S. J., Wells, W. M. 3., Jolesz, F. A., & Kikinis, R. (2004). Statistical validation of image segmentation quality based on a spatial overlap index. *Academic radiology*, *11*, 178–189. https://doi.org/10.1016/s1076-6332(03)00671-8

Zygote. (2014). Zygote solid 3d heart generations i & ii development report [Technical Development of 3D Anatomical Systems].

A

Interview

The relationship between the clinician and patient is very important. The patient's individual needs are at the center of the care. A key aspect of this is the communication between the healthcare provider and the patient and his or her family. The patient should be informed about his/her own health and be a part of shared decision-making. //

The following interview is conducted with the mother of a nine-year-old boy with a single ventricle. The aim of the interview is to gather information on how a physics-based computational model of a heart with a CHD can aid the patient and family. The patient's perspective can aid in the development of the model, as it is important to implement the patient's needs and aspirations into the model.

Date: January 27, 2022
Present: Carina (mother of Joas) and Puck
Topic: Patient perspective on patient-specific 3D cardiac models

Question: When and how did you hear that something was wrong with Joas's heart?

Answer: During the 20 week ultrasound, we learned that one of the ventricles was not fully grown. After the news, we were forwarded to the Radboud university medical center in Nijmegen. They made a lot of ultrasounds. This was difficult to do, because sometimes Joas was not positioned well in the belly and the picture was not good. In the end, they got a picture as complete as possible. I also gave birth there. An ultrasound was performed immediately after delivery. Then it turned out that they had not seen everything.

Question: How was that for you?

Answer: It was a little weird. You are going to a 20 week ultrasound and you know there are many scenarios. The sonographer went completely silent. You could tell from the sonographer that something was wrong. This was worse than hearing what was going on, the uncertainty and ambiguity of what exactly was going on. We were at a regular practice and we could only go to the Radboud three days later. That was terrible. It was all very uncertain. We were instructed not to google information. Well, what do you do first...? That's googling.

Question: How was the guidance from the doctors and hospital?

Answer: The doctors couldn't tell clearly what was going on. Maybe it was because of the equipment, because they couldn't see everything. Joas is our first child but second pregnancy. Before Joas I had a miscarriage at 12 weeks. We had never experienced the 20 week ultrasound before. There was no real guidance from there. It was more like: you have to go to a specialist hospital for this. Then they looked for the first place we could visit, the Radboud or the Utrecht MC. Radboud had a wait list of 3 days, UMC of 4 days. We got a lot of ultrasounds and then went to see a cardiologist. The cardiologist tried to draw it by hand. Then, we were sent home with the message: think carefully about whether you want to continue this pregnancy. A few days later, we had to come back to discuss what it would take if we were to continue with the pregnancy.

Question: How did things go after Joas was born? What kind of operations and treatments did Joas have?

Answer: Joas was born in the Radboud. After his birth, it turned out that not only something was wrong with his right ventricle; he has an HRHS. The right ventricle is barely there. He also has a transposition of the great vessels. This had all been seen on the ultrasound. On the ultrasound, they had not seen that his aorta was also very constricted. That meant that a day after his birth, he had to be transported by ambulance to the UMC. Because in the UMC they perform the heart surgeries and not in the Radboud anymore. At 8 days old, Joas had his first open heart surgery, the Norwood procedure. The second is called the Glenn procedure. Before his first open heart surgery, he had a coronary angiogram to visualize it all. Also, to make a plan about how they were going to do it. He's had a lot of coronary angiograms. We've seen pictures of that too. In the beginning, we couldn't do anything with the images. As Joas got older, he is now 9 years old. We have learned how to look at them. The first operation after 8 days was the most critical operation. Shortly after the operation, he was in the ICU and not doing well. That was a moment when we had to say goodbye. Then they had another operation on the spot in the ICU. As a mother, I completely missed that one. I don't know exactly what they did then. But then suddenly he started to recover. He spent quite some time in the ICU. Then he went home for a while. Some children remain in the hospital until the second operation. He had the Glenn procedure at 8 months. For his last operation, the Fontan procedure, he was just over 3 years old. The 2nd and 3rd operations went better.

Question: What kind of information did you receive from the hospital? How did you find more information yourself?

Answer: We as parents wanted to understand. We immersed ourselves in his situation and read about it. You are going to watch clips on how a normal heart works. We have experienced the patient care as very pleasant. But to really understand how his heart is put together was very difficult in the beginning. You have to learn a lot to understand how the images work. In Utrecht, they always showed images of what the surgeons had done. This was different for each cardiologist. Some cardiologists really took a moment to show and explain. We are not used to looking at such images. Before you understand a bit of how it works, you are a few years further. As parents, we received all the information. It's in other relationships that this is difficult too. Our parents and our families have always been very involved. We have to explain everything to them again, and we found that very difficult. We showed them the sketch we received. Some have had a little bit of biology at some point, but just the basic knowledge is difficult for others. How

everything works exactly requires some explanation. This is still the case. We still get questions very often. Sometimes you just don't feel like explaining everything completely.

Question: How is Joas doing now?

Answer: Joas is now 9 years old. He plays soccer. Soccer is his everything. He goes to school 5 days a week. He is a very fit, energetic boy. You would hardly say that he has such a huge heart defect. In the winter, he suffers from the cold. He then has trouble keeping his body warm. But he is very fit. He plays sports a lot, and he is doing really well.

Question: What does Joas think of it all?

Answer: It took quite a while before Joas understood everything. We have always been very open about it and we have told him everything. But something changed when he was in year 3. He was 6/7 years old. Until that moment, he had always been very sad. Joas knew he could not carry on activities for very long. He, for example, found a game of tag very complicated. He became very sad that he didn't succeed and that he had been the tagger during the whole break because he was unable to tag other children. Then he said it might be helpful that other children in the class also knew what was going on. He never really wanted to talk about it. I went to his class one time, and we talked to his classmates together and showed some pictures. Not too shocking for the other kids. Then in year 5, he gave his own speech about it. Since then, we have noticed a change. We borrowed a 3D heart from a biology teacher. This was to show what a normal heart looks like. We had that heart in our house for a few weeks for his speech. He then walked around a lot with it and asked a lot of questions about it. "How about it then?" "What does my heart look like?" "Do I then have a square heart?". He has absolutely no idea what is different. Then we try to explain: "We have two ventricles", "You have 1 large ventricle". At a later age he is more interested in it, giving a talk about it and explaining it to friends. Now comes a bit of acceptance. We, as parents, are happy about that.

Question: How does he see, and how do you see the future?

Answer: He is a boy. So he wants to be a professional soccer player like all the other boys. He sometimes thinks about his future differently. Sometimes he suddenly says "Maybe I'll be the camping boss after all". He likes camping very much. "Then I only have to work in the summer when it is nice and warm and in the winter, I don't have to do anything anymore." That way, he looks at his future, more from a practical point of view.

Since Joas has arrived, we have met quite a few other parents with children with CHDs. You hear very different stories. We don't really know what to expect or how things will go in the future. We have never met anyone with a similar image or a boy like Joas.

Question: The goal is that we will make dynamic (moving) models of hearts with congenital defects. Every condition is unique. Every child is unique. In addition, it is constantly changing due to the growth of the child and the surgeries. Ideally, we can create a model that is completely patient-specific. Correct dimensions, anatomy, flow directions and pressures. This is useful for the cardiac specialists, for the developers (technicians) of medical devices to be used during the procedures, but also for the parents and the patient. (Showed some videos and pictures of examples.) What do you expect from these heart models? What role can they play for parents and for the patient?

Answer: I like what I see. I think it could be helpful for children to look at when they grow up and think "Hey what exactly do I have?". Also to compare with another “normal” heart, to see what’s different. As a parent, a model would be very nice while explaining things to family and friends. You have something concrete to show what is going on. What we as parents encounter is that Joas’s heart is very specialized. In Utrecht, they know a lot about it. But we also occasionally visit the emergency room in our regional hospital. For example, if he suffers from pseudocroup. You have to go to a hospital quickly. We often notice that the doctors there are not so highly specialized. That is sometimes our greatest frustration. Sometimes it takes so long to explain things. Doctors don’t understand it or they make a mistake. Doctors often think he has asthma because you can hear him breathing. Then they want to give him a different medication. We then say no, it is not asthma. Before you actually get to the point where everyone understands what’s going on, it sometimes takes a lot of time. For us as parents, this is a point of frustration.

Question: What does Joas expect from it?

Answer: In his life, Joas is experiencing more and more that he has to explain to other people what is going on. Now it’s just at school, but it will always be the case.

Question: Do you have additional things you want to say or any questions?

Answer: If we have a check-up, we ask for the new developments. I know they are working on it in Utrecht. As parents, we always receive an invitation to a conference. It is with surgeons and cardiologists from all over the world. We went once as parents. It’s interesting to see what’s happening. You may be able to avoid major mistakes in the future. It is remarkable that during the pregnancy we were not very much encouraged to continue the pregnancy. Especially because it is a very tough process and you don’t know how children go through it. But in the past few years, we have been seeing a shift. Quality of life over survival is important. First, the primary concern was keeping these children alive. Now you see that it is much more focused on the quality of life of the child. A physiotherapist also followed Joas until he is 18. There you can see how Joas is going. He plays sports. This is very different from heart children 20 years ago. We also have a lot of contact with other parents. Somehow, we want to make life very malleable. Many pregnancies are terminated. You have to be willing to put in the time. It’s difficult and sometimes it’s hard to hear those stories. Especially because Joas is doing so well. When do you give a child the chance at a life?

Concluding remark: Thank you very much for letting me interview you.

B

Complete Results

Complete results organized per patient.

B.1. Patient 1

8-year-old female with a healthy heart.

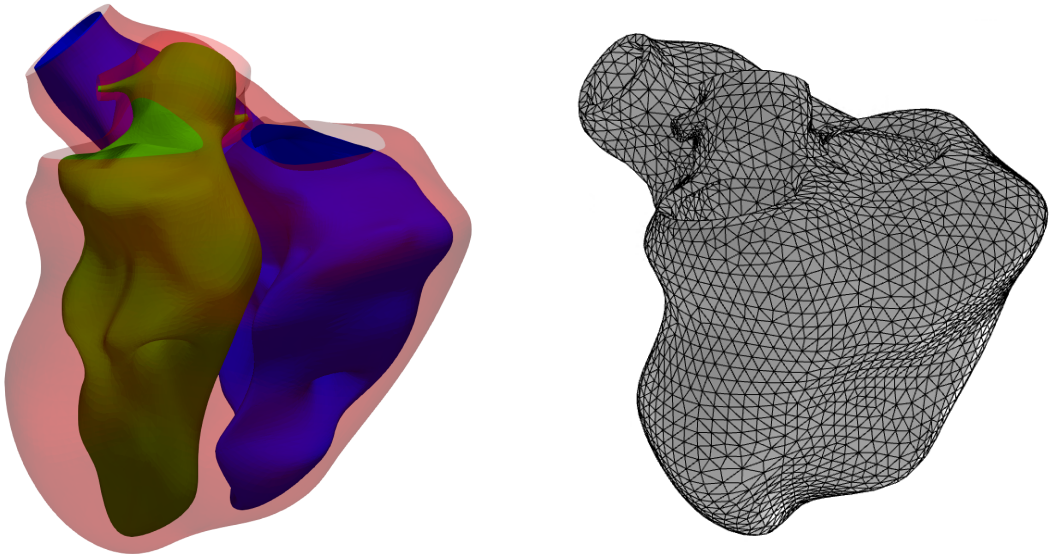

(a) Geometry. Red=epicardium, Green=LV endocardium, Blue=RV endocardium

(b) Mesh

Figure B.1: Biventricular geometry and mesh Patient 1

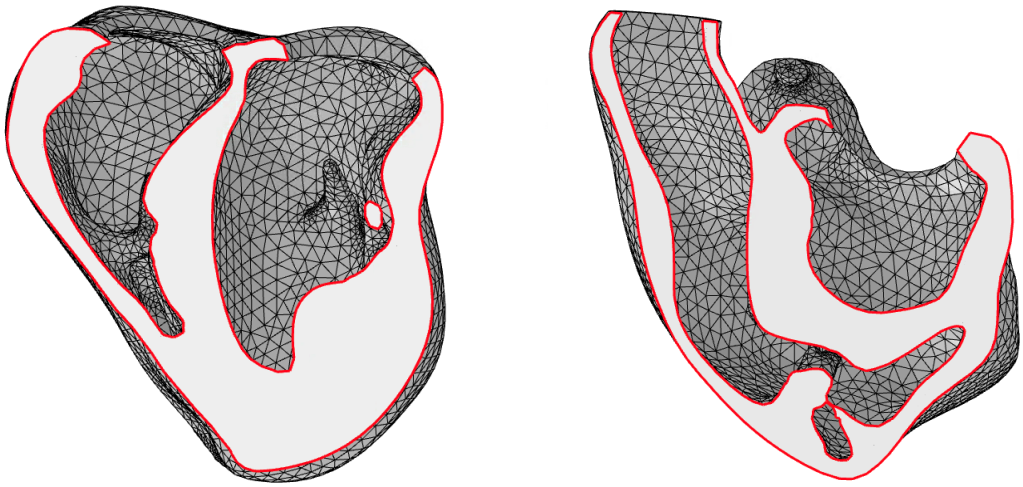

(a) Mesh cross-section 1 **(b)** Mesh Cross section 2

Figure B.2: Cross-sections of mesh Patient 1

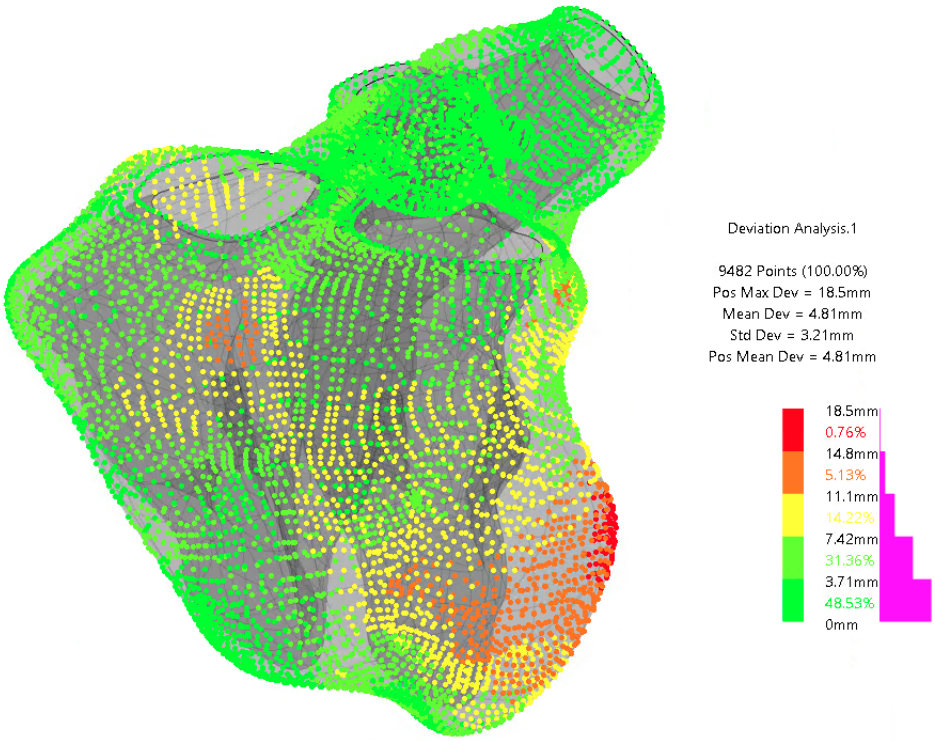

Figure B.3: Deviation analysis Patient 1

B.2. Patient 2

9-year-old female with a healthy heart.

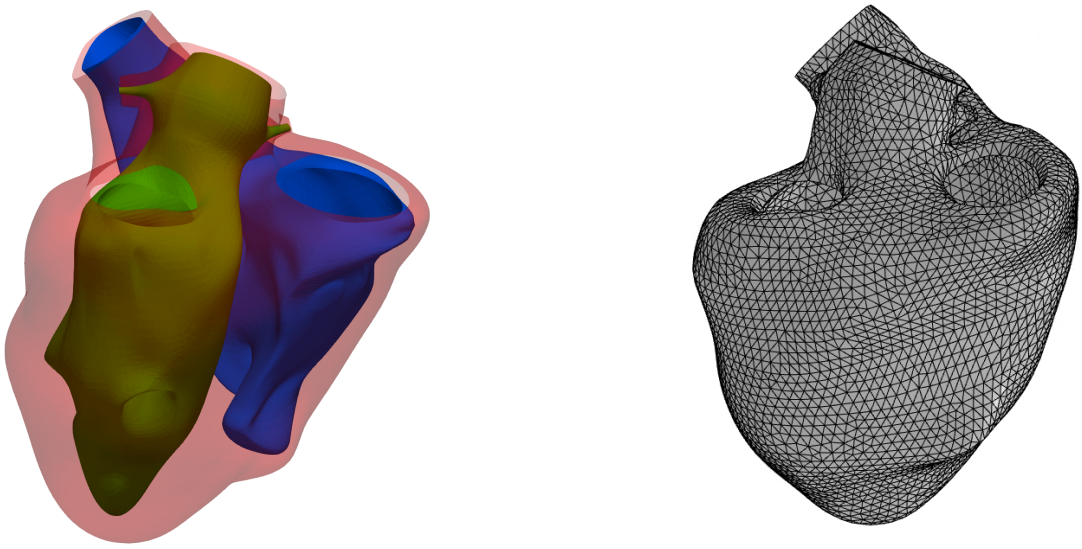

(a) Geometry. Red=epicardium, Green=LV endocardium, Blue=RV endocardium

(b) Mesh

Figure B.4: Biventricular geometry and mesh Patient 2

Table B.1: Local validation: Dice similarity coefficient results Patient 2

Scan slice	LV Blood volume	RV Blood Volume	Myocardium
1	n/a	0.894	0.673
2	0.939	0.877	0.617
3	0.973	0.933	0.773
4	0.979	0.902	0.730
5	0.969	0.863	0.833
6	0.929	0.824	0.768
7	0.948	0.732	0.789
8	0.865	n/a	0.842
9	0.898	n/a	0.730
Mean	0.937	0.861	0.750
SD	0.040	0.066	0.073

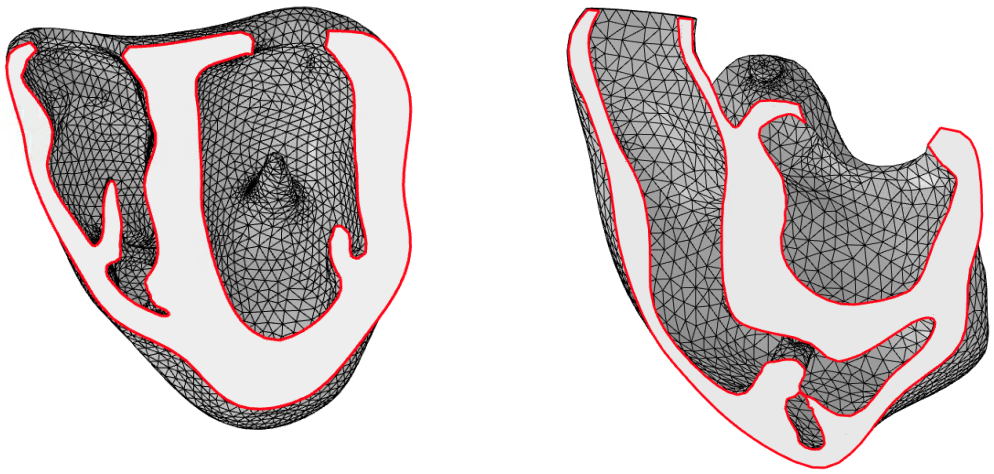

(a) Mesh cross-section 1 **(b)** Mesh Cross section 2

Figure B.5: Cross-sections of mesh Patient 2

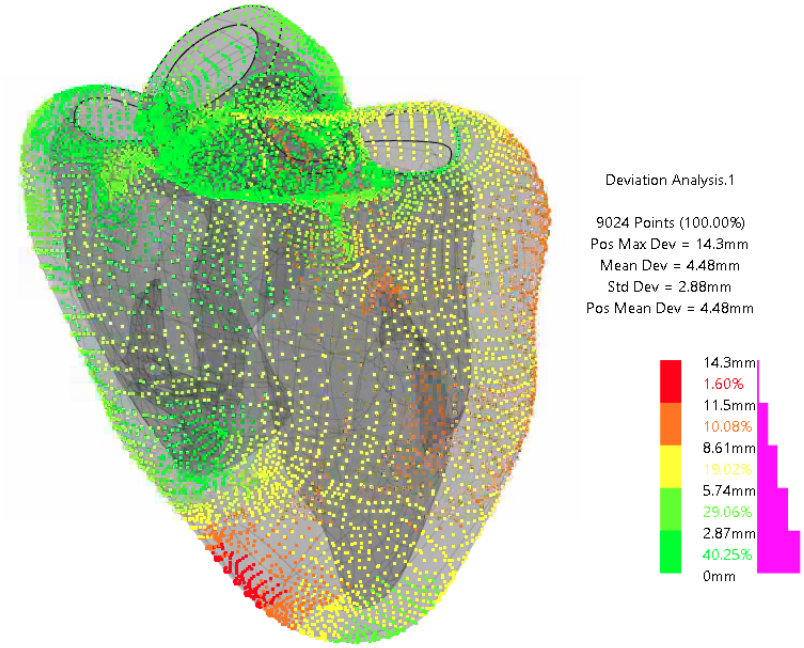

Figure B.6: Deviation analysis Patient 2

B.3. Patient 3

7-year-old male with TOF.

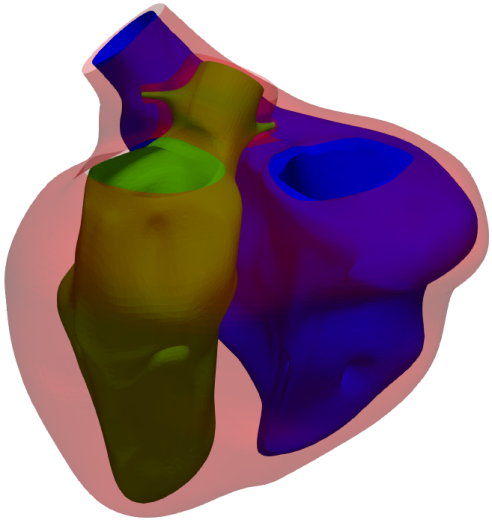

(a) Geometry. Red=epicardium, Green=LV endocardium, Blue=RV endocardium

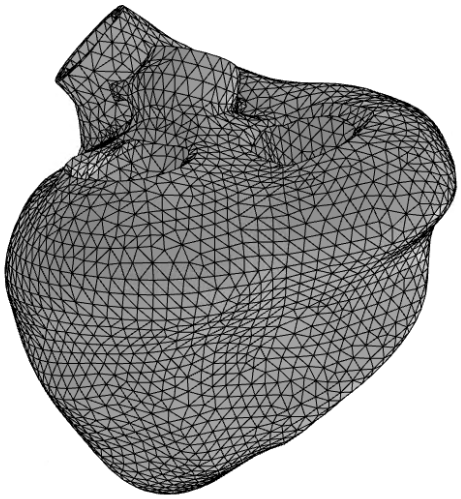

(b) Mesh

Figure B.7: Biventricular geometry and mesh Patient 3

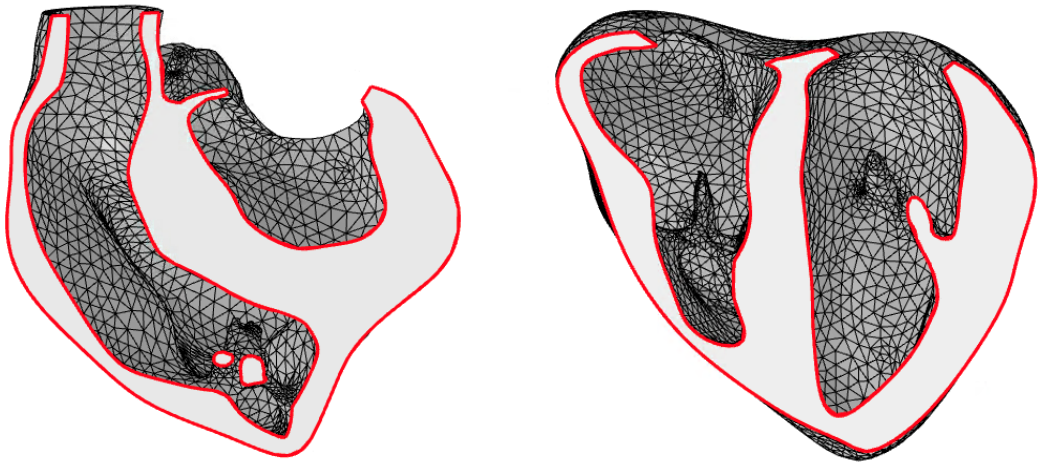

(a) Mesh cross-section 1 **(b)** Mesh Cross section 2

Figure B.8: Cross-sections of mesh Patient 3

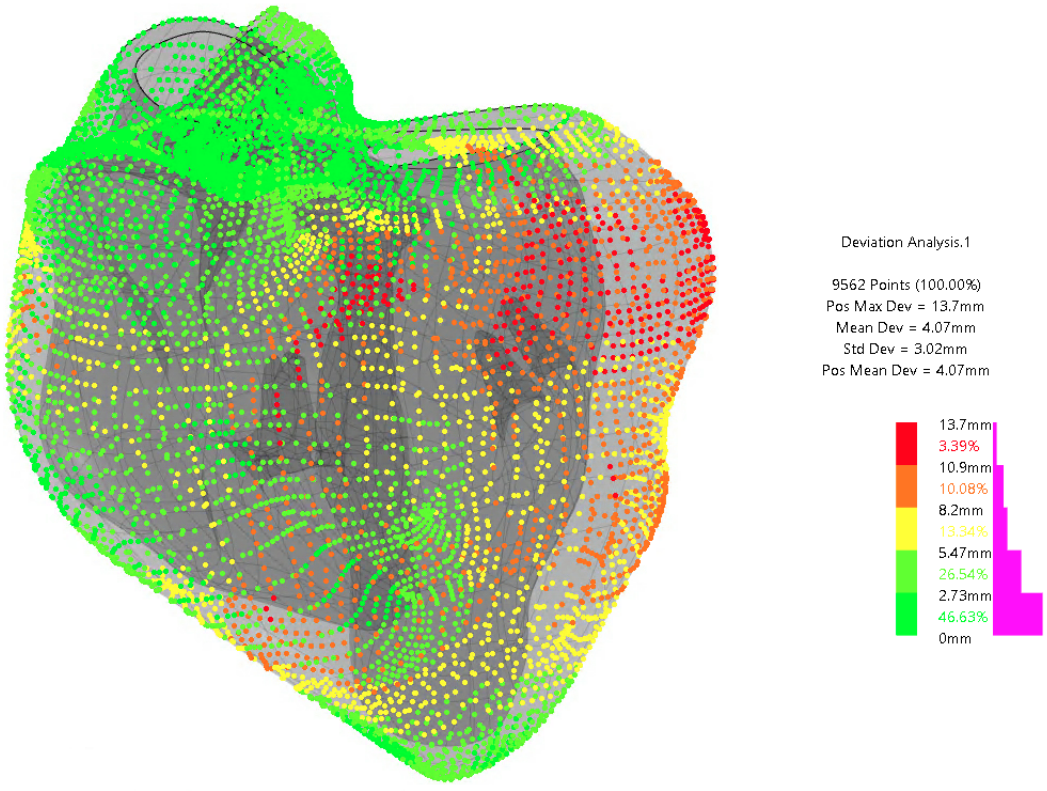

Figure B.9: Deviation analysis Patient 3

B.4. Patient 4

8-year-old male with TOF.

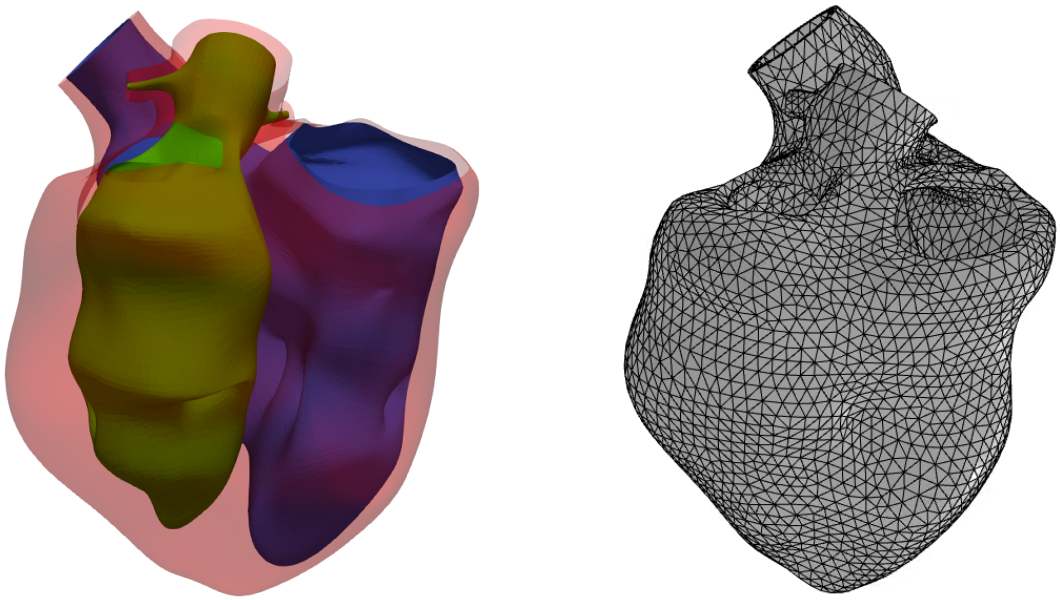

(a) Geometry. Red=epicardium, Green=LV endocardium, Blue=RV endocardium

(b) Mesh

Figure B.10: Biventricular geometry and mesh Patient 4

Table B.2: Local validation: Dice similarity coefficient results Patient 4

Scan slice	LV Blood volume	RV Blood Volume	Myocardium
1	0.981	0.555	0.414
2	0.975	0.888	0.778
3	0.981	0.857	0.754
4	0.968	0.840	0.743
5	0.975	0.775	0.805
6	0.979	0.850	0.788
7	0.929	0.897	0.599
8	0.954	0.880	0.809
Mean	0.968	0.818	0.711
SD	0.018	0.113	0.138

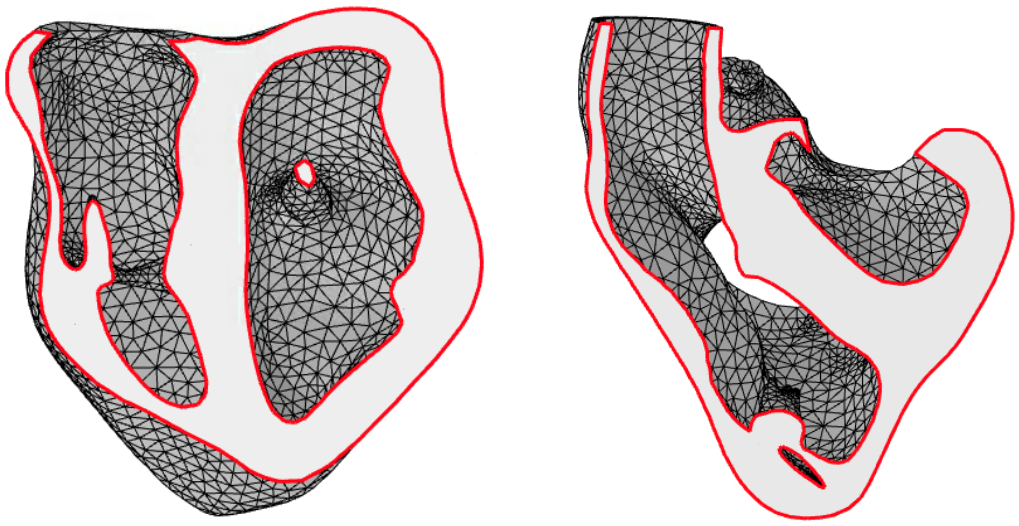

(a) Mesh cross-section 1 **(b)** Mesh Cross section 2

Figure B.11: Cross-sections of mesh Patient 4

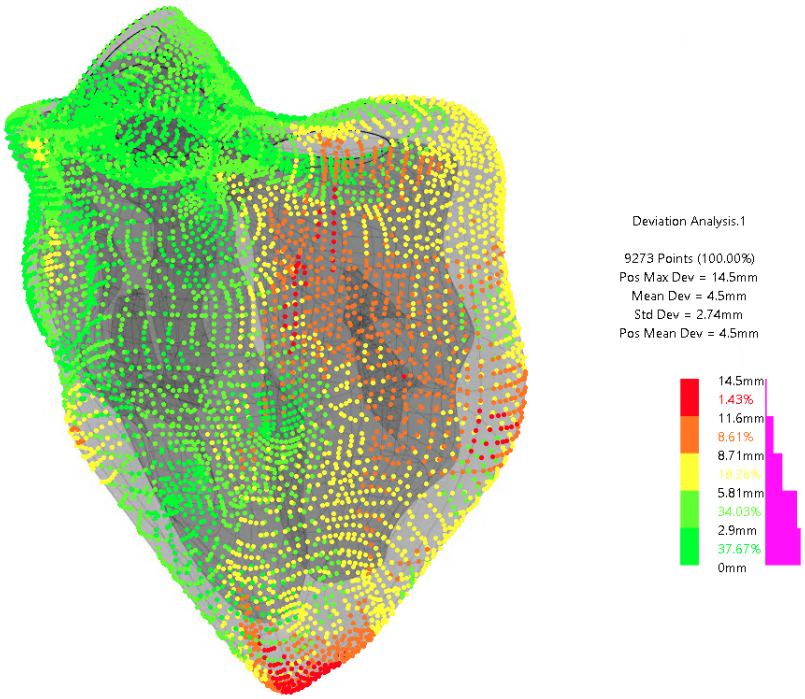

Figure B.12: Deviation analysis Patient 4

B.5. Patient 5

5-year-old male with Fontan physiology.

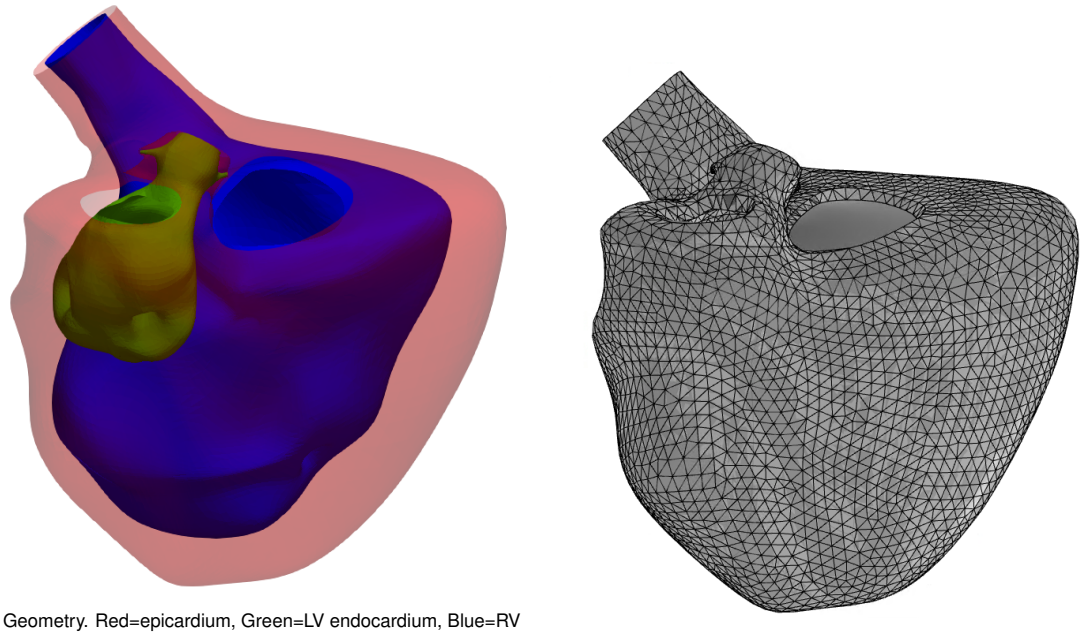

(a) Geometry. Red=epicardium, Green=LV endocardium, Blue=RV endocardium

(b) Mesh

Figure B.13: Biventricular geometry and mesh Patient 5

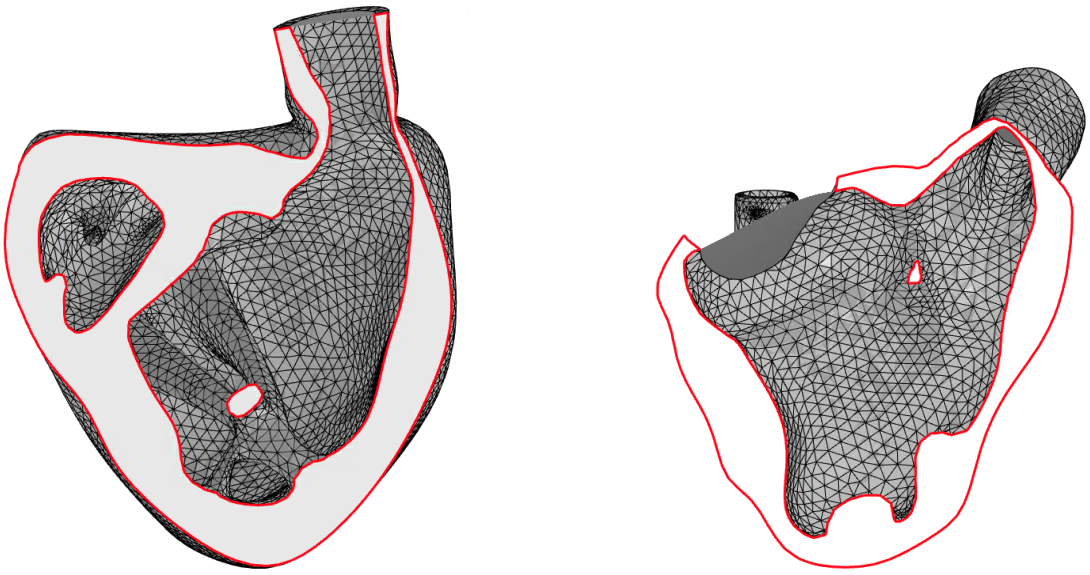

(a) Mesh cross-section 1

(b) Mesh Cross section 2

Figure B.14: Cross-sections of mesh Patient 5

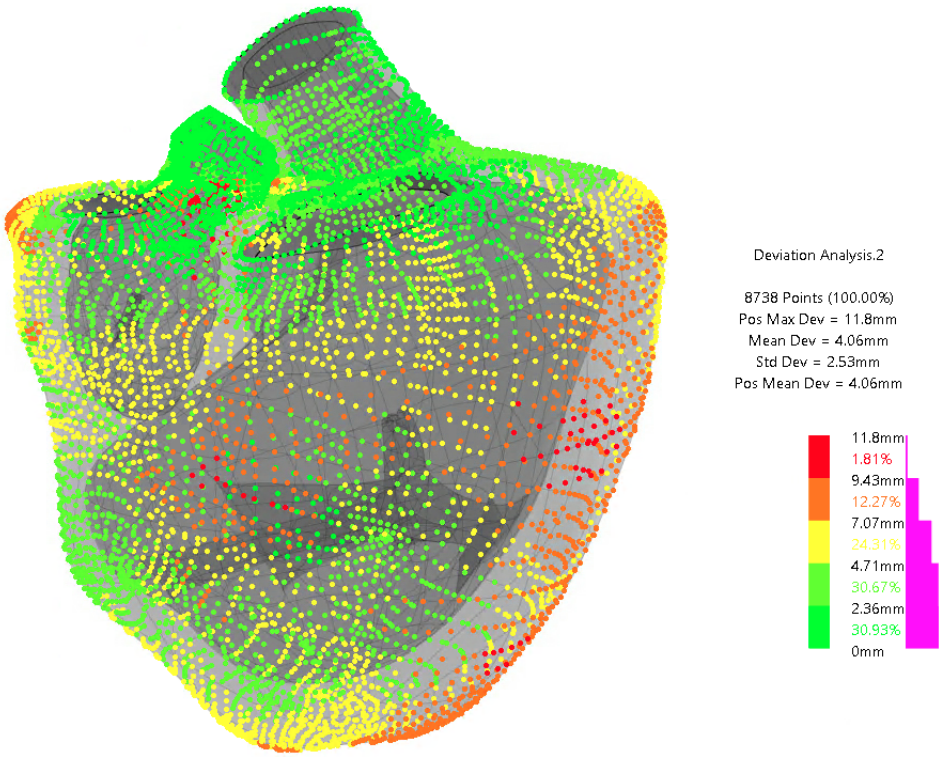

Figure B.15: Deviation analysis Patient 5

B.6. Patient 6

8-year-old male with Fontan physiology.

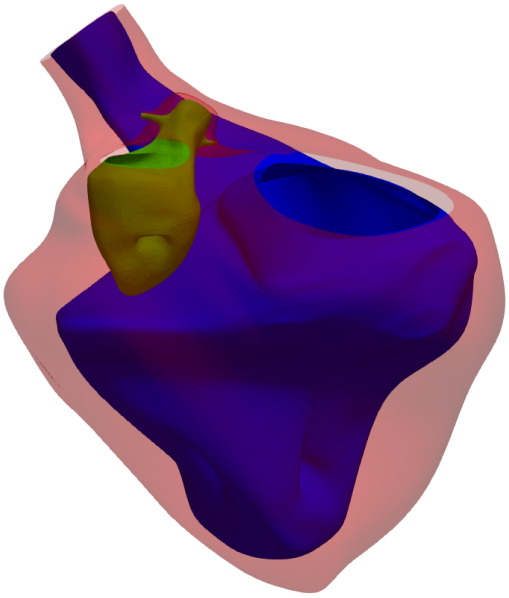

(a) Geometry. Red=epicardium, Green=LV endocardium, Blue=RV endocardium

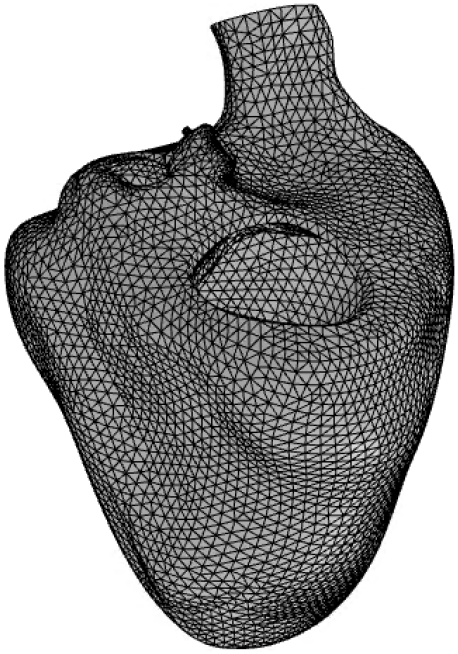

(b) Mesh

Figure B.16: Biventricular geometry and mesh Patient 6

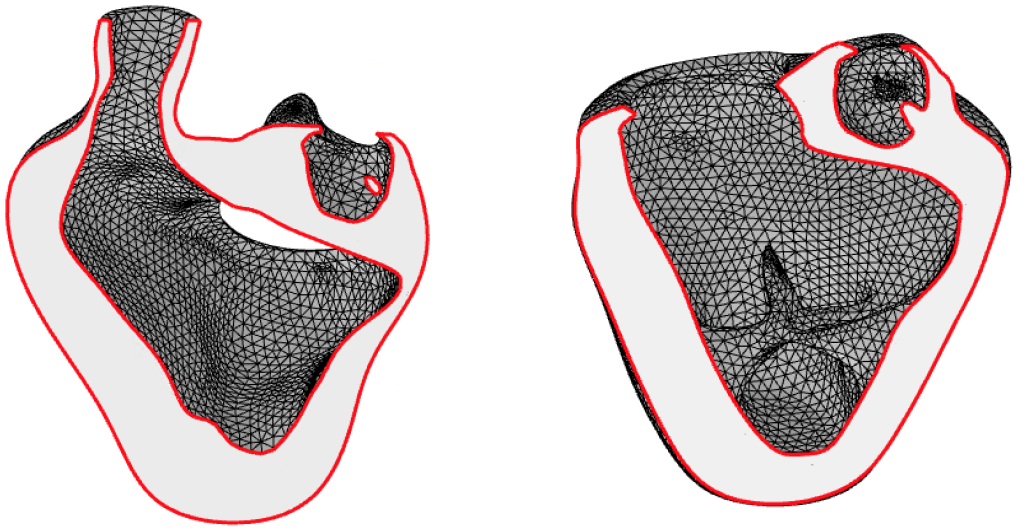

(a) Mesh cross-section 1 **(b)** Mesh Cross section 2

Figure B.17: Cross-sections of mesh Patient 6

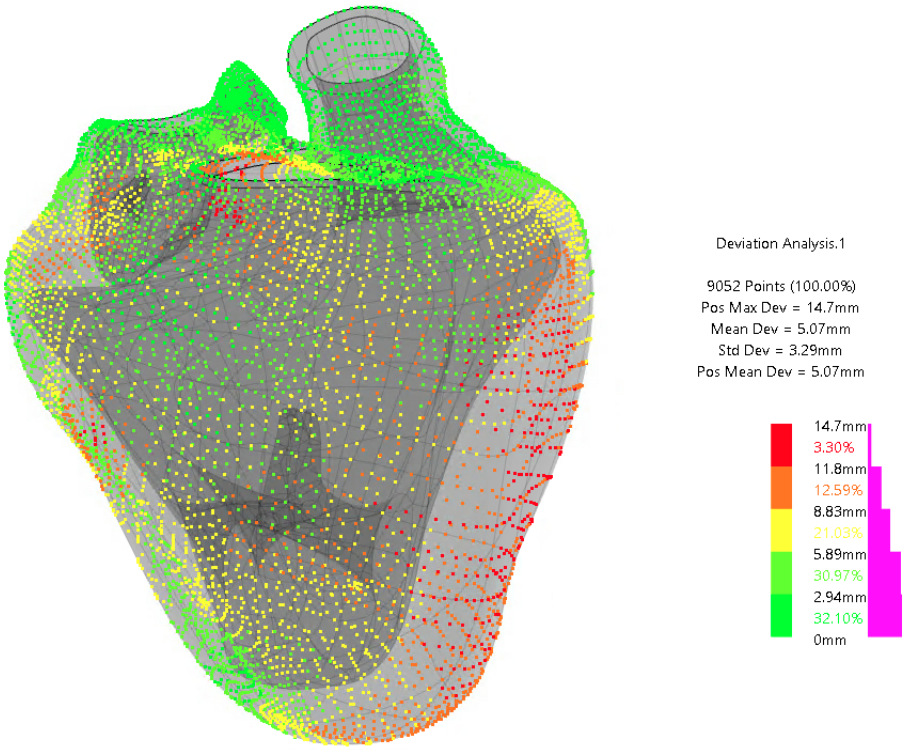

Figure B.18: Deviation analysis Patient 6

B.7. Patient 7

19-year-old male with Fontan physiology.

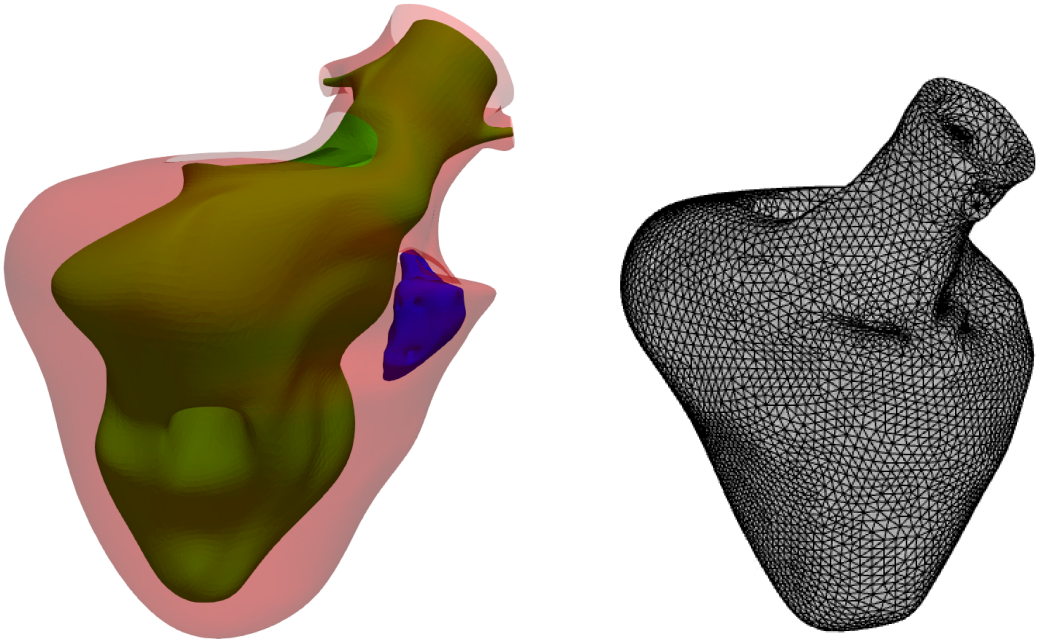

(a) Geometry. Red=epicardium, Green=LV endocardium, Blue=RV endocardium

(b) Mesh

Figure B.19: Biventricular geometry and mesh Patient 7

Table B.3: Local validation: Dice similarity coefficient results Patient 7

Scan slice	LV Blood volume	RV Blood Volume	Myocardium
1	0.916		0.838
2	0.975		0.831
3	0.914	0.935	0.766
4	0.946		0.821
5	0.905		0.821
6	0.977		0.890
7			0.843
Mean	0.939	0.935	0.830
SD	0.032		0.037

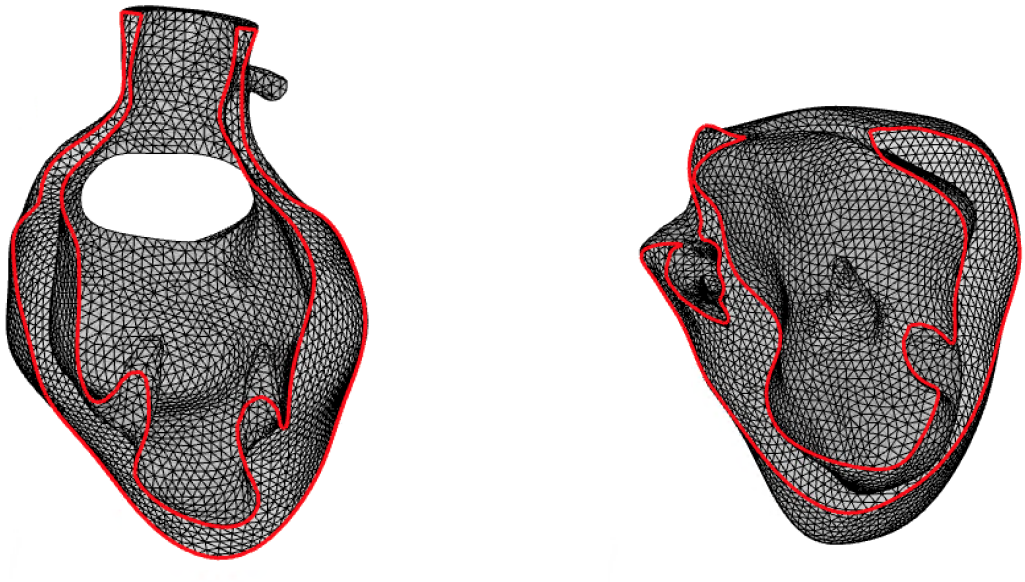

(a) Mesh cross-section 1 **(b)** Mesh Cross section 2

Figure B.20: Cross-sections of mesh Patient 7

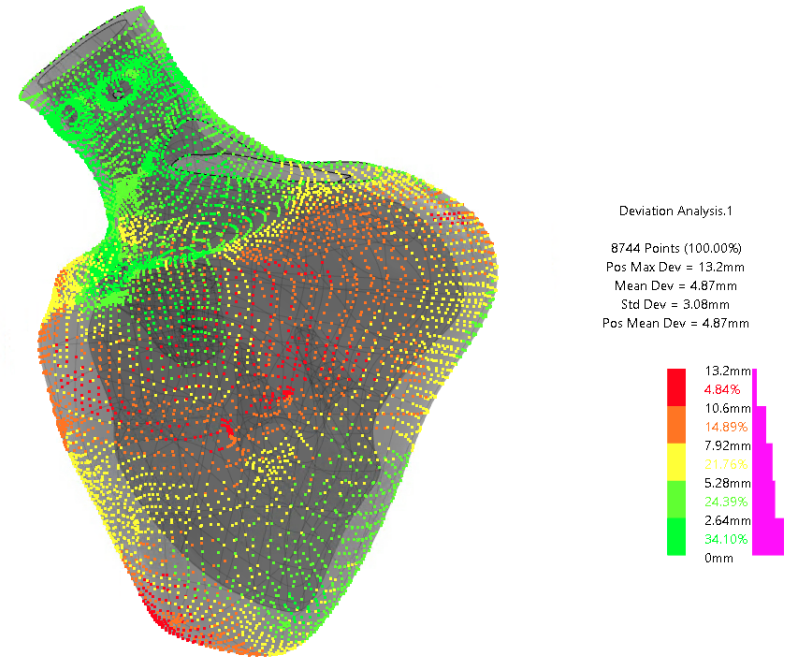

Figure B.21: Deviation analysis Patient 7

C

Manual Morphing Manual

This appendix provides a step-by-step description of the creation of a patient-inspired biventricular geometric model using parameter and manual morphing. The workflow in this appendix is equivalent to what is presented in Chapter 2 on methods and materials. The different sections describe the steps in detail. The final section is designated to the misalignment correction.

C.1. Data Acquisition

The first step is the acquisition of the imaging data. MRI data is used from 7 different patients. The age, sex and condition of these patients are listed in the Patient List in the Nomenclature chapter. Additional patient information is anonymized to protect the privacy of the patient. The MRI data is processed in Medis Suite.

1. Open Medis Suite
2. Select a patient and **Load** the patient data
3. Go to **QMass** to view the (already segmented) MRI slices.
4. Go to **Report** to view the measured ventricular data

A screen capture of Medis Suite is shown in Figure C.1. On the left side of the screen, the phases are shown and the right side shows an MRI slice. In this figure, the MRI is already segmented and the end-systole stage is visible. Color-coded contours are drawn to outline the locations of the ventricles. Here, the yellow contour represents the RV, green represents the LV epicardium, and red represents the LV endocardium. Additional contours can be added, such as the RV endocardium or the papillary muscles. Existing contours can also be adjusted.

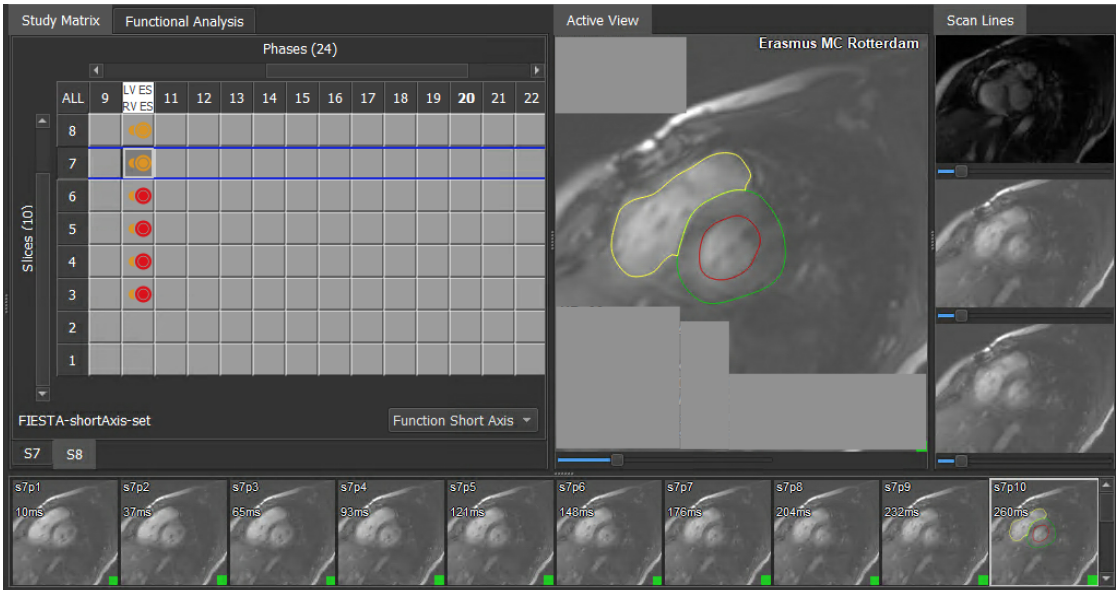

Figure C.1: Screen capture of Medis Suite.
MRI segmentation Yellow=RV, Green=LV epicardium and Red=LV endocardium

C.2. Image Processing

The second step is processing the imaging data into the reference geometry. This is done by using Paraview.

C.2.1. File format conversion from .vtp to .stl

1. Export the contours into .vtp files from Medis Suite.

   The exportation function may have to be activated. In that case, follow these steps:

   (a) Go to the file: `C:\ProgramFiles\Medis\Apps\QMass\8.1`.
   (b) Open the file **CF_Editor_User.cmd**.
   (c) Go to tab **Advanced** and in the menu select **Main**.
   (d) Make sure the option **Export Analysis File** is turned to **Enabled**.
   (e) Restart Medis Suite.

2. Open the .vtp files in Paraview.
3. The contours are numbered but not organized, as shown in Figure C.2.

   Group the contours of the endocardium and epicardium for each ventricle (or however desired). Select the individual contours, select **Add filter**, select **Append Geometry** and the click **Apply**. The contours of e.g. the epicardium of the left ventricle are now grouped, as shown in Figure C.3.
4. Turn the contours into solids by selecting the now called **AppendGeometry1**, select **Add filter**, select **Tube** and click **Apply**. The result of this step is shown in Figure C.4.
5. Save the data as .stl files.
6. Repeat steps 3-5 until all contours are saved as .stl files.

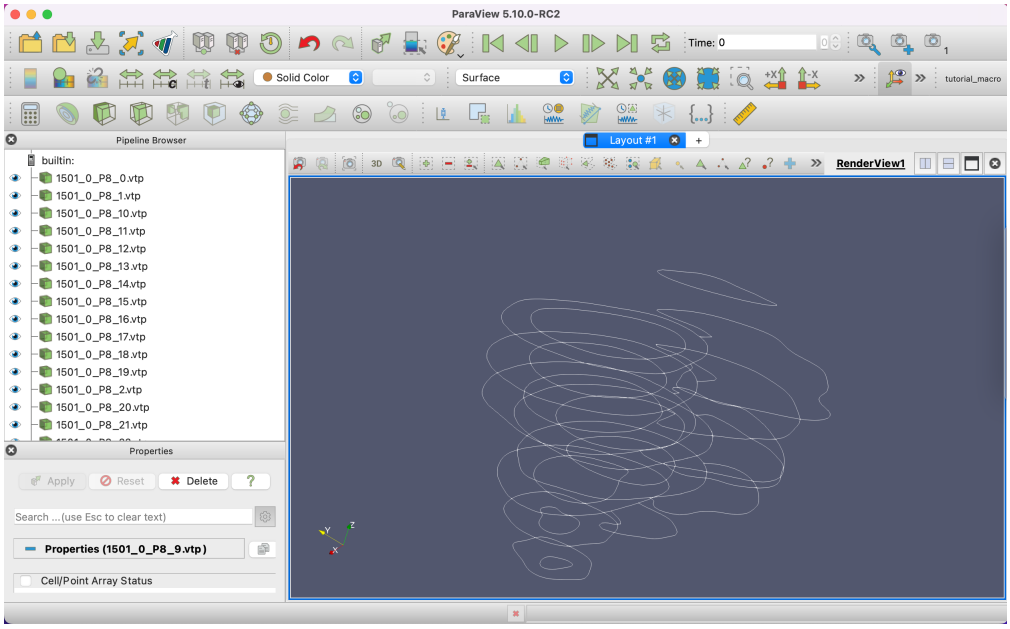

Figure C.2: Paraview capture of all contours

C.3. Geometry construction

The third step is the construction of the biventricular geometry. This section explains the use of the 3DEXPERIENCE platform and correctly scaling the ventricles.

C.3.1. 3DEXPERIENCE

The 3DEXPERIENCE platform by Dassault Systemes is used to design, construct, and analyze 3D models. 3DEXPERIENCE integrates multiple software products into a single platform.

1. Log in onto the 3DEXPERIENCE platform using the link: https://my.3dexperience.3ds.com/welcome.
2. First-time users can get familiar with the 3DEXPERIENCE platform by going to the **User Assistance**.
   (a) Select the **?** symbol at the top right corner to go to the **Help** menu and select the **3DEXPERIENCE User Assistance** option.
   (b) Familiarize yourself with the platform.
3. Another excellent resource for training is the **3DEXPERIENCE Edu Space** found here: https://eduspace.3ds.com/.
4. To get started, launch an application of CATIA (e.g. "Digitized Shape Preparation").

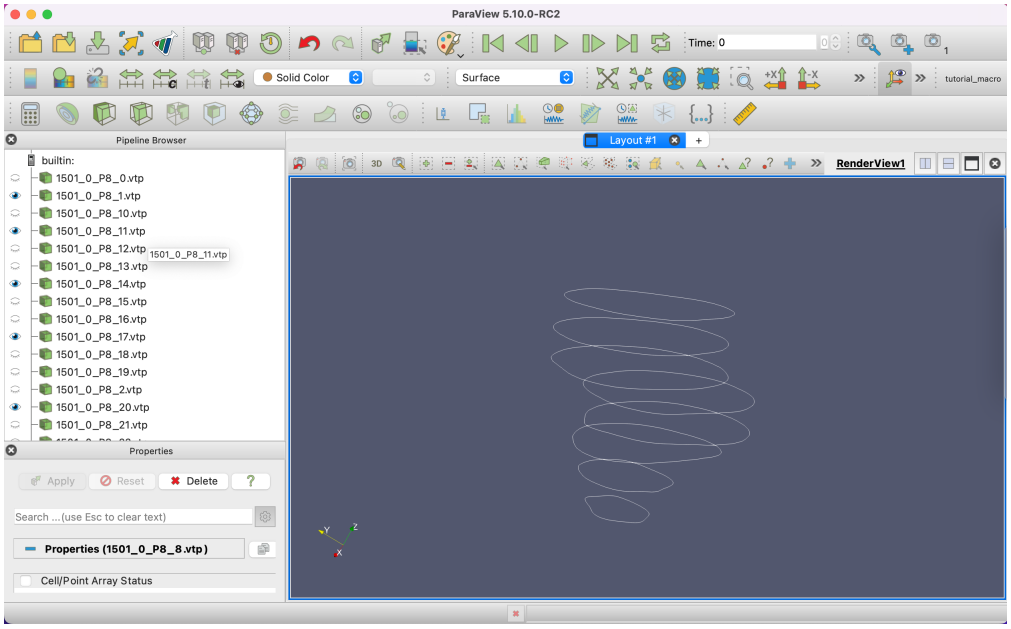

Figure C.3: Paraview capture of the LV contours

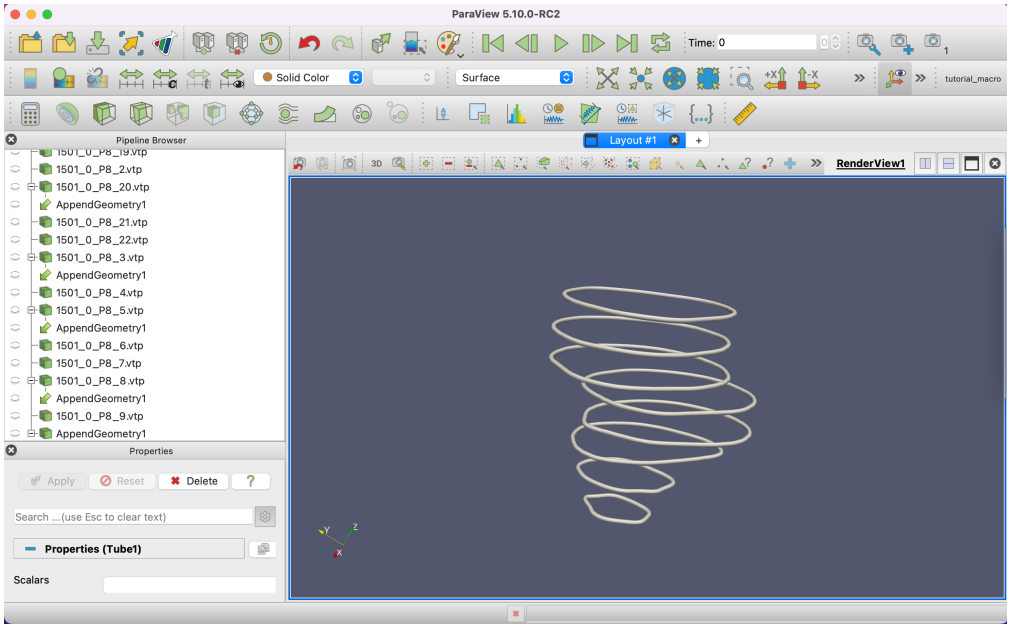

Figure C.4: Paraview capture of the LV contours.
After applying the tube filter

C.3.2. Scaling

Next in the geometry constructing is the scaling step. This section covers the steps of scaling the biventricular subdivision of the Living Heart Human Model to a size specific to a patient. The scaling is done inside CATIA and can be done using the "Digitized Shape Preparation" application.

1. Download and open the LHHM. The surface model of the LHHM is shown in Figure C.5.

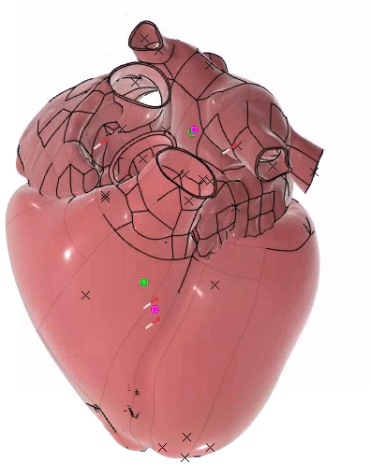

Figure C.5: LHHM

2. Work inside the Ventricles submodel of the LHHM or copy/paste the subdivision surfaces of the ventricles into a new product file.
3. Turn on the manual update mode.
4. Double-click the left endocardium subdivision to make the **Tools palette** appear (shown at the top in Figure C.6) and to start editing.
5. Select all nodes in the left endocardium and select the **affinity** tool.
6. Change the axis origin to **LHHM axis system** to ensure consistency when scaling different parts.
   (a) Select **Robot definition** and the **Pick** tool.
   (b) Pick the axis system **LHHM axis system** inside the model tree.
   (c) Click **Robot definition** again to exit this action.
7. Select **Edition**. The affinity dimensions appear as shown in Figure C.6.
8. Adjust the **Fx**, **Fy** and **Fz** values by multiplying them by the same scaling factor. The general size of the endocardium now fits the reference contours and click **OK** and exit. The result of this step is shown in Figure C.7. In this example, a scaling factor of 0.6 is used.
9. Repeat steps 4-8 for the right endocardium.
10. After scaling the left endocardium and right endocardium, the model looks like Figure C.8a. This figure shows Patient 5. Next, update the epicardium as shown in Figure C.8b.
11. In complex CHDs, such as HLHS, updating the epicardium can result into twisted and relocated nodes. An example of this is shown in Figure C.9. Here, a faulty thickness update is clearly visible as the epicardium intersects with the endocardium of the RV. There are also twisted and relocated nodes around the aortic arch. This can be detected by

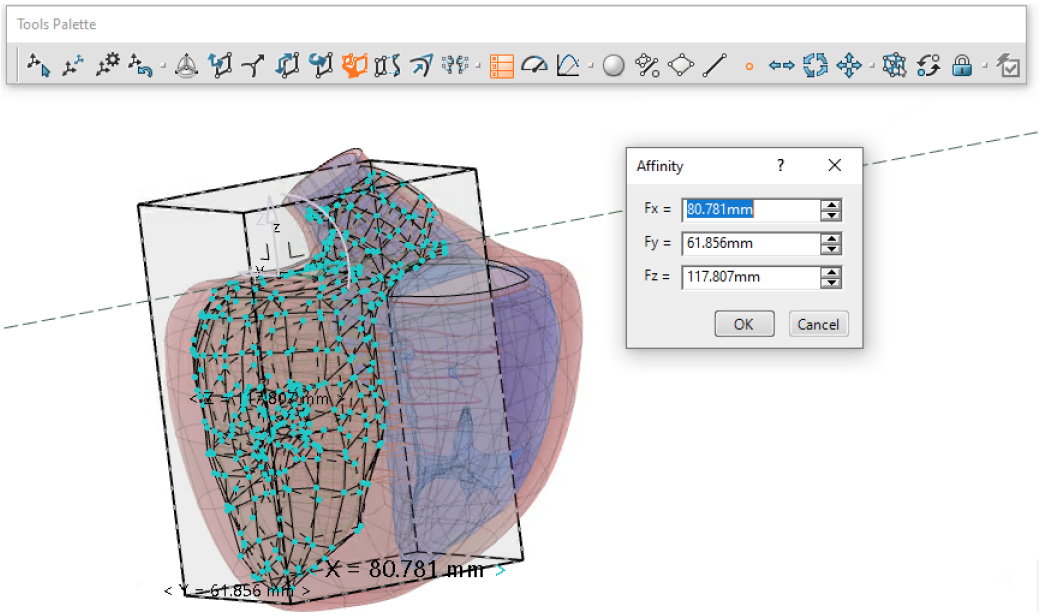

Figure C.6: Affinity dimensions.
Scaling opting with Tools Palette shown at the top.

the uneven and intersecting surfaces. The twisted surface has to be manually corrected. Techniques used to do this are explained in the manual morphing section below.

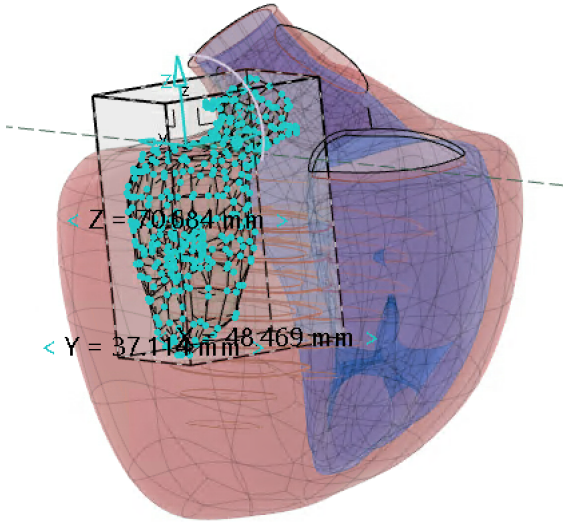

Figure C.7: Scaling of the left endocardium

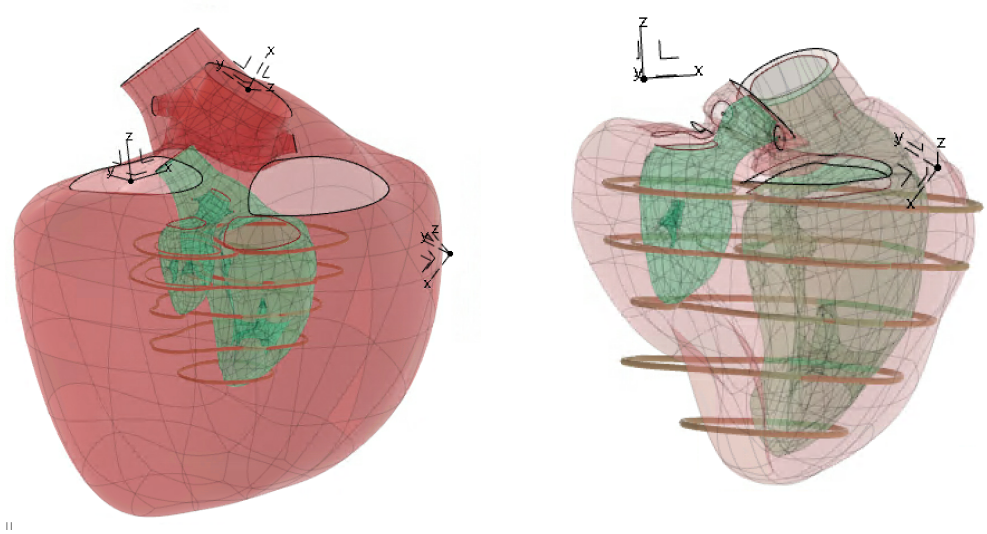

(a) Scaling of the left and right endocardium

(b) Updated epicardium

Figure C.8: Scaling surface model
Biventricular geometric surface model before and after updating the subdivision surface of the epicardium after scaling the endocardium. Also showing the reference geometry.

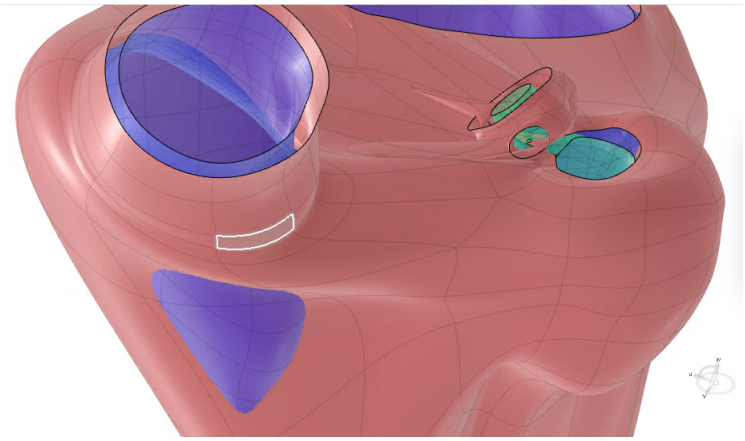

Figure C.9: Scaling errors.
Intersecting surfaces after updating the subdivision surface of the epicardium

C.4. Patient-Specific model

The fourth step is creating the patient-specific model. First, the reference geometry is aligned to the biventricular model, after which it can be edited using parameter and manual morphing.

C.4.1. Importing and aligning the reference geometry

The reference geometry is imported in CATIA using the "Digitized Shape Preparation" application.

1. Open the now scaled subdivision surfaced of the biventricular model.
2. Create a new geometrical set inside the model tree and import the reference geometry in this set.
   (a) Go to the **+** symbol at the top right corner, select **Import**, select **Digitization File**, click **Import a file**, find and open the correct file and click **OK**.
   (b) Name the file and click **OK**.
3. The subdivision surfaces and reference geometry are now in the same file, but not correctly aligned. Figure C.10 shows where the reference model is imported in regards to the biventricular model. A ruler is included for reference. In this example, they are about 1300 mm apart in the y-direction. The reference geometry has to be aligned with the model.

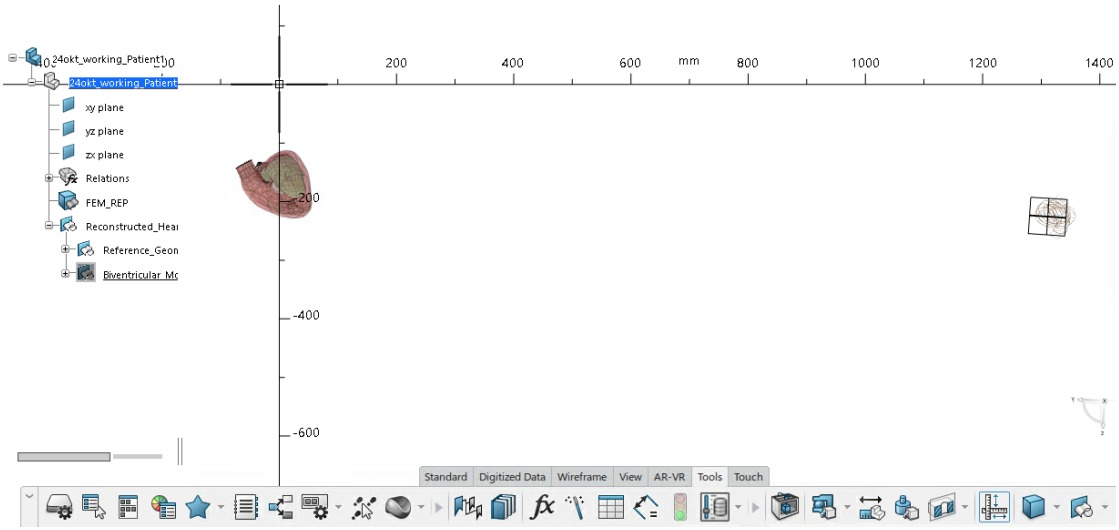

Figure C.10: Align the reference geometry using the robot

   (a) Go to the **Digitized data** tab inside the "Digitized Shape Preparation" application and select **Align using the robot**. See Figure C.11 for an illustration of this step.
   (b) For **Cloud to align**, pick the reference geometry.
   (c) Translate and rotate the reference geometry using the robot.
   (d) Reiterate this process until the reference geometry is correctly aligned with the subdivision surfaces of the ventricles.
   (e) If the aligning is performed one contour set at a time (for example the left endocardium separately from the right endocardium), use the **Axis To Axis tool** (Figure C.12) to transform the rest of the contours (from the other ventricle) to their corrected location.
      i. For **Element** select the contours to relocate.

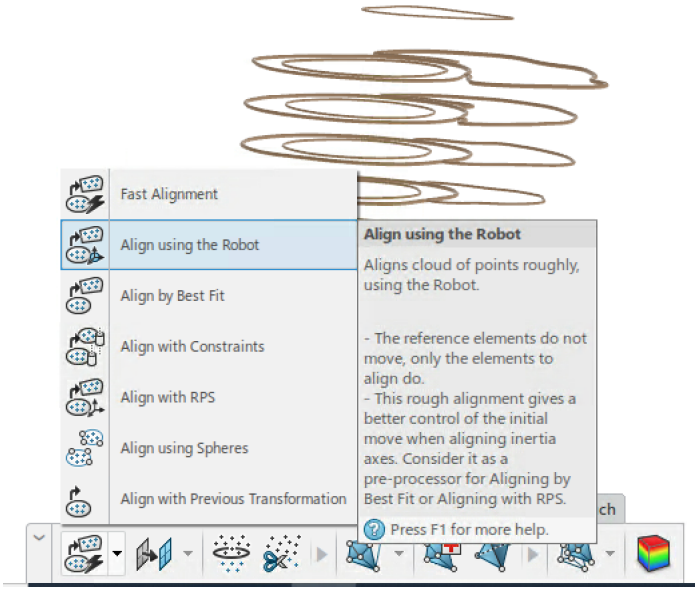

Figure C.11: Align using the Robot

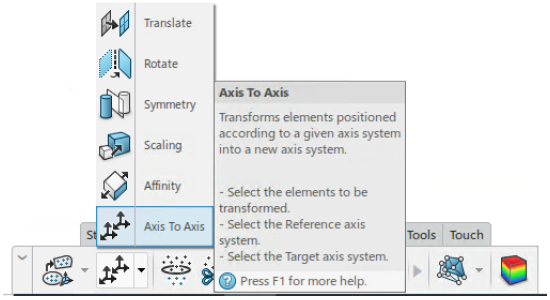

Figure C.12: Axis To Axis tool

ii. For **Reference** select AxisRef1 and for **Target** select AxisTrs1. These axis systems are created after translation using the robot and found under Axis Systems in the model tree.

iii. When multiple translations are performed, multiple reference and target axis systems are created. Repeat the axis to axis steps for all axis systems pairs.

(f) All contours should now be correctly transformed. **Isolate** the transformations to make them independent from the previous transformations.

4. The model is now ready to be (manually) morphed.

C.4.2. Parameter morphing

Before manual morphing of the model, parameter morphing can be used. This is a quick way to make modifications to the model. The parameter changes are performed on the endocardium of the left ventricle. The epicardium must be updated after changing the parameters. The parameters which can be morphed are listed below. A capture of the model tree with the

parameters is shown in Figure C.13.

- The Long Axis Length
- The Septal Long Axis Angle
- The Ant/Post Long Axis Angle
- Top LV Diameter
- Mid LV Diameter
- Apex LV Diameter

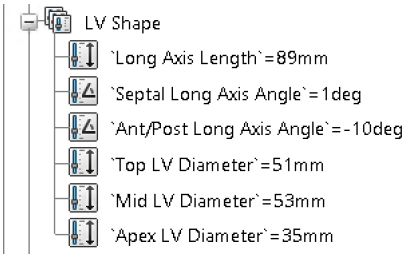

Figure C.13: Parameter morphing options from the model tree

The following steps describe the process of parameter morphing. The long axis length is taken as an example.

1. Turn on the manual update mode.
2. Go to the **Tools** tab and select the **Ruler**. Use the ruler to measure how much the long axis length of the ventricle needs to be increased or decreased.
3. Double-click the parameter to adjust the value.
4. Update the left endocardium.
5. Repeat until the parameters match the reference geometry. Figure C.14a shows the biventricular model before parameter morphing. Figure C.14b shows the same model after increasing the long axis length with 16 mm.

Figure C.15a shows the biventricular model before parameter morphing. Figure C.15b shows the same model after decreasing the septal long axis angle with 6 degrees.

(a) Long Axis Length = 89 mm

(b) Long Axis Length = 105 mm

Figure C.14: Parameter morphing: Long Axis Length

(a) Septal Long Axis Angle = +1 deg

(b) Septal Long Axis Angle = -5 deg

Figure C.15: Parameter morphing: Septal Long Axis Angle

Figure C.16a shows the biventricular model before parameter morphing. Figure C.16b shows the same model after decreasing the ant/post long axis angle with 12 degrees.

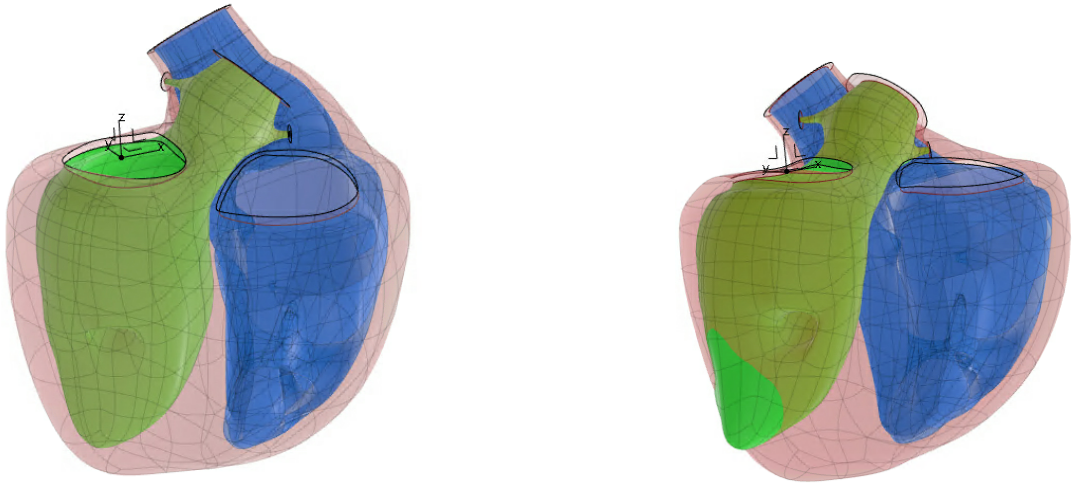

(a) Ant/Post Long Axis Angle = -10 deg

(b) Ant/Post Long Axis Angle = -22 deg

Figure C.16: Parameter morphing: Ant/Post Long Axis Angle

Figure C.17a shows the biventricular model before parameter morphing. Figure C.17b shows the same model after increasing the top LV diameter with 29 mm.

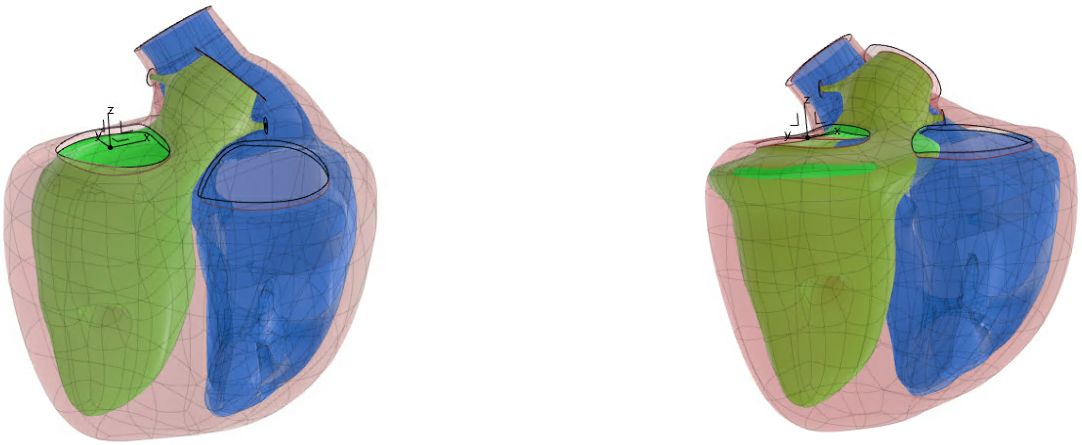

(a) Top LV diameter = 51 mm

(b) Top LV diameter = 80 mm

Figure C.17: Parameter morphing: Top LV diameter

Figure C.18a shows the biventricular model before parameter morphing. Figure C.18b shows the same model after increasing the mid LV diameter with 17 mm.

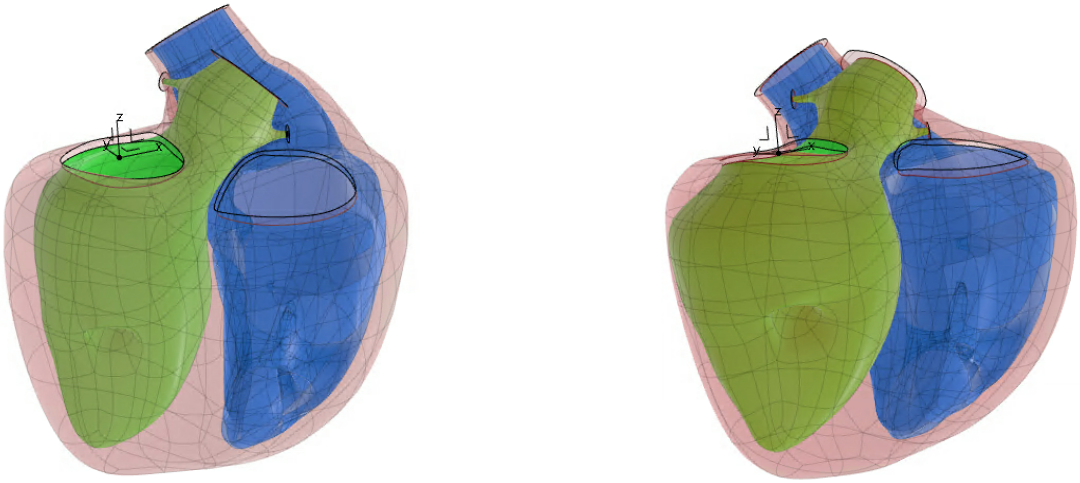

(a) Mid LV diameter = 53 mm **(b)** Mid LV diameter = 70 mm

Figure C.18: Parameter morphing: Mid LV diameter

Figure C.19a shows the biventricular model before parameter morphing. Figure C.19b shows the same model after increasing the apex LV diameter with 15 mm.

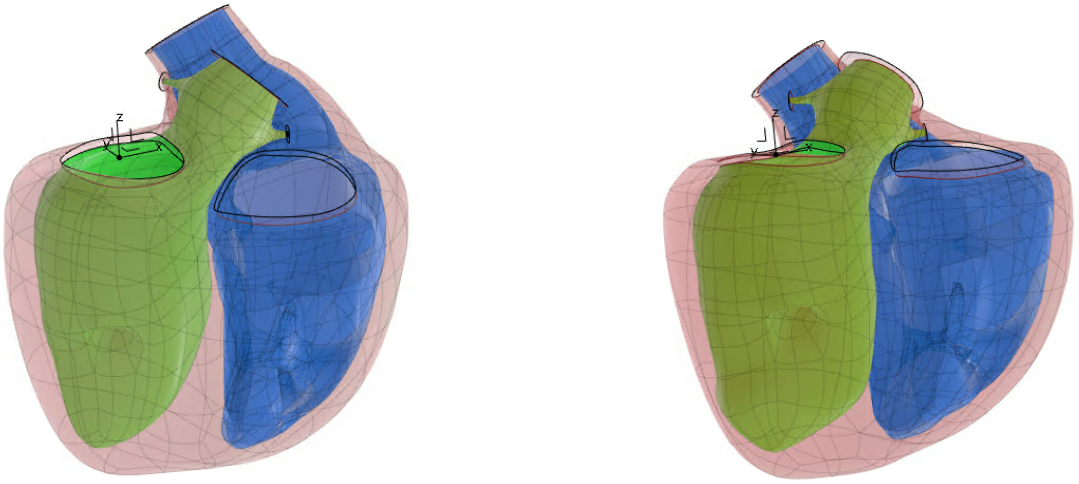

(a) Apex LV diameter = 35 mm **(b)** Apex LV diameter = 50 mm

Figure C.19: Parameter morphing: Apex LV diameter

C.4.3. Manual morphing

Manual morphing is performed to make local surface modifications to the biventricular subdivision surfaces. There are various different selection functions and surface modification tools available in the "Generative Shape Design" application in CATIA. The relevant functions and tools to this project will be highlighted here. All tools are found in the Tools Palette (Figure C.20).

Figure C.20: Tools Palette

1. To start manual morphing, double-click the subdivision of the left endocardium and the Tools Palette will appear.
2. Use the point tool to select an individual or group of nodes. There are some options:
   (a) Click and select individual nodes
   (b) Click and select multiple nodes by holding the **Control** (or **Command**) key.
   (c) Select multiple nodes by using **loop propagation**, see Figure C.21b. Here, the nodes around the mitral valve annulus ring are selected using loop propagation.

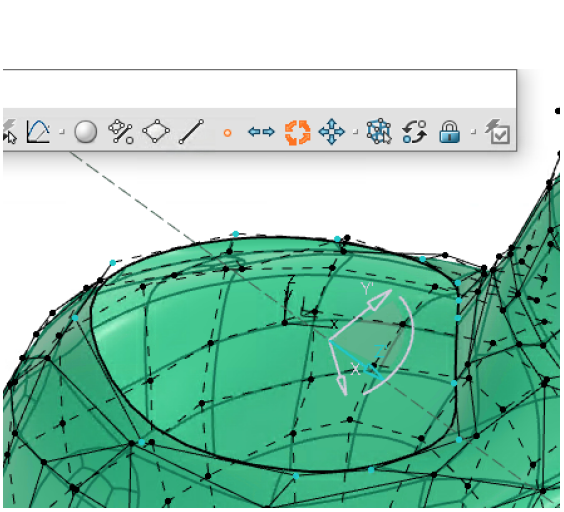

(a) Selecting nodes around the mitral valve annulus ring using loop propagation

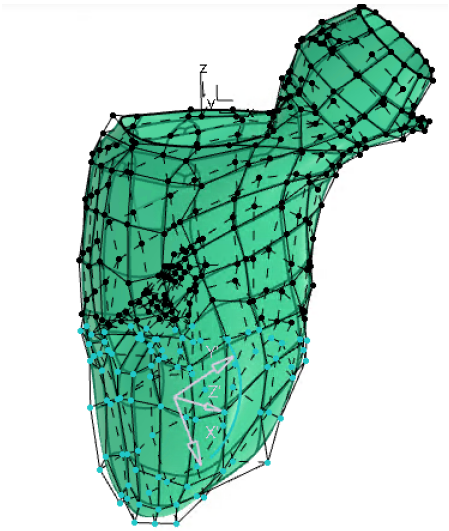

(b) Selecting multiple nodes using trapping

Figure C.21: Different options of selecting multiple nodes.

   (d) Select multiple nodes using **trapping**. Use **Control** + **Shift** + **select** the region to trap nodes. Figure C.21b shows that all nodes in the bottom part of the left endocardium are selected using trapping.

3. There are different surface modification tools that can be used.
   (a) The **translation** tool can be used to translate vertices based on the robot. The orientation of the robot can be adjusted. Figures C.22a and C.22b show this tool before and after a modification.

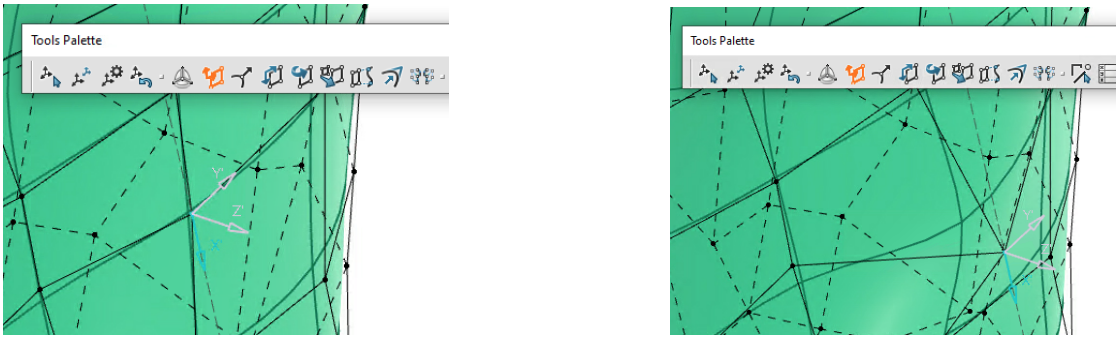

(a) Before **(b)** After

Figure C.22: Manual morphing using the robot tool

(b) The **local normal** tool can be used to translate vertices according to their normal directions, independent of the orientation of the robot. Figures C.23a and C.23b show this tool before and after a modification.

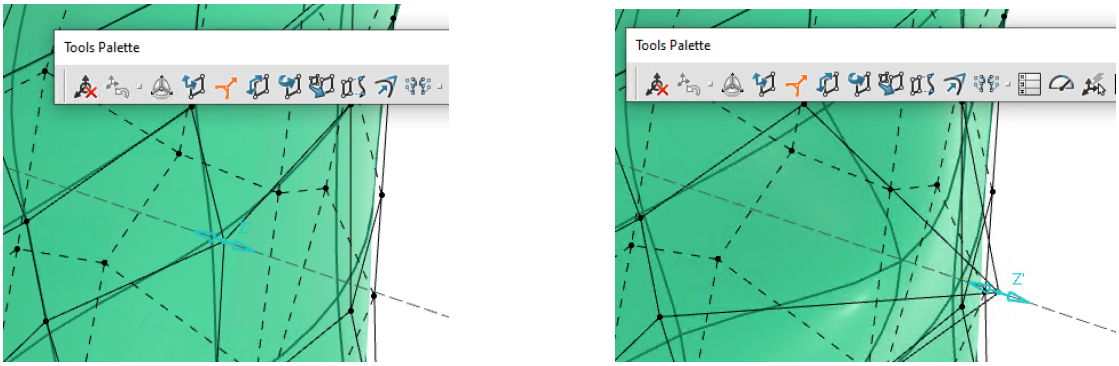

(a) Before **(b)** After

Figure C.23: Manual morphing using the local normal tool

(c) The **mesh lines** tool can be used to translate vertices along their links to other vertices. Figures C.24a and C.24b show this tool before and after a modification.

4. Use these functions and tools to continue refining the surface until it matches the reference geometry. As an example, Figure C.25a shows the LV endocardium of Patient 4 before manual morphing. Figure C.25b shows the same patient after manual morphing of the subdivision surface.
5. Repeat steps 1-4 and manually morph the right endocardium.
6. Update the epicardium.
7. Repeat steps 1-4 and manually morph the epicardium.

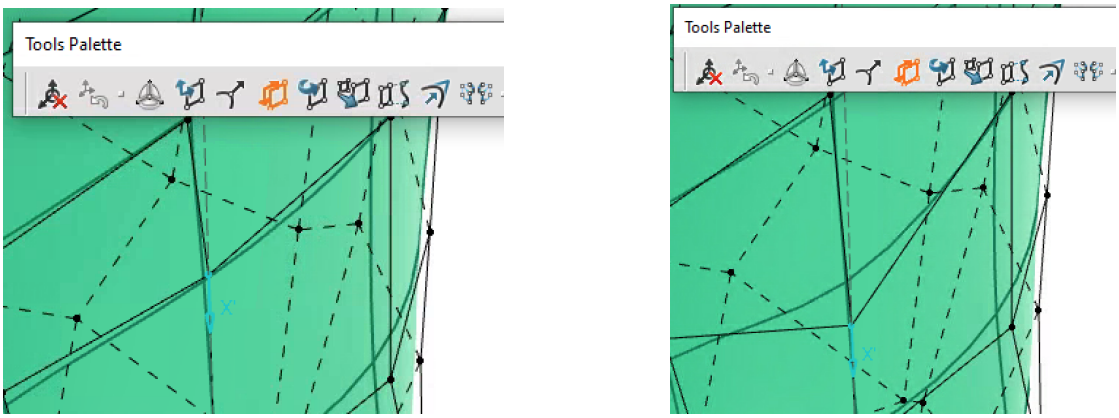

(a) Before **(b)** After

Figure C.24: Manual morphing using mesh lines

(a) Before **(b)** After

Figure C.25: Manual morphing
Comparing the LV endocardium of Patient 4 with its reference geometry before and after manual morphing

C.5. Mesh

The fifth and final step of the workflow is the creation of the mesh. Before that, a number of closed surfaces are to be made. These are used for volume measurements, but also as the basis for the mesh.

C.5.1. Blood volume

The first closed surface is made to measure the blood volume of the ventricle. It is created inside the "Generative Shape Design" application.

1. First, the construction geometry surfaces are created. These are fill surfaces on the openings of the ventricles.
   (a) In the **Surface** tab, select the **Fill** tool.
   (b) In **Outer boundaries** select all boundary lines of the mitral valve and click **OK**.
   (c) A fill surface is created to close the mitral valve opening in the subdivision surface of the LV.
   (d) Do the same for the aortic arch, left coronary artery and right coronary artery.
2. Select the **Join** tool and include the LV endocardium and the fill surfaces of the MV, AA, LCA and RCA. These surfaces are now joined.
3. Go to the "Part Design" application.
4. In the **Essentials** tab, select the **Closed surface tool**. Pick the just created Join to close. The result of a closed surface of the LV is shown in Figure C.26.

Figure C.26: Closed surface of the LV endocardium, Patient 1

   (a) If an error occurs, there is an overlapping surface or misplaced node.

   (b) Study the subdivision to find the error and go back to manual morphing to fix it.

5. Measure the blood volume of the ventricle.

   (a) In the **Tools** tab, select **Measure Inertia Part** and pick the closed surface as the input.
   (b) This tool then provides the volume of the ventricle, among other measurements.

6. Repeat steps 1-5 for the RV. This time, make fill surfaces for the tricuspid valve and pulmonary trunk.

C.5.2. Integrated ventricle

The next closed surface to create is the integrated ventricle, which represents the muscle layer of the heart. In short, this means the full heart volume minus the blood volumes of the two ventricles.

1. Again, fill surfaces are made. But this time, the openings between the epicardium and endocardium are filled. For clarity, they are called end surfaces.

   (a) In the **Surface** tab, select the **Fill** tool.
   (b) In **Outer boundaries** select all boundary lines of the MV of the epicardium. In the **Inner boundaries** select all boundary lines of the MV of the endocardium and click **OK**.
   (c) An end surface is created to close the opening between the epicardium and endocardium around the mitral valve.
   (d) Do the same for the aortic arch, left coronary artery and right coronary artery.

2. Repeat step 1 for the right ventricle. Figure C.27a shows the subdivision surfaces of the ventricles with the end surfaces depicted in gray.
3. Select the **Join** tool and include the epicardium, LV and RV endocardium, and the end surfaces of the MV, AA, LCA, RCA, TV and PT. These surfaces are now joined.
4. Go to the "Part Design" application.
5. In the **Essentials** tab, select the **Closed surface tool**. Pick the just created Join to close. Figure C.27a shows the subdivision surfaces of the ventricles with the end surfaces depicted in gray. Figure C.27b shows an enlarged view of the MV. There is clearly an overlapping surface. This will give an error.

   (a) Study the subdivision to find the error and go back to manual morphing to fix it.

6. Measure the mass of the integrated ventricle.

   (a) In the **Tools** tab, select **Measure Inertia Part** and pick the closed surface as the input.
   (b) This tool provides the volume among other measurements.
   (c) Multiply the volume by the density of cardiac muscle to obtain the mass of the ventricles.

C.5.3. Mesh

The mesh is created inside the "Structural Model Creation" application in SIMULIA.

1. Make a triangular surface mesh.

   (a) Go to the **Mesh** tab and select **Surface Triangle Mesh**.

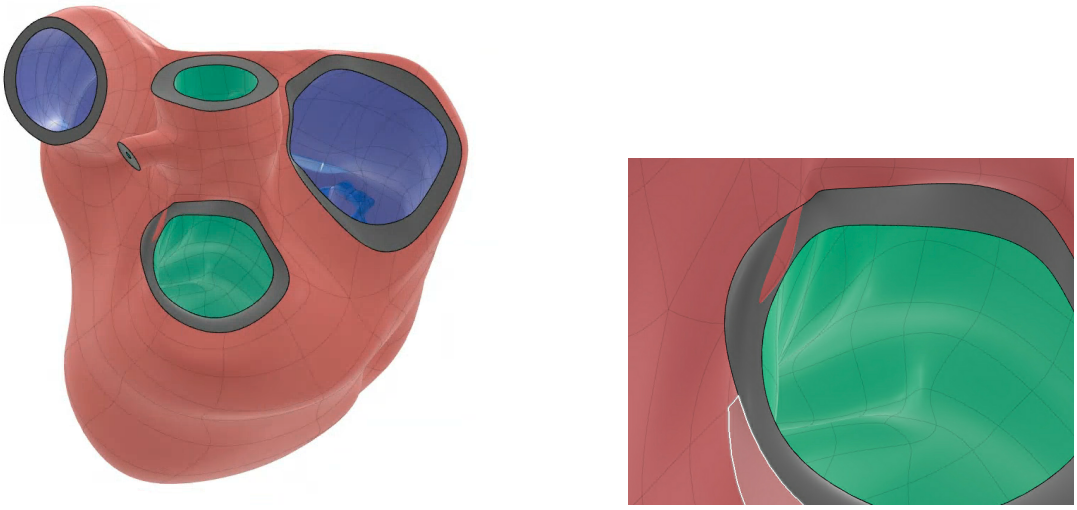

(a) Subdivision surfaces of the ventricles

(b) Enlarged view of the MV with overlapping surface

Figure C.27: Subdivision surfaces of the ventricles.
End surfaces depicted in gray

(b) Pick the integrated ventricle closed surface created in the previous section as the **Support**.
(c) Fill in **Mesh size** of 3 mm, **Absolute sag** of 0.2 mm and **Offset** of 0 mm.
(d) Click **Mesh** to create the mesh. See Figure C.28 for the Surface Triangle Mesh parameters.

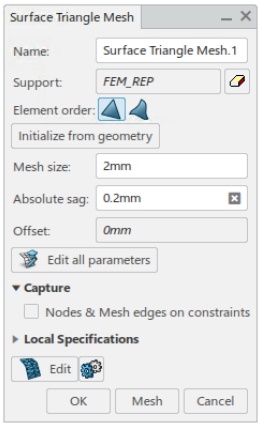

Figure C.28: Parameters Surface Triangle Mesh

2. Make a tetrahedron filler.

(a) Go to the **Mesh** tab and select **Tetrahedron Filler Mesh**.
(b) Pick the created Surface Triangle Mesh as the **Support**.
(c) Choose **Quadratic** as the **Element type**.

(d) Click **Mesh** to create the mesh. See Figure C.29 to see the Tetrahedron Filler parameters.

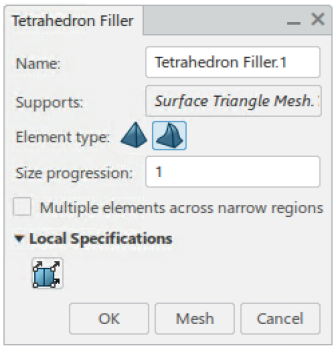

Figure C.29: Parameters Tetrahedron Filer

3. Right click the Tetrahedron Filler mesh in the model tree and select **Analyze**. The mesh **Quality Report** appears.
4. Bad elements lead to errors. If present, find the location of the bad elements and go back to the manual morphing step to edit the subdivision surface.
   (a) Bad elements can be caused by intersecting surfaces, surfaces that are not smooth, twisted nodes or a wall thickness that is too thin.
5. Reiterate until all bad elements are resolved. Figure B.13b shows an example of a created mesh (of Patient 5). Figure C.30b shows the same mesh made transparent displaying the left and right endocardium.

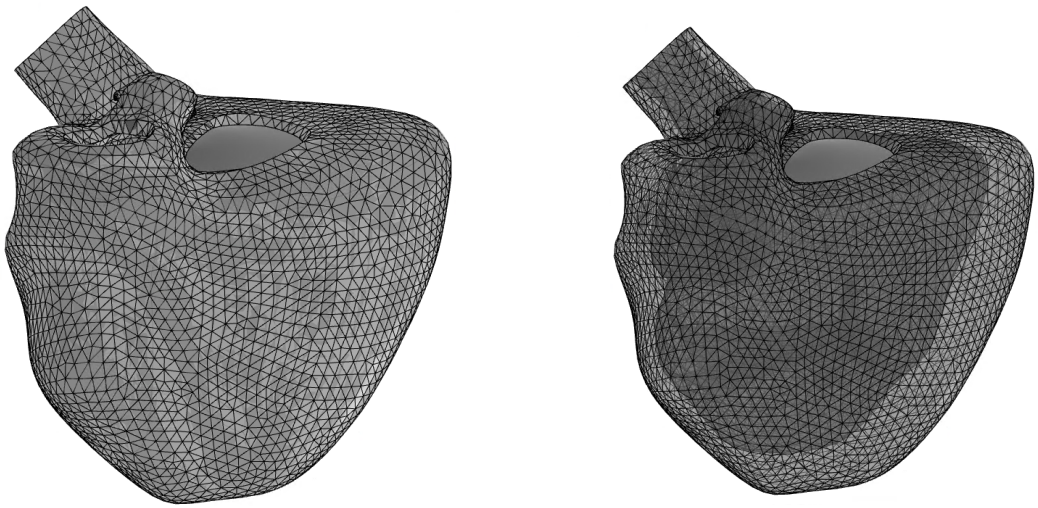

(a) Opaque mesh **(b)** Transparent mesh

Figure C.30: Mesh Patient 5

C.6. Misalignment correction

This section described the steps for a misalignment correction.

1. If a slice shift is suspected, the contours are to be individually imported in to the "Digitized Shape Preparation" application of CATIA.
   (a) Go to the **+** symbol at the top right corner, select **Import**, select **Digitization File**, click **Import a file**, find and open the correct file and click **OK**.
   (b) Name the file and click **OK**.
2. Create a point in the center of gravity for the individual contours.
   (a) Go to **Tools** and select **Measure inertia data**.
   (b) Select the contour, toggle on **Export center of gravity** and click **Create geometry** and then click **OK**.
3. Draw a line through the midpoints that are on the same axis.
   (a) Go to the **Wireframe** tab and select **Line**.
   (b) Pick the **Point-Point** option and select two midpoints.
   (c) For **Length type** pick **Creates line with infinite at end-point**.
   (d) Click **OK** to create the line.
4. Translate the rest of the contours onto the created line.
   (a) Go to the **Wireframe** tab and select **Point**.
   (b) Pick the **On curve** option. For **Curve** select the created line. For **Distance To Reference** pick **Distance along direction** and for **Direction** select the z-axis. Choose the **Offset** to be a multiplication of 8 mm (the vertical distance between the contours) and click **OK**. The parameters are shown in Figure C.31a. This generates a point on the created line. It will serve as the new center of gravity for the contour.

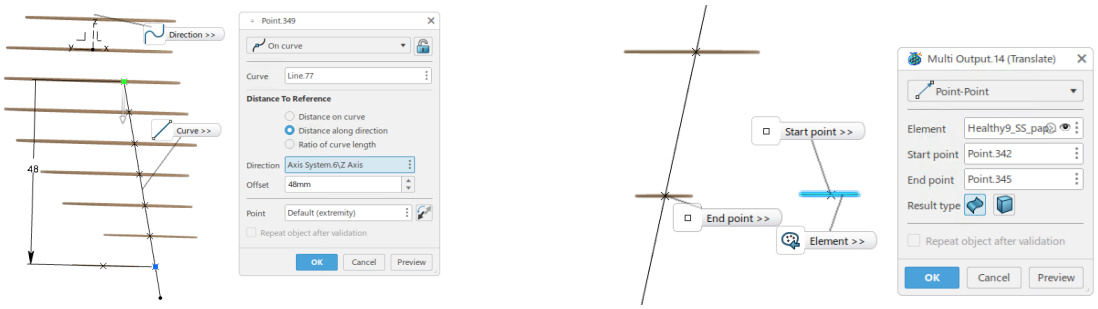

(a) Place a point on the created line

(b) Translate the contour to the new center of gravity

Figure C.31: Contour Translation.
Translating contours to corrected location for misalignment correction

   (c) Go to the **Digitized Data** tab and select **Translate**.
   (d) Select the **Point-Point** option.
   (e) For **Element** select the contour to translate, for **Start point** pick the original center of gravity and for **End point** pick the new center of gravity. The parameters are shown in Figure C.31b.
   (f) Click **OK** to translate the contour.
   (g) Repeat this step for the other contours in this ventricle.
5. Save the new corrected reference geometry.